DISS. ETH NO. 15499

CRUSTAL STRAIN RATES IN THE CENTRAL AND EASTERN MEDITERRANEAN AND IMPLICATIONS FOR SEISMIC HAZARD

A dissertation submitted to the

SWISS FEDERAL INSTITUTE OF TECHNOLOGY ZURICH

for the degree of

Doctor of Sciences

presented by

SARAH CLAIRE JENNY

Diploma of Natural Sciences (Dipl. Natw.)

Swiss Federal Institut of Technology (ETHZ, Switzerland)

born January 29, 1974

citizen of Fribourg (FR), Switzerland

accepted on the recommendation of

Prof. Dr. Domenico Giardini, examiner
Prof. Dr. Saskia Goes, co-examiner
Prof. Dr. Hans-Gert Kahle, co-examiner
Dr. Anselm Smolka, co-examiner
Dr. Massimiliano Stucchi, co-examiner

2004

Contents

Zusammenfassung

Die Bestimmung einer zeitlich gemittelten seismischen Gefährdung erfordert die Kenntnis von gemittelten seismischen Langzeit-Deformationsraten sowie Informationen über Häufigkeit und Stärke der Erdbeben. Von besonderem Interesse ist die Information über die grössten und zerstörerischsten möglichen Erdbeben. Seismische Kataloge können diese Information nur liefern, wenn sie lang und vollständig genug sind, um das Auftreten dieser grossen Ereignisse aufgezeichnet zu haben, und wenn die Fehler der Magnitude und der Lokalisation genügend klein sind. Trotz der langen historischen Erdbebenaufzeichnungen im Mittelmeerraum (eine Zeitspanne von 1000 - 2000 Jahren verglichen mit beispielsweise 150 Jahren Aufzeichnung in Kalifornien) sind die Unsicherheiten der durchschnittlichen, aus dem Katalog entnommenen, seismischen Deformationsraten gross. Besonders in Regionen, die sich langsam deformieren - wie der zentrale und westliche Mittelmeerraum - muss ein 1000-Jahre-Katalog nicht immer das grösstmögliche Ereignis in einem vorgegebenen Gebiet beinhalten.

Geodätische Daten, die im Verlauf von mehreren Jahren gemessen wurden, registrieren die Bewegung der Kruste mit einer Genauigkeit von 1 mm/yr oder weniger. Die geodätisch gemessene Deformation stimmt generell sehr gut mit den geologischen Daten überein, die über einen Zeitraum von einer bis mehreren Millionen Jahren protokolliert wurden und deshalb für eine langfristige tektonische Akkumulation der Strainraten repräsentativ ist. Daher liefern geodätisch gemessene Strainraten zusätzliche Erkenntnisse (eine obere Grenze) zur durchschnittlichen seismischen Rate der Strainfreisetzung. Nur wenige frühere Untersuchungen haben seismische und geodätische Daten zur bestmöglichen Abschätzung der langfristigen seismischen Aktivitätsrate kombiniert. In dieser Dissertation wurde zur besseren Abschätzung der seismischen Gefährdung für den sich relativ schnell verformenden östlichen Mittelmeerraum ($\sim$ 100 nanostrain, Geschwindigkeiten bis zu 4 cm/yr) (Kapitel 2) und den sich langsam verformenden zentra-

len Mittelmeerraum (10's von nanostrains, Geschwindigkeiten bis zu 5 mm/yr) (Kapitel 4) eine kombinierte geodätisch-seismische Analyse angewendet.

Ein Teil des Projekts beinhaltet Wiederholungsmessungen der geodätischen Referenzpunkte auf Sizilien und in der nherer Umgebung, wodurch die für Süditalien verfügbaren geodätischen Daten stark erweitert wurden. Diese neuen Daten dokumentieren eine jüngere (vor 0.5 - 0.8 m.y.) und früher nicht erkannte tektonische Neuordnung im zentralen Mittelmeerraum und verändern unser Verständnis der gegenwärtigen Tektonik grundlegend (Kapitel 3). Dies liefert einen wichtigen Anlass zur Überarbeitung der Abschätzung des seismischen Potenzials in Süditalien. Z. B. gehen im Norden Siziliens hohe Deformationsraten mit einem signifikanten seismischen Potential einher, dem bis jetzt in Risikokarten noch nicht Rechnung getragen wurde. Im Gegensatz dazu übertreffen die hohen Raten der seismischen Aktivität in Kalabrien während des 18. Jhd. die langfristigen tektonischen Deformationsraten und haben wahrscheinlich zu einer Überschätzung der seismischen Gefhrdung geführt.

In unserer Analyse des Mittelmeerraums sehen wir, dass seismischen Kataloge - selbst wenn sie kurz sind - den Stil der Deformation recht gut dokumentieren, da kleine und grosse Ereignisse im allgemeinen das gleiche Deformationsmuster widerspiegeln wie durch geodätische und geologische Daten bestimmt. Einige Ausnahmen wurden in Gebieten gefunden, wo ein grosser Teil der Deformation nicht mit Erdbeben verknüpft war (z.B. aseismisches Kriechen). Ein hinreichend langer Katalog ist jedoch entscheidend, um Magnituden der seismischen Deformationsraten zu erhalten. Für Deformationsrate, die so hoch sind wie im östlichen Mittelmeerraum, und für maximale Magnituden bis zu 7.5 würde ein Katalog von 100 - 200 Jahren eine langfristige Rate wiedergeben. Für kleine Deformationsraten, wie im zentralen Mittelmeerraum, ist ein 1000-2000- Jahre-Katalog erforderlich. Magnitude, Lokalisation und Unsicherheiten bzgl. der Vollständigkeit, vor allem für mittelgrosse Ereignisse ($M = 4.5 - 6.5$ in Griechenland, $M = 4 - 6$ in Italien), können die Zuverlässigkeit der auf dem Katalog basierenden Abschätzung der langfristigen seismischen Deformationsrate beeinträchtigen.

Im östlichen Mittelmeerraum korreliert das Ausmass der aseismischen Deformation mit dem tektonischen Regime: ungefähr 100 % der Deformation ist in strike-slip Zonen seismisch freigesetzt, etwas weniger in Extensionsgebieten und nur ca. 10-30 % entlang der Hellenischen Subduktionszone. Im zentralen Mittelmeerraum finden wir diese Kor-

relation nicht, aber es gibt ähnlich grosse Abweichungen im Verhältnis der seismichen zur totalen Deformation. Der östliche Mittelmeerraum hat relativ klar definierte Zonen hoher Seismizität, allerdings ohne deutlichen Hinweis auf eine Zeitabhängigkeit, die man während eines seismischen Zyklus erwarten würde. Im zentralen Mittelmeerraum ist die stark zeitabhänige Seismizität räumlich weit zerstreut, mit ähnlich starker Aktivität an einigen Inter- und Intraplattenzonen. Dabei wechseln sich Häufungen von starken Ereignissen mit Zeiten seismischer Ruhe ab.

Schliesslich wurde während eines Praktikums bei der MunichRe eine kombinierte Seismizität-Slip-Rate-Analyse in eine Risiko-Analyse für China (Kapitel 5) und Portugal (hier nicht enhalten) integriert, die den Nutzen des entwickelten Ansatzes aufzeigen soll.

Abstract

The determination of time-averaged seismic hazard requires the knowledge of average long-term seismic deformation rates, i.e., information on how often earthquakes occur and over what range of magnitudes. Of special interest is information on the largest, and most damaging, possible earthquakes. Seismic catalogues can only supply this information if they are long and complete enough to record the recurrence of these large events, and if errors in magnitude and location are sufficiently small. In spite of the long historical earthquake records in the Mediterranean (spanning 1000-2000 years compared with a 150 year record in for example California), the uncertainties in catalogue-derived average rates of seismic deformation are large. Especially, in slowly deforming regions like the Central and Western Mediterranean, a 1000-year catalogue may not always contain the largest possible event for a given area.

Geodetic data measured over the course of several years record crustal motions at the level of a mm/yr or less. The geodetically measured deformation is generally very consistent with that recorded geologically over time scales of 1 to a few m.y., and therefore representative for long-term tectonic accumulation rates of strain. Thus, geodetically measured strain rates provide an additional constraint (an upper bound) for average seismic rates of strain release. Only a few previous studies have combined seismicity and geodetic constraints for a best estimate of long-term seismic activity rates. In this thesis, the applicability of a combined geodetic/seismicity analysis for better constraints on seismic hazard was done for the relatively fast-straining Eastern Mediterranean ($\sim$ 100 nanostrain, velocities up to 4 cm/yr) (Chapter 2) and the slowly deforming Central Mediterranean (10's of nanostrains, velocities up to 5 mm/yr) (Chapter 4).

Part of this project included the remeasurement of geodetic benchmarks in Sicily and the surrounding region, thereby greatly expanding the geodetic constraints available for Southern Italy. These new data document a recent (0.5-0.8 m.y. ago) and previously

unrecognized tectonic reorganization in the Central Mediterranean and completely modify our understanding of the current tectonics (Chapter 3). This provides an important motivation for revising the estimates of Southern Italian seismic potential. For example, high deformation rates north of Sicily are accompanied by a significant seismic potential not accounted for in hazard maps up to now. In contrast, the high seismic activity rates of Calabria during the 18-th century exceed the long-term tectonic rates of strain accumulation, and may have led to overestimates of the seismic hazard.

In our Mediterranean analyses, we find that seismic catalogues - even if short - can document the style of strain quite well, because small and large events generally reflect the same deformation patterns, which are also consistent with styles inferred from geodetic and geologic data. A few exceptions were found in areas where a large portion of the deformation is not accompanied by earthquakes (i.e., aseismically creeping). However, a sufficiently long catalogue is crucial for obtaining magnitudes of seismic strain rates. For strains as high as in the Eastern Mediterranean and maximum magnitudes up to about 7.5, a catalogue of 100-200 years should reflect the long-term rate. For deformation rates as low as in the Central Mediterranean (maximum event size around 7), this requires a 1000-2000 year catalogue. Magnitude, location and completeness uncertainties, especially for intermediate-sized events ($M = 4.5 - 6.5$ in Greece, $M = 4 - 6$ in Italy) can compromise the reliability of catalogue-based estimates of long-term seismic deformation rates.

In the Eastern Mediterranean, the amount of aseismic deformation correlates with tectonic style: about 100 % seismic in strike-slip zones, somewhat less in the extensional regions and only about 10-30 % along the Hellenic subduction zone. In the Central Mediterranean, we found no such correlation, but there is a similarly large variation in the ratio of seismic over total deformation. The Eastern Mediterranean has relatively well-defined high seismicity zones, with no clear indications of time-dependence beyond what is to be expected during a seismic cycle. In the Central Mediterranean however, seismicity is spatially diffuse, with similar levels of activity at some inter- and intraplate zones, and strongly time-dependent, with clusters of large events and times of seismic quiescence.

Finally, during an internship at the MunichRe, a combined seismicity/slip rate analysis was integrated into hazard analyses for China (Chapter 5) and Portugal (not included

here), illustrating the usefulness of the approach developed.

Chapter 1

Introduction

Seismic hazard describes the potential for dangerous, earthquake-related natural phenomena such as ground shaking, fault rupture or soil liquefaction. These phenomena could result in adverse consequences like the destruction of buildings or the loss of life. Traditional seismic hazard maps convolve information about (1) the long-term average expected temporal, spatial and size distribution of earthquakes with (2) seismic wave attenuation between the sources and the points of interest for hazard evaluation and (3) site response. The results are plotted as maps showing the maximum expected ground acceleration (or velocity) in a certain time interval (e.g., 10, 30, 100, 1000 years depending on the application). Such maps are of great interest to engineers to guide the design of buildings and for governments to define building codes. Seismic risk is the probability of occurrence of the adverse consequences of ground motion. Seismic risk, used for example by insurance companies, is obtained by adding information on the vulnerability and value of structures in a given location. Although ultimately one would like to do a more time-dependent evaluation of hazard, in many areas of the world even the long-term average level of seismic recurrence is poorly defined.

This thesis mainly focuses on the first component of seismic hazard evaluation, i.e. assessment of the long-term average seismic potential. To do this one needs information about (1) the spatial distribution of seismicity, usually determined for regions called source zones and (2) the distribution of seismicity in time and with magnitude for each of these source zones. Generally, this information is obtained from evaluating historical (before the recording of earthquakes by seismic instruments, i.e. based on macroseismic data) and instrumental seismic catalogues. Historical catalogues predominantly record

the larger events and are affected by large uncertainties related to completeness, and earthquake magnitudes and locations. Instrumental catalogues are more complete, have better defined magnitudes and locations and include smaller events, but they are short. Especially in slowly straining areas, instrumental records are much shorter than the recurrence time of moderate and large events, and thus do not represent long-term average rates of seismicity well. To alleviate some of these shortcomings of the catalogues, we add, in this thesis, additional constraints from geodetic observations.

For mapping the distribution of seismic activity, a region of interest is usually divided into source zones, also called seismotectonic sources. Optimally, each of these zones covers a seismogenic fault. However, many subsurface faults are unknown and earthquake locations are often not constrained well enough to identify the responsible fault. This is especially true when one needs to rely on historical seismic data. With incomplete information on the distribution of damage all around the epicenter, pre-instrumental locations can be highly uncertain. Unless obvious seismic zones at larger distances are known, historical events were often assigned locations in the populated area where they were felt. However, when an active area was uninhabited and historical documents are absent all together, its activity may have gone unrecognized and even large earthquakes may have remained undetected. Also in instrumental catalogues, location errors are often not small enough to unequivocally identify the fault structures responsible for the observed seismicity. Therefore, seismic source zones generally span broader zones that include a population of faults. Within each source zone, the seismicity is assumed to be homogeneous, i.e. the style of deformation and the seismic potential is similar throughout the source zone. For short observation times and given uncertainties in magnitude and location, source zones have to be large enough to encompass a number of events that are statistically representative of the seismicity.

The temporal seismic activity is defined as the occurrence of earthquakes within a certain magnitude range for a given time period, in the form of a magnitude-frequency distribution. Magnitude-frequency distributions are generally parameterized in terms of a power-law distribution, often referred as the Gutenberg-Richter distribution, from the names of the researchers who first observed this power law distribution of earthquake numbers N with magnitude M

$$logN = a - bM \tag{1.1}$$

Here a represents the recurrence rate of small events and the b-value describes the decrease in recurrence frequency with increasing magnitude. At the largest magnitudes, the power-law distribution has to break down because of limited fault sizes and limits on the total energy that can be released [*Kagan*, 2002a; *Koravos et al.*, 2003]. In our studies, we use a simple Gutenberg-Richter distribution truncated at a maximum magnitude M_{max}. Although other more complex distributions with alternative definitions of a critical or maximum magnitude may better describe magnitude-frequency data in detail [*Kagan*, 2002a; *Koravos et al.*, 2003], the truncated Gutenberg-Richter distribution can often not be rejected by the available data, and we use it for its simplicity. Recurrence rates of small events are usually defined from instrumental seismicity; recurrence rates of large earthquakes are constrained by historical and sometimes paleoseismic (i.e., geological) data. Even within one catalogue (historical or instrumental), completeness may vary with magnitude. Even with the best attempts at correcting for this differential completeness, a magnitude-dependent uncertainty remains, which may affect the estimates of the b-value, which is a measure of the number of large versus small events. Furthermore, the uncertainty in magnitude varies through time. Magnitude uncertainties are smallest in the instrumental catalogues. For older events, historians often have to assign a magnitude to an earthquake with information as qualitative as a description of the shaking of a bookshelf and the toppling down of books, with consequently much larger uncertainties, which may vary considerably between events. Furthermore, a conversion from the damage-related intensity scale to the instrumental magnitude scale is also not always straight-forward. These magnitude uncertainties contribute further to uncertainties in magnitude-frequency distributions and consequently in b-values.

b-values are typically close to 1 [*Godano and Pingue*, 2000; *Kagan*, 2002b]. Regional variations of the b-value (between about 0.5 and 1.5) have been observed by many authors (see e.g., *Hattori* [1974]; *Okal and Romanowicz* [1994]). Some studies [*Utsu*, 1971; *Kagan*, 1991, 2002a] argue that differences in b-value could be due to systematic errors in magnitude determination and strongly support the universality of $b = 1$ (see also, *Kagan* [1997]; *Godano and Pingue* [2000]; *Main* [2000]; *Leonard et al.* [2001]). Most of these studies have analysed instrumental data. Our detailed study of the Eastern Mediterranean (Chapter 2) also indicates spatially variable b-values. It has been argued that the smooth Gutenberg-Richter distribution only applies when one averages over

several faults. For single faults, the distribution may change to a so-called characteristic distribution, dominated by the recurrence of one large, "characteristic", event. In this case, the characteristic event has much shorter recurrence times than would be expected based on the extrapolation of the frequency of smaller events. Since the smaller event side of the distribution is usually best constrained (by the instrumental catalogues), it is important to know whether the distribution is smooth or characteristic to evaluate seismic hazard. Modeling of Ben-Zion and coworkers [*Ben-Zion and Zhu*, 2002; *Ben-Zion et al.*, 2003] shows that such characteristic distributions may depend on the distribution of heterogeneity on the fault plane (which is possibly linked to the maturity of the fault). In practice, it is usually difficult to conclusively establish (within the catalogue uncertainties) if the distributions deviate from a smooth Gutenberg-Richter trend and the existence of characteristic distributions is a matter of ongoing debate [*Utsu*, 1999; *Kagan*, 2002a; *Koravos et al.*, 2003].

a- and *b*-values are not only believed to vary significantly in space but also in time [*Wiemer and Wyss*, 2002; *Schorlemmer et al.*, 2004a, b]. For hazard purposes, it is important to know how much variation in recurrence time may occur through time. The variability can theoretically range from perfect periodicity (regular recurrence times and thereby good predictability and increasing hazard with time since the last event), to earthquake clustering (strong variations in recurrence time from very short to very long and decreasing hazard with time since the last event). It is clear that by interaction between faults and fault segments, recurrence regularity is disturbed [*Ward and Goes*, 1993; *Papadimitriou and Sykes*, 2001; *Robinson and Benites*, 2001]. We know clustering happens in aftershock sequences, and during such a sequence, the probability of earthquake occurrence decreases with time since the main shock. But the recurrence pattern of main shocks is still a matter of much debate. Recent research is focusing on trying to establish relations between stress changes and seismicity to infer whether a region is far from or close to a next big event [*Stein et al.*, 1994; *Lin and Stein*, 2004; *Gomberg et al.*, 2004]. For specific faults or fault segments it may be possible to obtain such information [*Stein et al.*, 1997; *Harris and Simpson*, 2002]. But for most faults and larger regions, our understanding of the earthquake process and the data are insufficient. The intermediate assumption, without additional information, is a Poisonian distribution, i.e., earthquakes occur randomly in time with an average frequency = 1/(recurrence time),

and hazard is constant in time. This is what we use here.

Earthquakes represent deformation or strain. The amount of strain that an earthquake represents can be estimated from its seismic moment. Seismic moment is a more physical measure of earthquake strength than the empirical magnitude scale. Moment M_0 is equal to μAD, where μ is the elastic shear modulus of the medium surrounding the fault, A is the fault area, and D the average earthquake slip. Magnitude M_w is related to moment as [*Kanamori*, 1977]:

$$M_w = \frac{2 \times log_{10} M_0}{3} - 10.7 \tag{1.2}$$

Strain ϵ is the amount of slip D, divided by the width of the deforming zone. Thus moment equals $\mu V \epsilon$, where V is the volume of the deforming area [*Kostrov*, 1974]. Integrating the recurrence rates of events over the full range of magnitudes thus provides a seismic strain rate for the area studied.

At best, seismic catalogues can give an estimate of the short-term seismic deformation rate, averaged over the catalogue's duration. Although the largest events represent the largest proportion of strain, the much larger number of small and moderate events can contribute significantly to the seismic deformation rate when b is larger than 1. This small event strain remains largely undetected by historical catalogues. Even when not significantly affected by catalogue completeness and uncertainties in magnitude and location, the short-term seismic deformation may not be representative for long-term seismic moment rates, if the recurrence times of the largest events much exceed the catalogue length. Seismic hazard analyses, which estimate long-term average magnitude-frequency distributions, thus correspond to an estimate of average strain rate. When based solely on seismicity data, these estimates are hampered by the aforementioned limitations of the catalogue. What is generally not done is to compare these implied strain rates with other strain rate measurements, such as, for example, those obtained geodetically.

Geodetic data give measurements of total tectonic strain accumulation rates [*Stein*, 1993], when data affected by short-term fluctuations due to for example co- and post-seismic deformation are excluded. Uncertainties in geodetic strain rates (apart from filtering out short-term fluctuations) are mainly due to lack of dense enough data network to define the concentration of strain. Geodetic (tectonic) strain rates represent

an upper bound of strain that can, on average, be released seismically in a given time interval. Based on historical seismicity, earlier hazard studies [*Erdik et al.*, 1999; *Slejko et al.*, 1999] have defined earthquake recurrence parameters that, when converted, correspond to strain rates that are up to ten times larger than strain rates observed geodetically. This indicates the usefulness of including geodetic constraints in seismic hazard evaluation.

The long-term tectonic deformation may be larger that the long-term seismic deformation, if part of the overall deformation occurs aseismically. Even close to the surface, not all deformation is reflected in earthquakes. This is most clearly documented along San Andreas fault, which has both continuously creeping zones without large earthquakes, and locked zones with large earthquakes [*Thatcher*, 1990], but also for subduction zones worldwide very different ratios of seismic/total deformation have been estimated, ranging from close to 0 to 100 % [*Scholz and Campos*, 1995; *McGuire and Segall*, 2003]. Conditions that determine whether deformation occurs unstably, i.e., by earthquakes, or by steady slip are not well understood. It is clear that temperature plays a role (because of the correlation of earthquake activity along ridges and trenches with thermal structure, e.g., *Lay and Wallace* [1995] and *Stein and Wysession* [2003]), but this is not an explanation along the San Andreas fault. Often the proportion of seismic versus aseismic deformation is expressed in a seismic coupling width. In this case, each fault is considered 100 % seismic, but over a variable depth interval ranging from only a few kilometers to 40-50 km in subduction zones. In this thesis, we will keep the seismic width fixed and estimate ratios of seismic/total deformation rates assuming they are accommodated over the same depth interval.

The goal of this thesis is to define earthquake recurrence parameters (a, b and M_{max} in source zones) that are consistent with all data available: seismic and geodetic strain rates, geological and tectonic information. Although significant uncertainties in the seismic potential estimates remain, it is important to use recurrence rates that at least satisfy all data we do have. This is done for a fast-straining area (the Eastern Mediterranean, covering Greece and western Turkey) and a slow-straining area (the Central Mediterranean, focusing on South Italy).

The Mediterranean encompasses the convergence between the African and European plates. This convergence occurs at slow rates of 0.5-1 cm/yr and becomes increasing

oblique when moving from the eastern to the western end of the Mediterranean (Fig. 1.1). Deformation inside the collision zone is complex as illustrated by the distributed seismicity (Fig. 1.1). It contains extruding blocks like Anatolia, rotating blocks like Adria and fast-retreating subduction zones like the Hellenic trench.

In the Eastern Mediterranean, the high strain rates and the large density of geodetic data allow a detailed comparison between the short-term seismic strain rate documented by earthquake catalogues and the tectonic strain rate field measured geodetically, and evaluation of how these types of information can be merged for estimating seismic potential (Chapter 2). After reevaluating the current tectonics of Southern Italy based on newly collected geodetic data (Chapter 3), we redefine the source zones for this region. Then we use what was learned from the Eastern Mediterranean study to assess seismic potential of the much more slowly deforming South-Central Mediterranean (Chapter 4). Some indication of how such information can be incorporated in hazard/risk analyses is given in the report in Chapter 5.

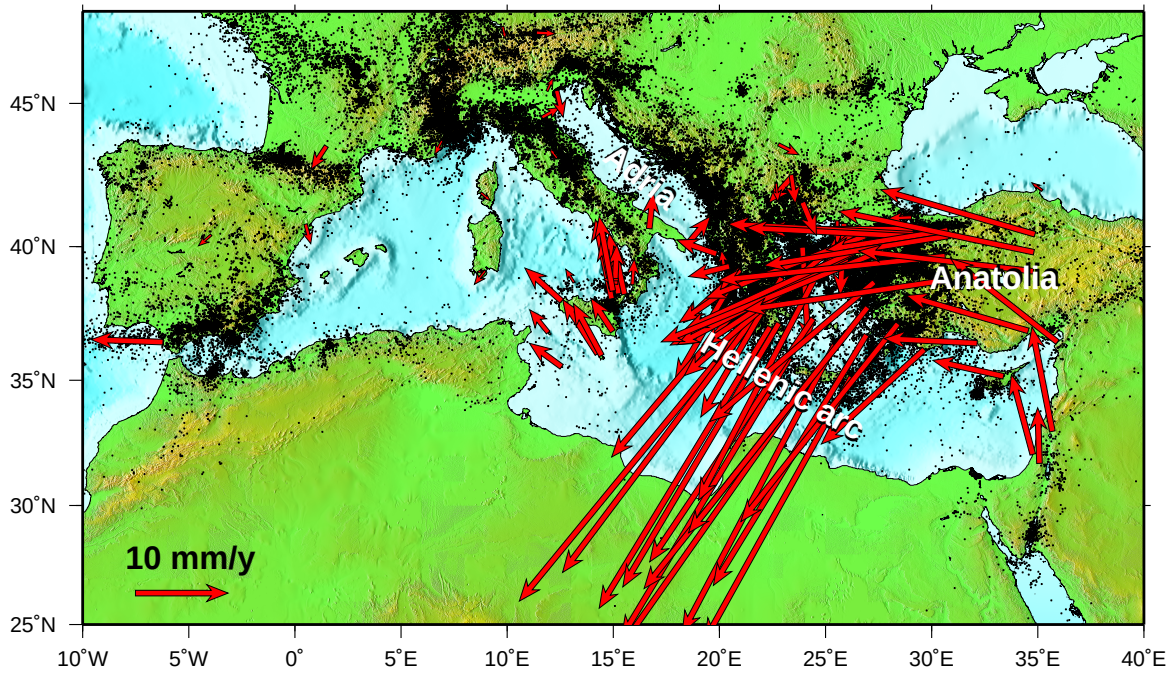

Figure 1.1: Mediterranean area. Seismicity is from the PDE-NEIC catalogue [U.S. Geological Survey] for depths $\leq 40km$. Geodetic data relative to Europe are from *Boucher et al.* [1998], *Cocard et al.* [1999], *McClusky et al.* [2000], *Kotzev et al.* [2001] and *Hollenstein et al.* [2003]. The southernmost vector in the Central Mediterranean, on the island of Lampedusa, reflects stable Africa's motion.

Chapter 2

Earthquake recurrence parameters from seismic and geodetic strain rates in the eastern Mediterranean

Sarah Jenny, Saskia Goes, Domenico Giardini and Hans-Gert Kahle

Geophysical Journal International, 157, 1331-1347, 10.1111/j.1365-246X.2004.02261.x, 2004

2.1 Abstract

Although the parameters used in seismic hazard analyses imply a long-term seismic strain rate, they are usually not checked against such alternative estimates. In this study, we determine hazard parameters for the eastern Mediterranean (a value, b value, m_{max} and the corresponding long-term seismic moment rate $\dot{M}_0^{seis}$) consistent with seismicity data, tectonic information and geodetic strain rates. The dense data coverage in this region permits a detailed comparison of the horizontal seismic strain rate field, $\dot{\varepsilon}_s$, as recorded in the 500-year long historical catalogue and the tectonic strain rate field, $\dot{\varepsilon}_g$, measured geodetically. We find that $\dot{\varepsilon}_s$ is very similar in style over all magnitude ranges

within each different tectonic regime in the study region. Furthermore, $\dot{\varepsilon}_s$ is similar in style to $\dot{\varepsilon}_g$. Except along the Hellenic arc, $\dot{\varepsilon}_s$ is consistent with $\dot{\varepsilon}_g$ in amplitude. We verify that for the high strain rates accommodated in the eastern Mediterranean and historical catalogues spanning at least 100-200 years, $\dot{\varepsilon}_s$ should reflect the long-term seismic strain release when averaged over each tectonic zone. To estimate such seismic strain reliably, accurate knowledge about the rates of recurrence of intermediate size events ($M_w = 4.5 - 6.5$) is needed. For $b \geq 1$, these events can accommodate up to 60 % of the strain. The combined analysis of $\dot{\varepsilon}_g$ and $\dot{\varepsilon}_s$ provides an estimate of the seismic/total strain. The major strike-slip zones in the region, the Northern Anatolian fault and the Kephalonian fault, experience little to negligible aseismic deformation. In the remaining eastern Mediterranean up to 10-30 % of the total deformation is aseismic. The Hellenic trench is largely uncoupled, with at least 50 % and up to 90 % of the compressive strain released aseismically. Only the extensional component of strain at the eastern end of this trench appears significantly seismically active.

2.2 Introduction

Knowledge of long-term seismic strain rates is essential for determining the seismic hazard of a region. Probabilistic seismic hazard analyses make an implicit estimate of long-term seismic strain rates. In hazard studies, the region of interest is divided into seismic source zones in which seismicity is assumed to be homogeneously distributed. For each source zone a magnitude-frequency seismicity distribution is determined, usually in terms of a Gutenberg-Richter relation and a maximum magnitude. The integrated moment rate of this distribution is equivalent to a seismic strain rate estimate. However, the strain rate fields implied by the seismic hazard data are generally not checked against other strain rate data. For example, for some regions, the hazard parameters from the Global Seismic Hazard Assessment Program (GSHAP) [*Giardini and Basham*, 1993; *Giardini*, 1999] yield tectonically unrealistic strain rates that exceed geodetically inferred strain rates by a factor of 2-10. Although unrealistic strain rates do not necessarily lead to unreliable short-term hazard maps, it is preferable to use a set of hazard parameters that is consistent with all available data. The objective of this study is to evaluate how different sources of data can be used and integrated for this purpose.

Our study focuses on the Eastern Mediterranean. First, we determine the geodetic and seismic strain rate fields for the region independently. By comparing these two fields, we estimate long-term seismic strain rates, where long-term is defined as encompassing many large-earthquake cycles. Then we translate strain rates into earthquake recurrence parameters as used in hazard analyses. The dense geodetic data distribution, relatively long historical catalogues and high activity rates make this region ideal for constructing independent estimates of seismic and geodetic strain rates. Once the strengths and weaknesses of the individual data sources are known, future applications to regions with less dense data coverage become feasible.

Geodetic and seismic strain rates are mapped using the method of *Haines and Holt* [1993], which allows the determination of strain rate fields and corresponding velocity fields within a zone of continuous deformation by integrating seismic, geodetic and geological information. Using the latest GPS measurements [*Clarke et al.*, 1998; *Davies et al.*, 1997; *Reilinger et al.*, 1997; *Cocard et al.*, 1999; *McClusky et al.*, 2000; *Kotzev et al.*, 2001], we are able to map geodetic strain rates in more detail than done in previously proposed deformation models for the Eastern Mediterranean [*Makris*, 1978; *McKenzie*, 1978; *Le Pichon and Angelier*, 1979; *Le Pichon et al.*, 1995; *Giunchi et al.*, 1996a; *Mantovani et al.*, 2000]. The data we use exclude short-term co- and postseismic deformation [*McClusky et al.*, 2000; *Cocard et al.*, 1999]. On a global scale, it has been demonstrated that geodetic strain rates and tectonic deformation rates inferred from geology agree well [for example, *Argus and Heflin*, 1995; *DeMets et al.*, 1994; *Ward*, 1990]. A similar agreement has been found along the western and eastern parts of the North Anatolian Fault Zone (NAFZ) [*Armijo et al.*, 1999; *Straub et al.*, 1997; *Westaway*, 1994]. Therefore, we take the geodetic strain rate field as representative for long-term tectonic deformation.

To define a seismic strain rate field, the style is obtained from moment tensors, using Kostrov summation, while the magnitude is inferred from historical catalogs going back to 500 BC. Others have performed analyses of seismic deformation rates using around 100 yr seismic historical data [*Jackson and McKenzie*, 1988; *Jackson et al.*, 1992]. [*Papazachos and Kiratzi*, 1992] combined historical data back to the eighteenth century and moment tensors within a study area in central Greece. We map seismic strain rates on the same grid as used for the geodetic field, and evaluate uncertainties

due to uncertainties in mechanism, magnitude and completeness. The main factors that contribute to uncertainties in estimates of long-term seismic moment rate from historical catalogues have been analysed in detail by *Field et al.* [1999].

We compare geodetic and seismic strain rates to obtain an estimate of long-term seismic moment rates. Such moment rates should neither exceed tectonic moment rates, nor require unreasonably large magnitude events. Seismic moment rates that are low compared to tectonic strain rates may indicate that deformation occurs in part aseismically (or in other words, that the depth of seismic coupling varies). Using the observed magnitude-frequency distributions of seismicity and their uncertainties, we translate the seismic moment rates into earthquake recurrence parameters for the simple truncated Gutenberg-Richter distribution often used in hazard analyses. *Ward* [1998a] has previously estimated and compared seismic and geodetic moment rates in Europe for a less dense geodetic data set and using the seismicity of 20th century from the NEIC catalogue. He found that overall, the seismic moment rates are less than geodetic moment rates. This however does not imply significant aseismic deformation, as short catalogues are more likely to under- than overestimate long-term moment rates [*Ward*, 1998a, b]. *Jackson et al.* [1994] compared seismic and geodetic strains in the Aegean. The distribution of geodetic data at the time allowed only a coarse grid study. They found a seismic strain rate deficit for the whole Aegean area. Recently, *Koravos et al.* [2003] performed a significantly more detailed study of the seismicity distribution and moment release rates in the Aegean. To obtain maximum magnitude estimates they relied on the geodetic strain of *Jackson et al.* [1994]. In the analysis done here, we update both seismic and geodetic deformation fields and compare them in style as well as in amplitude.

2.3 Tectonic Setting of the Eastern Mediterranean

The Aegean-Anatolian region is an area of intense seismic activity relative to the surrounding areas. The region can be divided into five different tectonic regimes: 1) strike-slip motion along the North Anatolian Fault Zone (NAFZ) and its extension into the northern Aegean, the North Aegean Trough (NAT) 2) extension in Central Greece, including the Gulf of Corinth and Peleponesos, 3) extension in western Anatolia, 4) convergence along the Hellenic arc and 5) the Kephalonian transform fault (Fig. 2.1).

The NAFZ accommodates right-lateral strike-slip motion between Anatolia and stable Europe. Releasing steps in the fault form pull-apart basins in the Marmara Sea [*Barka*, 1997]. The westward extrusion of Anatolia is probably a response to Arabian indentation [*Jackson and McKenzie*, 1988; *Le Pichon et al.*, 1995]. The NAFZ is a relatively recent tectonic feature of the region. It formed around 10 m.y. ago in eastern Turkey [*Barka*, 1992] and propagated westward [*Taymaz et al.*, 1991b; *Armijo et al.*, 1999]. At present, the fault zone extends into the NAT where several linear trends of strike-slip earthquakes can be discerned. This strike-slip motion is transferred into normal faulting (with the direction of the principal extension being constant) in continental Greece [*Hatzfeld et al.*, 1999]. Slip rates along the NAFZ have been estimated by seismic moment summation [*Jackson and McKenzie*, 1988; *Eyidoğan*, 1988; *Kiratzi*, 1993; *Westaway*, 1994], geological information [*Barka and Kandinsky-Cade*, 1988; *Taymaz et al.*, 1991a; *Lyberis et al.*, 1992] and geodetic velocities [*Straub et al.*, 1997; *McClusky et al.*, 2000]. The velocities obtained by recent GPS campaigns constrain the rates of the westward motion of the Anatolian plate along the NAFZ to 26 $\pm$ 3 mm/yr relative to Eurasia.

N-S directed extension is presently localized in central Greece, around the Gulf of Corinth and the regions north and south of it [*Sorel*, 2000]. Around 25-30 m.y. ago extension occurred further south and in the Aegean Sea [*Jolivet et al.*, 1994; *Gautier et al.*, 1999]. The Southern Aegean is at present seismically very quiet and is often treated as a rigid block. Some extension is also observed in western Anatolia, but it is less pronounced geodetically [*Jackson and McKenzie*, 1984; *Seyitoglu and Scott*, 1996; *Kahle et al.*, 1999]. The extension in Greece and western Anatolia is probably a response to trench roll-back [*Jolivet*, 2001].

Convergence along the Hellenic arc is currently active from the Kephalonian transform fault in the northwest to Rhodes in the southeast. The trench is marked by recently deformed sediments and a high level of seismicity consisting predominantly of small events. Very few large thrust events have been documented and the level to which the subduction zone interface is coupled and, thus the seismic strain rate, is not well constrained [*Jackson and McKenzie*, 1988; *Meijer and Wortel*, 1997]. The Hellenic trench is also associated with active extension parallel to the arc [*Lyon-Caen et al.*, 1988; *Armijo et al.*, 1992].

The Kephalonian fault marks the western termination of the active subduction at present. Active subduction north of Kephalonia ceased around 5 m.y. ago [*King et al.*, 1993; *Robertson and Shallo*, 2000], and was replaced by continental collision between the Adriatic and the Balkans. The Kephalonian fault exhibits dextral strike-slip motion, at a rate of 2-3 cm/yr [*Kahle et al.*, 1996; *Cocard et al.*, 1999; *Louvari et al.*, 1999].

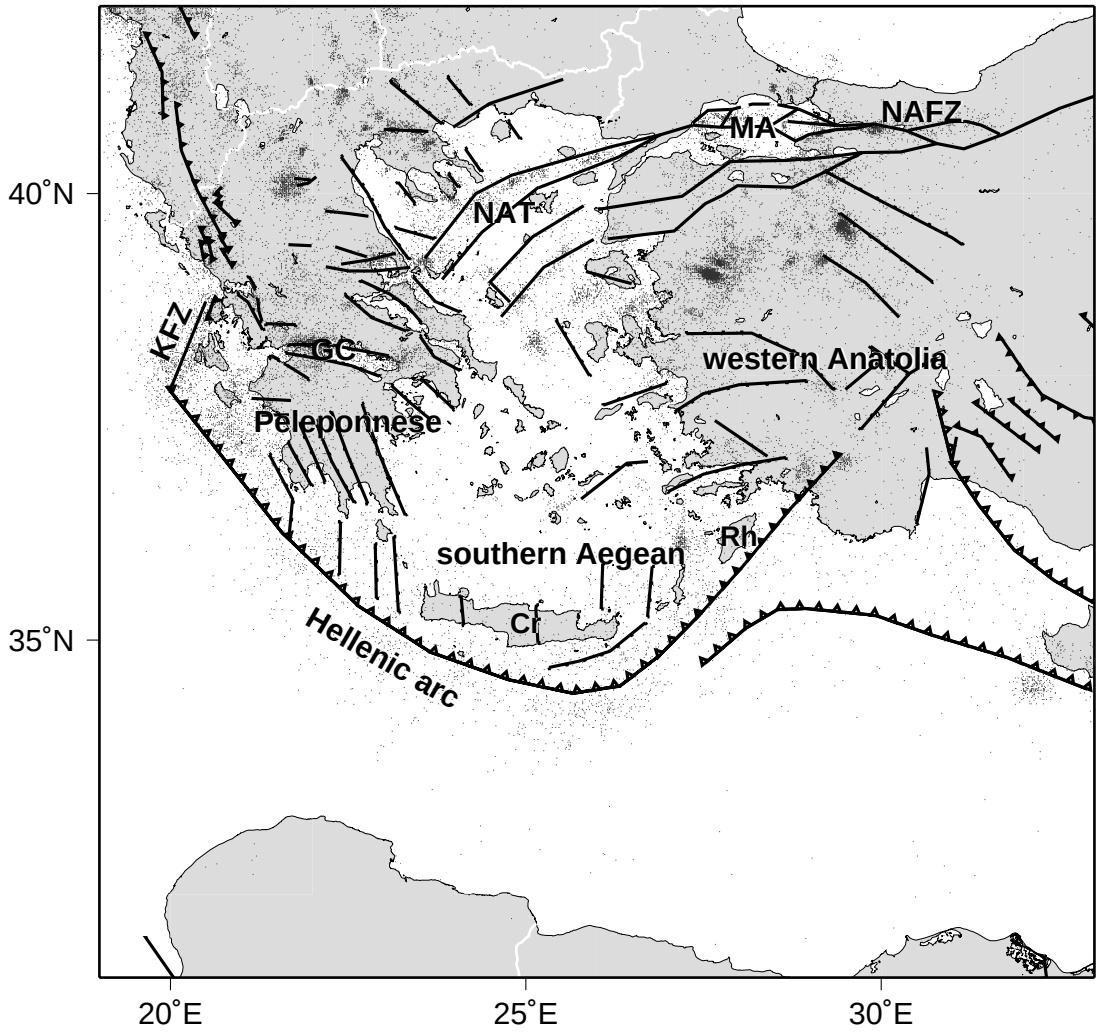

Figure 2.1: Tectonic setting of the study region showing major faults (after *Kahle et al.* [2000]) and seismicity from the PDE-NEIC catalogue [U.S. Geological Survey] for depths $\leq$ 40 km and a time span of 1/1/1977-31/12/2001. Cr = Crete, GC = Gulf of Corinth, KFZ = Kephalonian Fault Zone, MA = Marmara Sea, NAFZ = North Anatolian Fault Zone, NAT = North Anatolian Trough, Rh = Rhodes.

2.4 Strain mapping method

We treat deformation as continuous within the Aegean-Anatolian region. We use the method developed by *Haines and Holt* [1993], upgraded and discussed in more detail by *Haines et al.* [1998] and *Beavan and Haines* [2001], and applied in various regions [for example, *Kreemer et al.*, 2000; *Shen-Tu et al.*, 1999; *Holt and Haines*, 1995]. *Haines and Holt* [1993] show that velocity and strain rate on a sphere can be expressed in terms of the rotation vector function $\mathbf{W}(\hat{\mathbf{x}})$, which describes the velocity field $\mathbf{u}(\hat{x})$,

$$\mathbf{u}(\hat{x}) = r\mathbf{W}(\hat{x}) \times \hat{x} \tag{2.1}$$

where $\hat{\mathbf{x}}$ is the unit radial position vector on the Earth's surface and r is the radius of the Earth. This method provides a consistent strain rate field (compatible and related to $\nabla\mathbf{u}(\hat{x})$) and allows for the combination and comparison of different data types (seismic, geodetic and geologic). Their method determines $\mathbf{W}(\hat{\mathbf{x}})$ at the knot points of a curvilinear grid assuming a bi-cubic spline interpolation between the nodes to obtain a continuous $\mathbf{W}(\hat{\mathbf{x}})$ field that satisfies strain rate compatibility constraints. $\mathbf{W}(\hat{\mathbf{x}})$ at the nodes is obtained from a weighted least-squares minimization between observed and predicted values of velocity (in the case of geodetic data) and/or strain rate (in the case of seismic data). Weights are given by the estimated data covariance. Depending on the data distribution some smoothing over one to several neighboring grid cells is usually required. In the case of seismic data, strain rates are estimated from Kostrov summation [*Kostrov*, 1974]:

$$\dot{\varepsilon}_{ij} = \frac{1}{2\mu VT} \sum M_0 m_{ij} \tag{2.2}$$

where μ is the shear modulus, V is the cell volume (the grid area times the seismogenic thickness), T is the time period of the earthquake record, M_0 is the seismic moment, and m_{ij} is the unit moment tensor. We use a shear modulus of $3.5\times10^{10} Nm^{-2}$ and an average 15 km thickness of the seismogenic zone. Values of μ and seismogenic thickness affect the magnitude but not the style of the estimated strain rate tensors. To determine self-consistent strain rate fields associated with GPS observations, velocities are matched subject to the constraint of minimal strain rate magnitude. Covariances are taken

directly from the geodetic data [*Hollenstein et al.*, 2003].

The choice of the grid is important. It should be fine near major faults to allow for large spatial variations in strain, but coarser in areas where sparse data do not provide detailed constraints. It should follow tectonic features so that smoothing is performed consistently with tectonics. For Kostrov summation grid cells should delimit areas of homogeneous tectonic deformation. Based on the main tectonic domains, seismicity maps and moment tensor data, a curvilinear grid is defined across the eastern Mediterranean region, covering an area between 13° to 36° E and between 30° to 47° N (Fig. 2.2).

Plate rigidity can be simulated by setting the spatial derivatives of $\mathbf{W}(\hat{\mathbf{x}})$ to zero. This is done for the part of the African plate marked in Fig. 2.3. The geodetic velocity field is calculated relative to a Eurasian reference frame. The northern boundary of the grid is kept fixed in this reference frame.

2.5 Data

2.5.1 Seismic data

The style of seismic deformation within the Aegean-Anatolian region is derived from focal mechanism solutions of the Harvard Centroid Moment Tensor (CMT) catalogue [*Dziewonski et al.*, 1981, http://www.seismology.harvard.edu] and a compilation of large events by *Jackson et al.* [1992] (Fig. 2.2). The CMT catalogue contains solutions for approximately all events with magnitude $M_w > 5.5$ since January 1977; we use events up to August 2003. Catalogues spanning the entire 20th century for the Eastern Mediterranean have been compiled by *Anderson and Jackson* [1987], *Jackson and McKenzie* [1988] and *Jackson et al.* [1992], but contain only large events ($M \geq 6.0$) and have larger uncertainties. The mechanisms from the short CMT catalogue agree well with the data of *Jackson et al.* [1992]). Most of the slight differences between the deformation styles in the two data sets disappear when the moment tensors are averaged. To obtain strain rate estimates, we include all events at depths less than 40 km, which reflect lithospheric deformation related to horizontal surface motions. Most of the events (90 %) are located above 15 km , the depth used in the Kostrov strain calculation, but to allow for depth uncertainties, we set the depth cut-off to 40 km.

Historical catalogues provide information about moment rates over a much longer

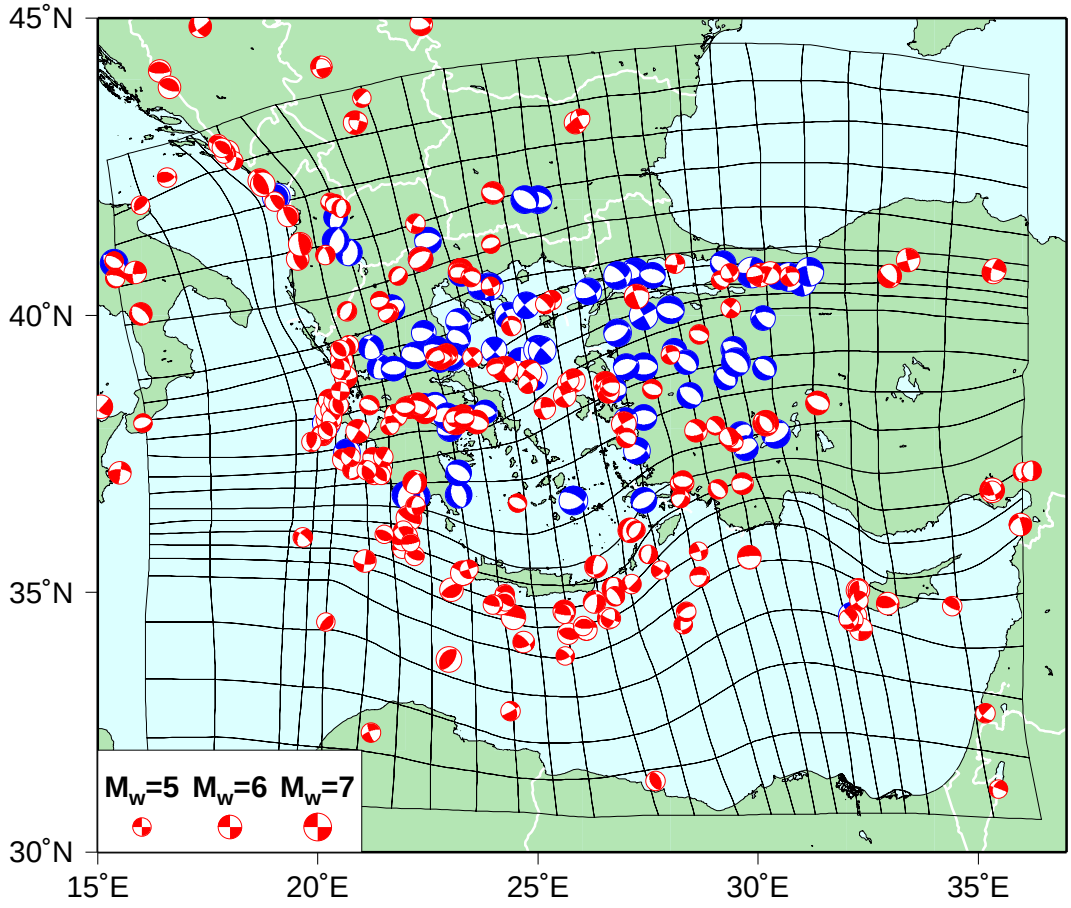

Figure 2.2: Focal mechanisms with $M \leq 6.5$ from the CMT catalogue in black [*Dziewonski et al.*, 1981]. Focal mechanisms with $M > 6.5$ from the Harvard CMT catalogue and from *Jackson et al.* [1992] in gray. All events have depths ≤ 40 km. Also shown is the grid on which Kostrov summation and strain rate mapping are performed.

period and give constraints on the magnitude of the seismic strain rates. To assess uncertainties and improve the catalogues, we combine the results of several catalogues. The catalogue of *Ambraseys and Jackson* [2000] for the Marmara Sea contains all earthquakes between 1500 and 2000 AD with $M_s \geq 6.0$ and is believed to be complete above $M_s \geq 6.8$. *Ambraseys* [2001a] further compiled a catalogue for the time interval 1900-1999 in the eastern Mediterranean including Greece and the Middle East for shallow earthquakes ($h \leq 40km$) with $M_s \geq 6.0$. Seismicity in Greece west of 30 °E for the period 550BC-1999 is available from *Papazachos et al.* [2000]. For Turkey a declustered catalogue has been prepared for the Global Seismic Hazard Assessment Program (GSHAP) [*Giardini*, 1999, http://seismo.ethz.ch/GSHAP/turkey/seisgshap.prn]. Finally the NEIC-PDE Catalogue [U.S. Geological Survey], although short, contains a

considerable number of small events for the time span 1973 to present which allows the mapping of tectonic features that are moving seismically (Fig. 2.1). These different sources were merged and carefully cross-checked to produce our own historical catalogues. The magnitude and location of events are not always in agreement amongst the various authors. To assess the impact of these uncertainties on the determination of the moment rates and the earthquake recurrence parameters, we define two catalogues. Both catalogues comprise the catalogue of *Papazachos et al.* [2000] west of 30° E and the the GSHAP-Turkey and the NEIC-PDE catalogues east of 30° E. The first one, CAT1, spans only the last 500 years, and where available, the data of *Ambraseys and Jackson* [2000] and *Ambraseys* [2001a] for events larger than $M_w = 6$ are used, instead of those of *Papazachos et al.* [2000] and GSHAP. The second catalogue, CAT2, spans the full 2550 years, and the data were not modified from *Papazachos et al.* [2000] and GSHAP. To assess the effects of uncertain completeness intervals, we use published estimates [*Papazachos*, 1999; *Papazachos et al.*, 2000] west of 30° E, as well as our own estimates (Table 2.1) based on the method of *Mulargia et al.* [1987] that identifies changes in seismicity rate. The same range of completeness intervals is used for CAT1 and CAT2.

The other large sources of uncertainty are the earthquake magnitudes. The magnitude reported by *Papazachos et al.* [2000] is an equivalent moment magnitude, calculated by relations that transfer magnitudes of locally used scales to moment magnitudes M_w [*Papazachos et al.*, 1997]. *Papazachos et al.* [2002] showed that these equivalent magnitudes are practically equal to M_w, with an overall standard error $\sigma = 0.23$. The catalogues of *Ambraseys and Jackson* [2000] and *Ambraseys* [2001a] use M_s, which is similar to M_w in the range $5.0 \leq M_s \leq 7.5$ [*Hanks and Kanamori*, 1979]. The GSHAP catalogue lists M_w. In their study of the Aegean region, *Koravos et al.* [2003] used only the catalogue of *Papazachos et al.* [2000]. They revised the magnitudes of all events before 1904 down by 0.4. This revision is based on the probable magnitude overestimate of two large events for which alternate data are available [*Abe and Noguchi*, 1983; *Ambraseys*, 2001b]. Rather than applying a systematic shift, we prefer to use two catalogue alternatives, where it should be noted that many of the magnitudes of *Ambraseys and Jackson* [2000] and *Ambraseys* [2001a] (including those of the two afore mentioned events) are lower than those in CAT2. In addition, we assign the following magnitude errors [*Papazachos et al.*, 2000]: ±0.25 for the instrumental period (1911-2000), ±0.35

date	M_w range	500 yr catalogue CAT1	2550 yr catalogue CAT2
for area west of 30° E:			
$\geq$ **-550** / *0 - 1499*	$\geq$ 8.0		3
$\geq$ **1500** / *1600 - 1844*	$\geq$ 7.3	1,2,3	3
$\geq$ **1845** / *1750 - 1899*	$\geq$ 6.5	1,2,3	3
$\geq$ **1900** / *1845 - 1910*	$\geq$ 6.0	1	3
$\geq$ **1911** / *1900 - 1949*	$\geq$ 5.5	3	3
$\geq$ **1950** / *1911 - 1969*	$\geq$ 5.0	3	3
$\geq$ **1970**	$\geq$ 4.5	3	3
for area east of 30° E:			
$\geq$ **1500** / *1800 - 1844*	$\geq$ 7.3	1,4	1,4
$\geq$ **1845** / *1900 - 1899*	$\geq$ 6.5	1,4	1,4
$\geq$ **1900** / *1925 - 1924*	$\geq$ 6.0	1.4	1.4
$\geq$ **1925** / *1950 - 1972*	$\geq$ 5.5	4,5	4,5
$\geq$ **1973** / *1980 - 1999*	$\geq$ 4.5	5	5

Table 2.1: The two combined historical seismic catalogues and the corresponding completeness length used in this study. In bold: completeness intervals, in italics: alternate completeness intervals. Sources: 1 = *Ambraseys* [2001a], 2 = *Ambraseys and Jackson* [2000], 3 = *Papazachos et al.* [2000], 4 = GSHAP-Turkey, 5 = NEIC-PDE. The sources are listed in order of priority.

for the historical period (1500-1911) and ± 0.5 for data prior to 1500. Errors in magnitude due to the approximation $M_s = M_w$ are included in these errors. Magnitude and completeness uncertainties are propagated through our analyses.

2.5.2 Geodetic data

The GPS measurements of crustal motions we use are from *McClusky et al.* [2000], *Cocard et al.* [1999], and *Kotzev et al.* [2001]. *McClusky et al.* [2000] compiled geodetic velocities for the period 1988-1997 at sites extending from the Caucasus mountains to the Adriatic Sea and from the southern edge of the Eurasian plate to the northern edge of the African plate. *Cocard et al.* [1999] carried out repeated GPS measurements in the period from 1993 to 1998 across the entire West Hellenic Arc. *Kotzev et al.* [2001] measured a regional GPS network in Bulgaria over the period 1996 to 1998. Fig. 2.3 shows the GPS velocities relative to Eurasia. For the motion of the rigid African Plate, we used the recent AFR-EUR rotation pole at -10.88° N, -16.16° E with a rate of 0.066°/m.y. [*Fernandes et al.*, 2003]. This pole results in a NNW velocity for northeastern Africa

and is based on a combination of geodetic observations. The velocities are significantly less than in NUVEL-1A. The necessity of lower AFR-EUR convergence velocities has been previously noted [*Westaway*, 1990; *Sella et al.*, 2002; *Kreemer et al.*, 2003].

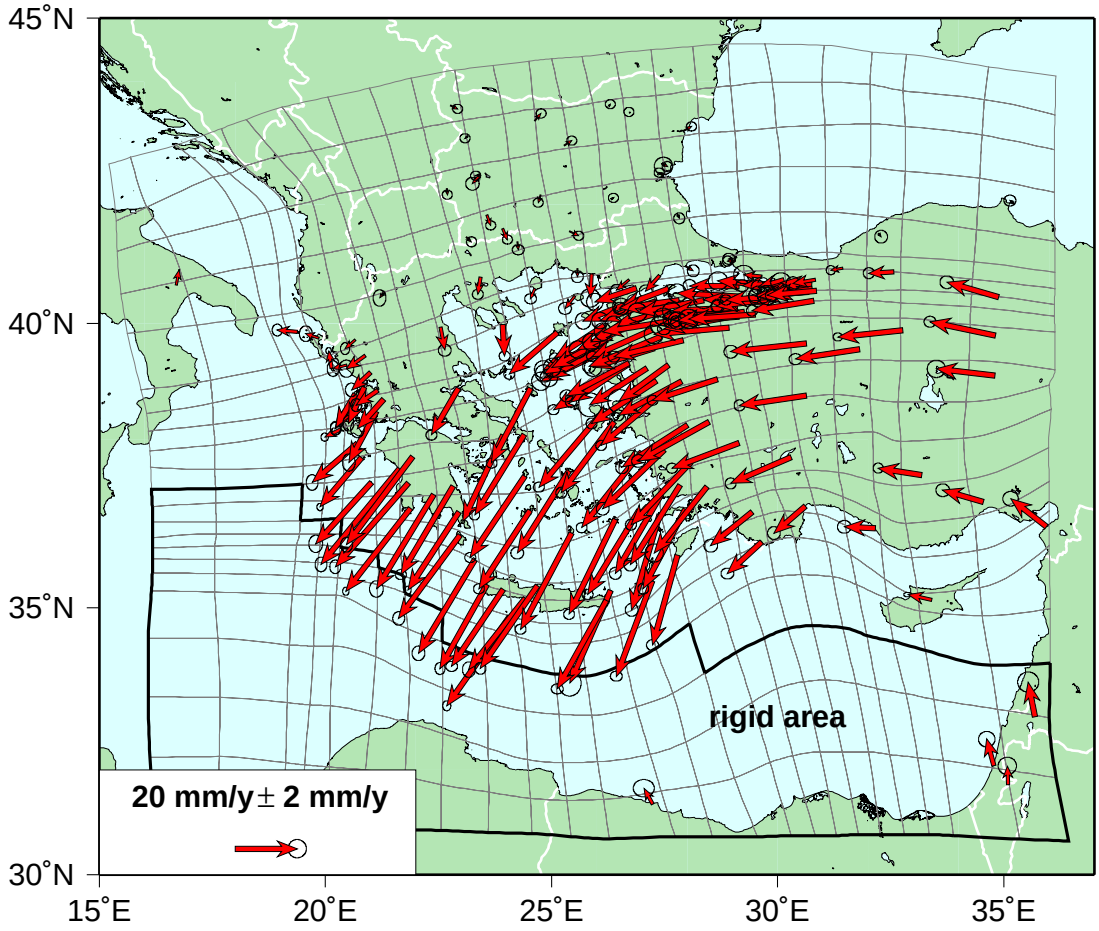

Figure 2.3: GPS velocities relative to Eurasia used in the inversion. Data are from 1) *Kotzev et al.* [2001] for the period 1996-1998 in Bulgaria, 2) *McClusky et al.* [2000] for the period 1988-1997 at sites within Greece and eastern Turkey and 3) *Cocard et al.* [1999] for the period 1993-1998 across the west Hellenic arc. The black line delimits the rigid African plate which is moving according to the rotation pole of *Fernandes et al.* [2003].

2.6 Strain rate style

2.6.1 Seismic

Although focal mechanisms from a few decades might not be expected to yield a reliable estimate of long-term seismic strain styles, *Amelung and King* [1997] found a very good agreement between seismic strain patterns inferred from earthquakes over several units

of magnitude and regional tectonic strain patterns for the strike-slip regime of the San Andreas Fault in California. The results of *Kreemer et al.* [2000] for various tectonic regimes in Indonesia also showed gross agreement in deformation patterns over several units of magnitude, but differences in detail. Our study region also contains tectonic regimes other than strike-slip faulting. Therefore, we test the similarity of strain rate patterns of the seismic data over different magnitude ranges and compare these patterns with those of, presumably long-term tectonic, strain inferred from the GPS data.

The strain rates are determined by summing the moment tensors plotted in Fig. 2.2 within each cell of the curvilinear grid. The obtained moment tensors are smoothed over one neighboring cell to obtain a strain rate field for most of the grid, that is, also where no focal mechanisms are available. Fig. 2.4(a) shows the direction only of the principal strain rate axes inferred by summing events up to $M_w = 5.9$ and up to $M_w = 6.5$ from the CMT catalogue. Similarly, Fig. 2.4(b) shows the direction of the principal strain rates axis inferred by summing events up to $M_w = 6.5$ and larger events of the CMT catalogue and from the catalogue of *Jackson et al.* [1992] which contains events up to $M_w = 7.6$. A similar style of deformation is observed for earthquakes in all magnitude ranges, for most of the study area. Note that differences between the principal axes of less than about 20 ° are within the uncertainties in the CMT solutions. Uncertainties in the older mechanisms are likely to be somewhat larger. Most of the small differences are due to smoothing into areas with poor data coverage (for example, eastern Hellenic arc and southwestern Turkey, around Crete, the southern part of the Peleponesos, compare with Fig. 2.2). Given the overall consistency of the strain fields from larger and smaller events and because of the better quality and uniformity of the CMT catalog, we use the events with $M_w \leq 6.5$ to define our best estimate of the style (not the magnitude) of the seismic strain rate field.

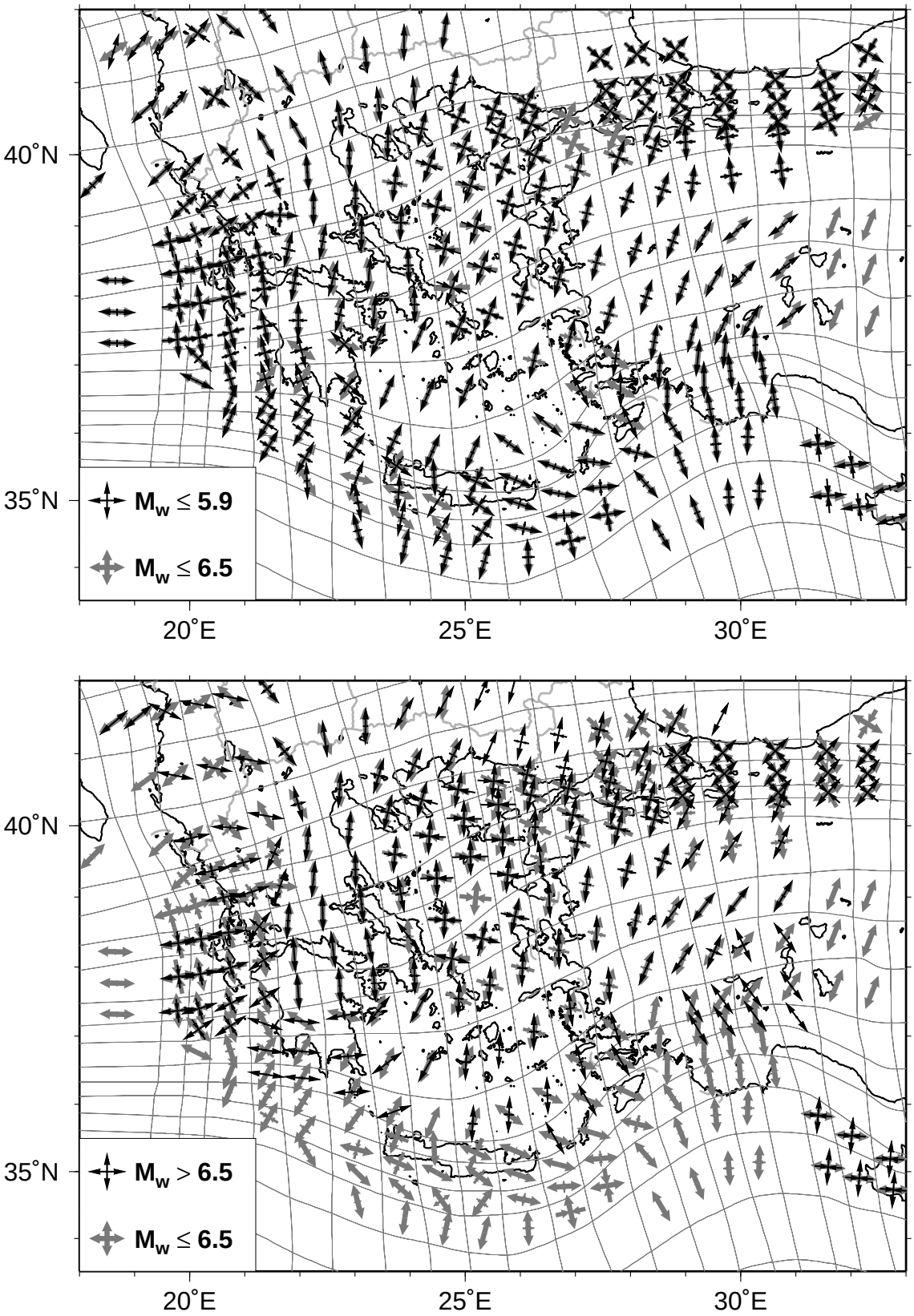

Figure 2.4: Style of the seismic strain rate field. (a) Direction of the principal strain rate axes of the unit moment tensors inferred by summing events up to $M_w = 5.9$ (in black) and up to $M_w = 6.5$ (in gray) of the CMT Catalogue. (b) Direction of the principal strain rate axes of the unit moment tensors inferred by summing events up to $M_w = 6.5$ of the CMT catalogue (in gray) and larger events of the CMT and *Jackson et al.* [1992] (in black). The direction of the principal strain rate axes is consistent over a large range of magnitudes.

2.6.2 Geodetic

Using the method of *Haines and Holt* [1993], the geodetic velocities (Fig. 2.3) are inverted for a horizontal strain rate field. The principal axes of the geodetic strain are very similar in direction to the pattern of seismic strain (Fig. 2.5). Again, some differences are due to (different) smoothing of the seismic and/or geodetic strain rate field into areas of low data coverage (for example, Central Turkey and Central Greece for the GPS data). Note that, along the eastern part of the Hellenic arc, the compressional part of the geodetic strain rates perpendicular to the arc is almost absent in the seismic strain rates. In areas where seismic and geodetic strain rate fields reflect the same style of deformation, these data can be combined to constrain earthquakes recurrence rates (Section 2.8).

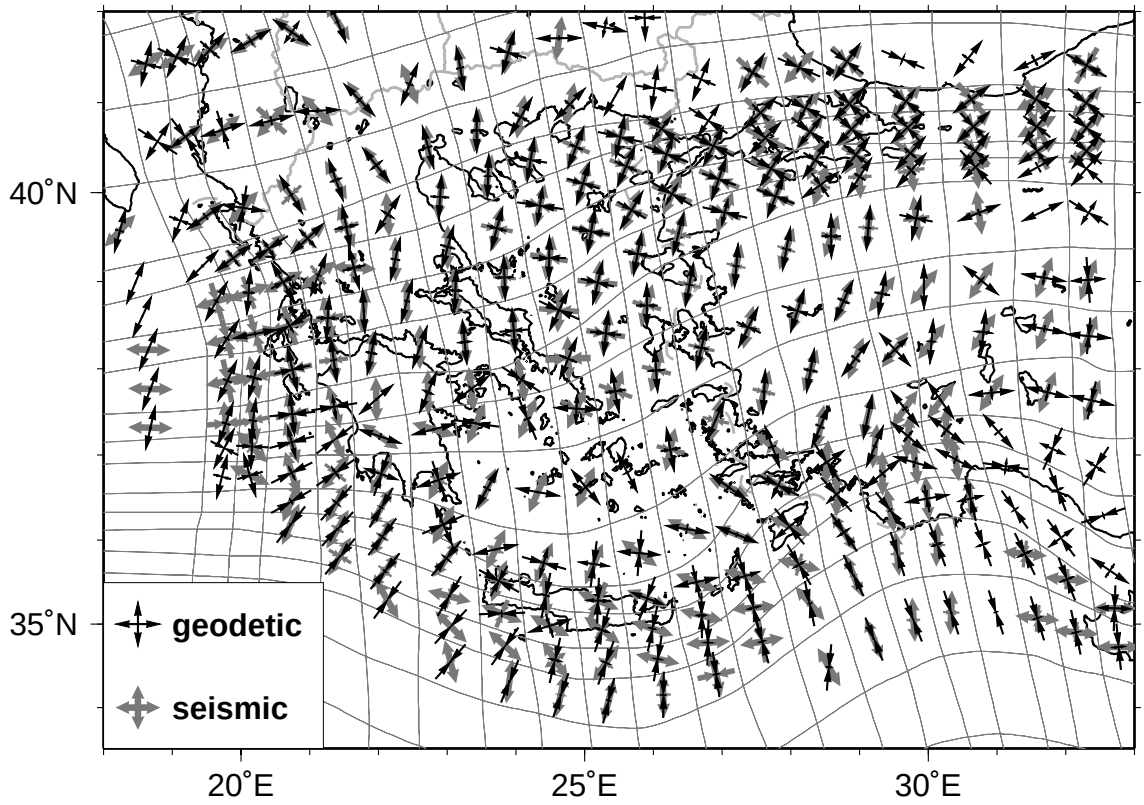

Figure 2.5: Comparison of the direction of the principal strain rate axes of the unit moment tensors inferred by summing events of the CMT catalogue up to $M_w = 6.5$ (in gray) and obtained by the inversion of GPS data in Fig. 2.3 (in black).

2.7 Strain rate magnitude

2.7.1 Seismic from the catalogues

The moments of the events in our seismic catalogue CAT1 are summed within each grid cell, and converted into rates by dividing over the appropriate completeness interval for each magnitude range (Table 2.1: in bold). Only events with $M_w \geq 4.5$ are taken into account. If, as with most geodetic data sets, the vertical strain rate is unknown, the moment rate associated with a best-fitting double couple can not be defined unambiguously. If also the predominant faulting style in the region is not known, *Savage and Simpson* [1997] propose to estimate scalar moment rates from horizontal strain rates as follows:

$$\dot{M}_0 = 2\mu V Max(\mid \dot{\epsilon}_1 \mid, \mid \dot{\epsilon}_2 \mid, \mid \dot{\epsilon}_1 + \dot{\epsilon}_2 \mid) \tag{2.3}$$

where μ is the shear modulus, V is the volume of the seismogenic zone and $\dot{\epsilon}_1$ and $\dot{\epsilon}_2$ are the principal horizontal strain rate axes.

Although the seismic moment tensors do provide faulting style in most of the study area, moment rates are converted into horizontal strain rates using Equation 2.3 for consistency with the treatment of the geodetic strain rates. Fig. 2.6 shows the principal horizontal axes of the total seismic strain rate tensor obtained by combining the historic seismic moment rates of CAT1 with the styles from the $M_w \leq 6.5$ events of the CMT catalogue (Fig. 2.4). Note that only the strain rate styles are smoothed over one neighboring grid cell; the moment rate magnitudes are unsmoothed.

The largest strain rates are found 1) along the NAFZ east of the Marmara Sea 2) in the NAT, along the continuation of the NAFZ 3) within the eastern part of the Gulf of Corinth and just NE of it 4) along the Kephalonian fault and 5) along the Hellenic arc especially along the eastern part. Although the strain rate field is dominated by larger events ($M_w \geq 7.0$), high strain rates also correlate with high seismicity rates, and smaller events in the range $M_w = 4.5 - 6.5$ contributed up to 60 % of the total seismic moment rate in certain areas. Note that data in southwestern Turkey are sparse and the quality of the seismicity data here is poorer than in the rest of our study area.

The uncertainty in moment rates due to uncertainties in magnitude, location and completeness of the catalogues are estimated by comparing our two catalogues, CAT1 and CAT2, along the NAFZ where the data in the catalogues differ the most. This

yields a variation of up to a factor of 2 in moment rates. Similar uncertainties probably exist in other regions as well and a factor of 2 uncertainty is assigned to the whole study area. The seismic moment rates are scaled to strain rates with a constant seismogenic thickness of 15 km, which is a reasonable estimate of the depth range over which the bulk of the seismic strain is accommodated in continental areas. Different values of μ $\times$ seismogenic thickness lead to a change of up to 30-40 % in the moment rates, that is, much less than the effect of catalogue uncertainties. At the trench, the effective seismogenic thickness may be twice as large, which would reduce the estimated seismic strain rates by a factor of two.

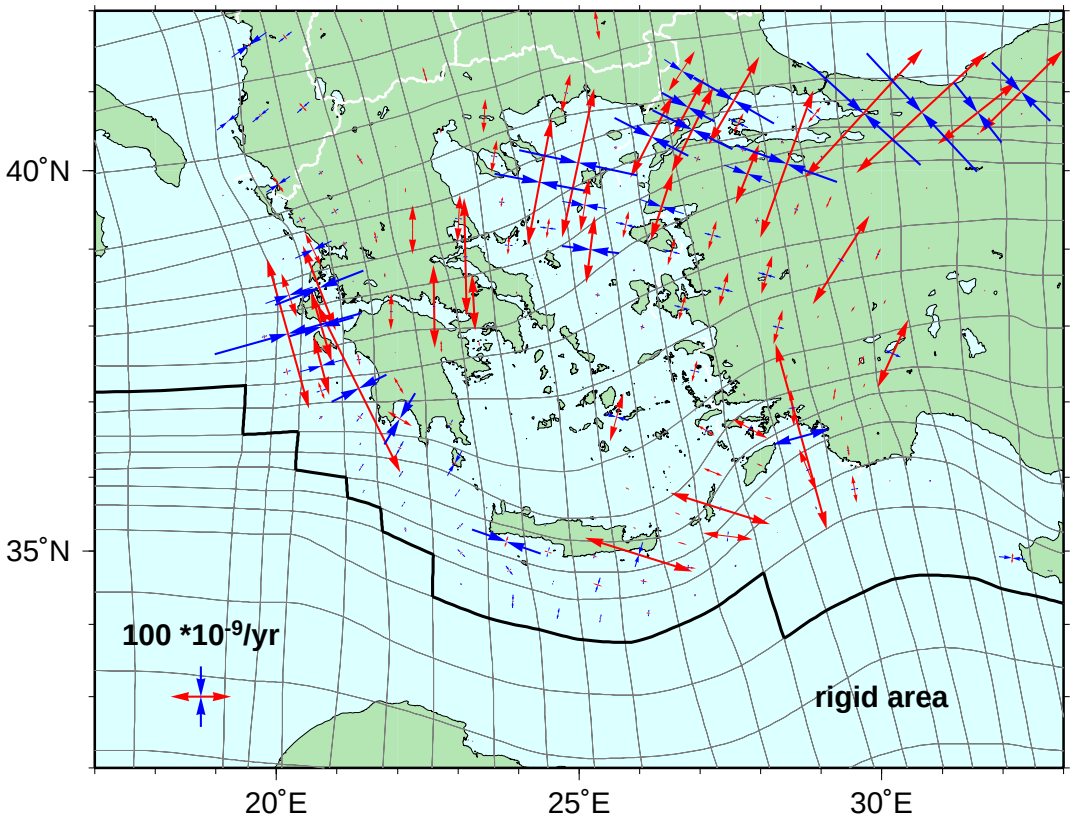

Figure 2.6: Principal horizontal axes of the total seismic strain rate tensor obtained by combining the seismic moment rates of the 500 yr catalogue (CAT1) with the styles inferred from the $M_w \leq 6.5$ events of the CMT catalogue.

2.7.2 Tectonic from GPS data

The principal horizontal axes of the total geodetic strain rate field are shown in Fig. 2.7 on the same scale as the seismic strain rates in Fig. 2.6. The strain rate field is con-

sistent with the fields obtained with similar data but different methods [*Kahle et al.*, 2000; *Nyst*, 2001]. The geodetic deformation field (Fig. 2.7) is dominated by one broad band of right-lateral strike-slip deformation along the NAFZ and its prolongation in the Aegean, extension around the Gulf of Corinth, and strike-slip in the area of the Kephalonian fault. These regions coincide with the regions of the highest seismic strain rates (Fig. 2.6). In addition, a strong component of compression is found in the geodetic strain rates along most of the Hellenic arc which is absent in the seismic strain rates. The concentration of strain along the arc is dictated by the constraint of a rigid African plate, just south of the trench. We defined the extent of the rigid African plate based on the seismicity. Although some deformation and seismicity occurs south of the trench in the Mediterranean Ridge accretionary complex [*Kreemer and Chamot-Rooke*, 2004], most seismicity is located near the trench and we assume that, for the 15 km depth interval considered, the trench accommodates the around 4 cm/yr Aegean-African convergence.

The geodetic strain rate field is much smoother than the seismic strain rate field. In part this is the result of smoothing induced by the bicubic spline approximation in the inversion of geodetic data, where the seismic strain rates were smoothed only in style. But largely it reflects the differing characters of long-term tectonic and short-term seismic strain rates. The geodetic data measure both distributed (short-term) elastic loading and concentrated permanent deformation (seismic as well as aseismic) which, when averaged over length scales exceeding those of elastic loading, add up to long-term tectonic rates. By contrast, whereas the seismicity reflects permanent, seismic, strain only, measured over the duration of a catalogue that is generally less than several earthquake recurrence cycles. A useful comparison of geodetic (that is, tectonic) strain rates and seismic catalogue strain rates can only be made on scales that exceed the intrinsic (elastic) and applied smoothing of the geodetic deformation field. Such a comparison is made in the next section.

2.8 Estimating earthquake recurrence parameters

The seismic and geodetic strain rates together with seismic magnitude-frequency data are used to define, for a set of source zones, the three parameters a, b, and m_{max} of the truncated Gutenberg-Richter distribution commonly used in hazard analyses. The

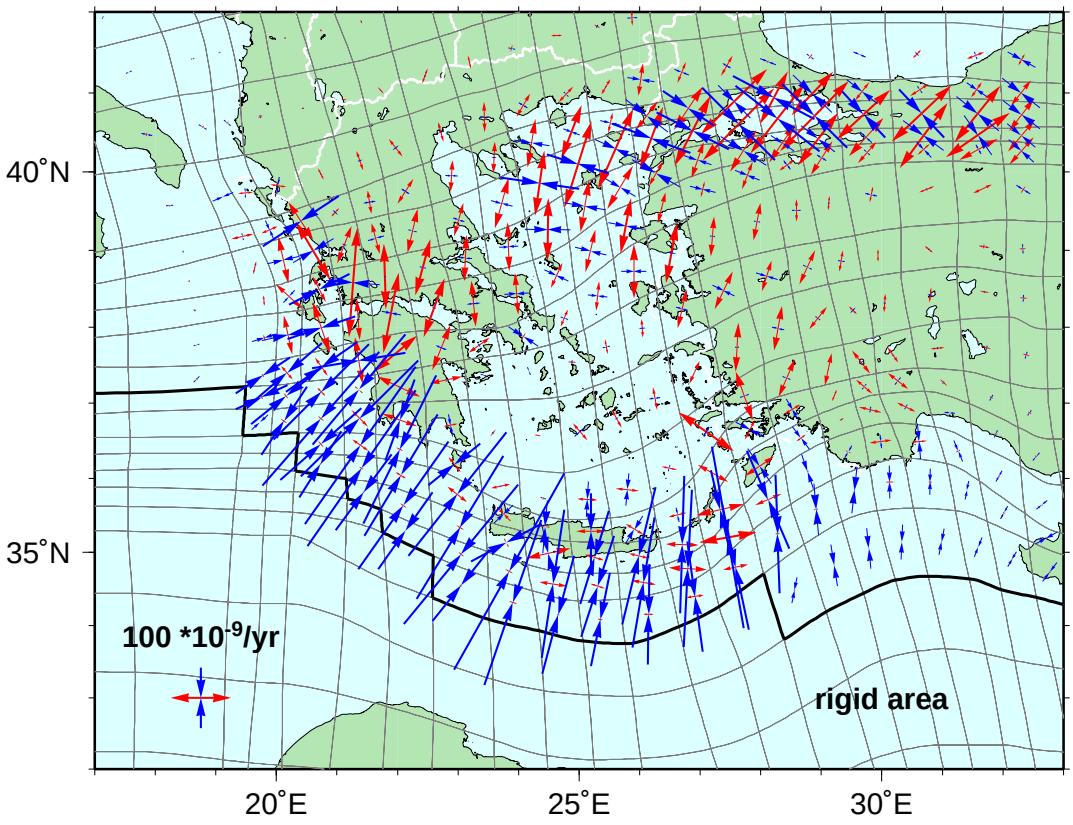

Figure 2.7: Principal horizontal axes of the total geodetic strain rate field obtained with the method of *Haines and Holt* [1993] from fitting the GPS velocities plotted in Fig. 2.3.

a-value is the recurrence rate of small events, the b-value describes the decrease in recurrence frequency with increasing magnitude, and m_{max} is the largest magnitude event expected. Although other distributions may better describe magnitude-frequency data in detail [*Kagan*, 2002a; *Koravos et al.*, 2003], the simpler truncated Gutenberg-Richter (TGR) can often not be rejected by the available data.

We use the data to define a plausible range of a, b, and m_{max} combinations. Such combinations should satisfy the following constraints. 1) The a- and b-values should be compatible with the magnitude-frequency data. 2) m_{max} should not greatly exceed m_{max}^{cat}, the maximum observed event size. The length of the catalog, T_{cat}, relative to the recurrence interval of m_{max} events (T_{rec}^{max}) determines how large a difference between m_{max} and m_{max}^{cat} is plausible. The larger T_{cat}/T_{rec}^{max}, the closer m_{max} and m_{max}^{cat} should be. 3) The combination of a, b, and m_{max} should result in a total, long-term, seismic moment rate, $\dot{M}_0^{seis}$, that is less then or equal to the tectonic moment rate, $\dot{M}_0^{tec}$, determined

geodetically. If $\dot{M}_0^{seis}$ is less than $\dot{M}_0^{tec}$, it indicates that part of the deformation is aseismic, which can be expressed in a percentage of aseismic deformation, as a smaller width of the seismogenic zone, or as a coupling factor less than 1. 4) $\dot{M}_0^{cat}/\dot{M}_0^{seis}$ has to be reasonable for the catalog length relative to T_{rec}^{max}. If T_{cat} is large, the average catalogue moment rate, $\dot{M}_0^{cat}$ should be close to the long-term average $\dot{M}_0^{seis}$. If however, the catalogue is relatively short, $\dot{M}_0^{cat}$ can be much smaller, or even larger than $\dot{M}_0^{seis}$, depending on whether the catalogue happens to include or miss some of the largest events. Table 2.2 summarizes the used terminology for the different maximum magnitude and moment rate estimates.

	seis	*cat*	*tec*
$\dot{M}_0$	Estimated long-term seismic moment rate	Moment rate obtained from catalogue	Geodetically estimated $\dot{M}_0$
m_{max}	Estimated long-term max. magnitude	Largest event size in the catalogue	Max. magnitude required to give $\dot{M}_0^{seis} = \dot{M}_0^{tec}$

a_1, b_1, m_{max}^1:	$b_1 = 1$, $m_{max}^1 = m_{max}^{cat}$	$\Rightarrow a_1$ = max. estimate of a
a_2, b_2, m_{max}^2:	a_2: max. likelihood for $m_w = 4.5 - 6$, $b_2 = 1$	$\Rightarrow m_{max}^2$
a_3, b_3, m_{max}^3:	a_3 and b_3: max. likelihood for $M_w = 4.5 - m_{max}^{cat}$	$\Rightarrow m_{max}^3$

Table 2.2: Terminology

2.8.1 Source zones

To determine the earthquake recurrence parameters, the study region is divided into ten areas (Fig. 2.8), where each area is characterized by a uniform style of deformation. The Northern Anatolian Fault Zone was separated into an eastern section (up to 33 °E), where the strike-slip fault is well-defined (zone 4) and a Marmara Sea section (zone 3), which may contain several splays and accommodates some extension. The diffuse continuation of the NAFZ in the northern Aegean is contained in zone 2. All extension in central Greece and western Anatolia is grouped in zones 6 and 7, respectively. Zone 5

encompasses the Kephalonian strike-slip fault. The active Hellenic trench is divided into a central section (zone 9), where geodetically measured compression is mainly trench-perpendicular, and an eastern section (zone10), where motion is oblique. These two zones may incorporate a small amount of arc-internal deformation, but were drawn to span the dipping interface and allow for larger off-shore earthquake location errors. Zones 1 and 8 contain the low straining region in northwestern Greece and the southern Aegean, respectively. Hazard studies usually define earthquake recurrence parameters within finer source zones. For example, superimposed on Fig. 2.8 are the source zones of the SESAME seismic hazard project (http://seismo.ethz.ch/gshap/sesame/). However, the density of geodetic and seismic data and location errors of the historical earthquakes do not allow a smaller scale study. Furthermore, the size of each zone is defined such that the number of events included is large enough to determine statistically significant a- and b-values. Nevertheless, our coarser grid study provides constraints which earthquake recurrence rates for smaller source zones should satisfy.

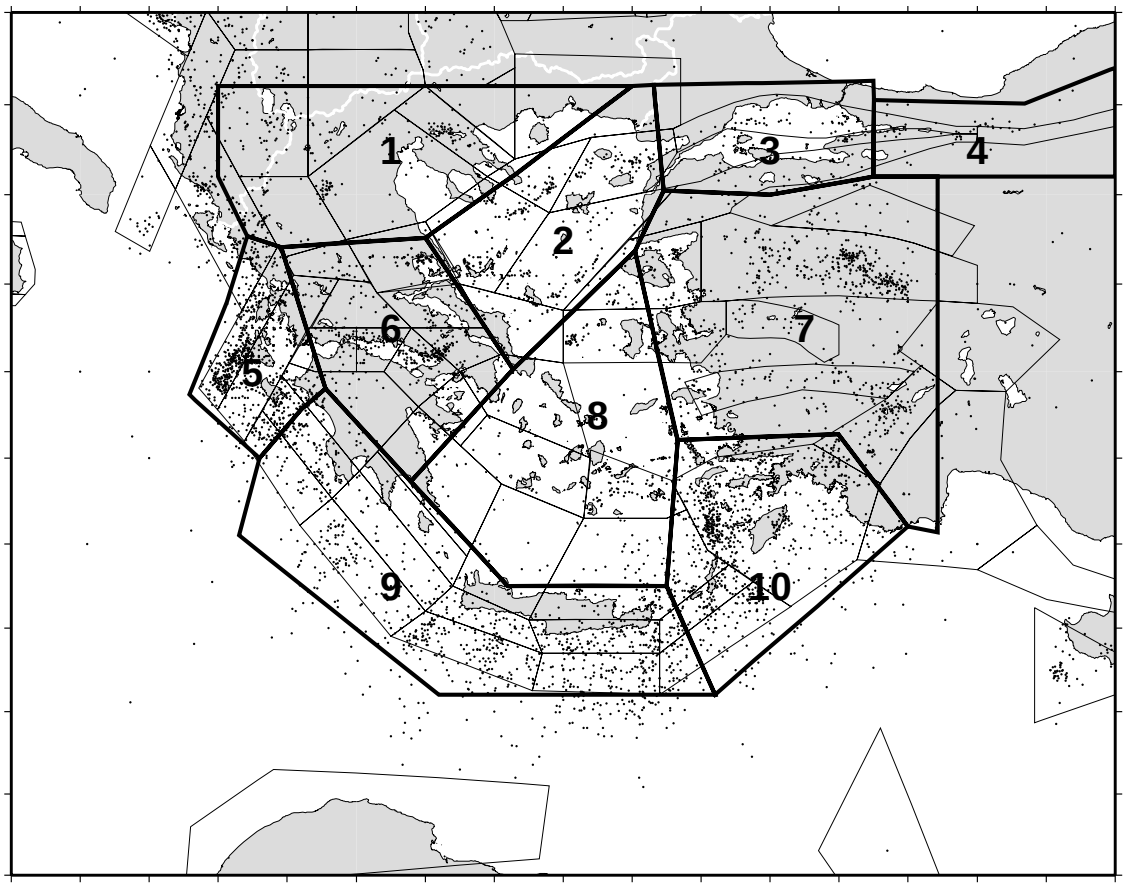

Figure 2.8: The ten tectonic areas used to define the earthquake recurrence parameters. Superimposed are the SESAME sources and seismicity (dots) of the historical catalogue CAT1 (Table 2.1).

2.8.2 Magnitude-frequency data

Fig. 2.9 shows the cumulative magnitude-frequency distribution of the two catalogues discussed in Section 2.5.1. The two data sets show a similar trend. A systematic increase of the cumulative number of earthquakes occurs around $M_w = 6$. Systematic errors in magnitude assignment, in completeness length estimate, missing events with $M_w = 5 - 6$, or a real increase of the rate of recurrence can explain this change in the distribution with magnitude. Although an increase in recurrence rate may occur in some regions, especially along single faults, it is quite unlikely to occur within all areas and we suspect a systematic catalogue inadequacy to be the cause. In Fig. 2.9, the gray area delimits the range of magnitude-frequency distributions obtained when random uncertainties in magnitude and completeness length are taken into account. To define this range, magnitudes and completeness intervals are randomly chosen within the uncertainty bounds given in Section 2.5.1 and in Table. 2.1 yielding 1000 alternate versions of both CAT1 and CAT2. For most of the regions, the uncertainties do not allow to distinguish a characteristic distribution. Note that the uncertainty ranges in Fig. 2.9 do not account for possible systematic errors in the catalogs. *Koravos et al.* [2003] did prefer a characteristic distribution for many of their source regions, but it should be noted that the -0.4 magnitude correction they applied tends to enhance characteristic behaviour. Although our data do not unambiguously define a linear trend, we feel they provide insufficient constraints to fit a more complex distribution than the three-parameter truncated Gutenberg-Richter distribution.

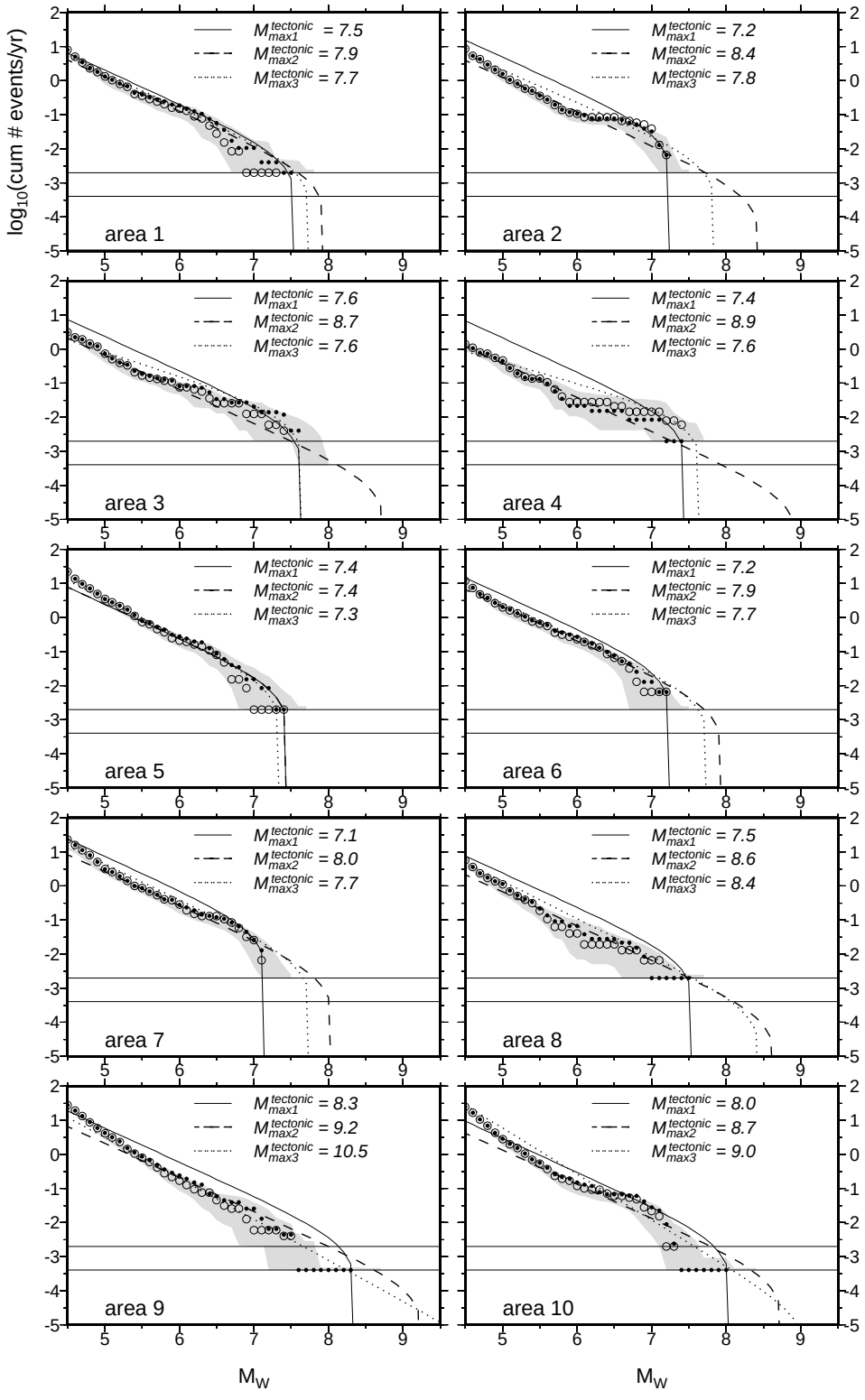

Figure 2.9: The log_{10} of the cumulative number of events versus magnitude for the historical seismic catalogues CAT1 (plain circles) and CAT2 (filled circles) (Table 2.1) in each of the areas shown in Fig. 2.8. The curves represent truncated Gutenberg-Richter approximations to the magnitude-frequency data. The various curves provide an estimate of the range of m_{max}^{tec} necessary if all tectonic deformation ($\dot{M}_0^{tec}$) is accommodated seismically. The different curves are discussed in the text and the parameters are listed in Table 2.3. Solid lines: a_1, $b_1 = 1$, m_{max}^1, dashed lines: a_2, $b_2 = 1$, m_{max}^2, dotted lines: a_3, b_3, m_{max}^3. The two horizontal lines mark the recurrence time equal to the length of the two historical seismic catalogues. The gray area illustrates the uncertainties in the magnitude-frequency data due to non-systematic uncertainties in magnitude and completeness.

2.8.3 a, b values and m_{max}

As a first step, we determine several end-member a, b, and m_{max} fits to the magnitude-frequency data. Subsequently, we test how catalogue length affects the possible range of $\dot{M}_0^{cat}$/ $\dot{M}_0^{seis}$. The combinations of a, b, and m_{max} determined here (Table 2.3), all assume that $\dot{M}_0^{seis} = \dot{M}_0^{tec}$, that is, they provide an upper bound estimate, m_{max}^{tec}, for m_{max}. The tectonic moment rate $\dot{M}_0^{tec}$ is determined from the geodetic strain rates in Section 2.7.1, using Equation 2.3. Assuming homogeneous $\dot{M}_0$ in each small grid cell, $\dot{M}_0^{tec}$ in the 10 larger areas are determined by summing the geodetic moment rates of all grid cells contained in them. If only part of a grid cell overlaps with a seismogenic source zone, the geodetic moment rates are included in proportion to the area intersected.

area	$\times 100$ km^2	$\dot{M}_0^{tec}$	a_1	a_2	a_3	b_3	m_{max}^{seis}	T (in yr)
1	714.66	2.88e+18	1.3	1.1	1.2	1.0	7.5-7.7	400-1500
2	522.53	4.95e+18	1.7	1.1	1.2	0.9	7.2-7.7	100-500
3	343.63	3.70e+18	1.3	0.8	0.6	0.7	7.6-7.8	550-1000
4	293.48	2.70e+18	1.3	0.6	0.4	0.6	7.4-7.8	200-1000
5	271.01	3.09e+18	1.4	1.4	1.6	1.1	7.4-7.5	450-500
6	532.57	4.64e+18	1.6	1.3	1.4	1.0	7.2-7.7	100-950
7	1224.46	6.63e+18	1.8	1.4	1.7	1.0	7.2-7.7	100-700
8	904.87	3.39e+18	1.4	0.8	1.2	1.1	7.5-7.8	450-1050
9	1103.10	2.09e+19	1.7	1.3	1.7	1.2	7.5-8.0	350-2500
10	674.25	7.46e+18	1.4	1.1	2.1	1.3	7.5-8.0	400-2500

Table 2.3: $\dot{M}_0^{tec}$ = geodetic (long-term tectonic) moment rate in Nm/yr, a_1 and a_2 resp. a_3 and b_3 are the earthquake recurrence parameters obtained in Section 2.8.3. b_1 and b_2 are equal to 1 in all areas. $a = log_{10}$ of the cumulative number of events with $M_w \geq 4$, b = slope of the Gutenberg-Richter relationship, m_{max}^{seis} = best estimate of m_{max}, T = recurrence time of m_{max}^{seis}.

Some studies [for example, *Kanamori and Anderson*, 1975; *Wesnousky*, 1999; *Godano and Pingue*, 2000; *Kagan*, 2002a, b] have argued for a universal b value of 1. For cases 1 and 2, we fix b to 1. a_1 is a maximum a-value obtained by setting m_{max} equal to the minimum possible value m_{max}^{cat}. a_2 is a minimum value, estimated from a maximum likelihood fit [*Aki*, 1965] to the distribution for events with $M_w = 5-6$, which represents the lower part of the data trend. Note that uncertainties in magnitude are taken into account to estimate the maximum likelihood fit. It is clear from Fig. 2.9 that $b = 1$ is

not always an appropriate value to characterize the frequency-magnitude relationship. For case 3, we find both a_3 and b_3 by a maximum likelihood fit to CAT1. We find that b_3-values less than 1 provide a better approximation to the data of the northeastern part of our study region, and b_3 values larger than 1 better approximate the data along the Kephalonian fault and the trench. This is consistent with results from *Papaioannou and Papazachos* [2000], who determined a, b and m_{max} for smaller Greek source zones. They found b-values systematically increasing from 0.8 in northern Greece to 0.9 in central and southern Greece and southwestern Anatolia, to 1.0 along the Kephalonian fault and Hellenic Trench. The b_3-values we find in our larger study region range from 0.6 to 1.3.

With the exception of areas 1 and 5, the a_1-curves imply that the historical catalogues underestimate the recurrence rates of all events with $M_w < 6.5 - 7$. By contrast, the a_2-curve implies, for most areas, that the catalogues overestimate the recurrence of events $M_w = 6.5 - 7.5$, and that significantly larger events than have been observed can occur. The a_3,b_3- curves represent the data quite well for the NAFZ areas 3 and 4 with a b-value of 0.7 and 0.6, respectively, and for the Kephalonian Fault (area 5), with a b-value of 1.1. Thus, for these three zones, a reasonable combination of a, b, and m_{max} with $\dot{M}_0^{seis} = \dot{M}_0^{tec}$ can be found, implying that all deformation is accommodated seismically. A slightly more characteristic distribution for the NAFZ would still give $\dot{M}_0^{seis} = \dot{M}_0^{tec}$ for a m_{max}^{seis} that does not deviate much from m_{max}^{cat}. However, the shape of the seismicity distribution in zone 4 may be affected by the poorer data quality east of 30 °E. For areas 1, 2, 6 and 7, m_{max}^3 exceeds m_{max}^{cat} by only about 0.5 and we can not reject the possibility that $\dot{M}_0^{seis} = \dot{M}_0^{tec}$. In zones 2 and 7, the recurrence times of the missing $M > 7$ events are small enough compared to T_{cat} that a few more events should have been recorded. However, in these two zones, the catalogues may be incomplete. In areas 9 and 10, but also in area 8, $m_{max}^{2,3}$ are much larger than m_{max}^{cat}, and larger than we think plausible. In areas 9 and 10, not only the largest events, but also other events with $M \geq 7.5$ expected from the curves, are absent in the catalogues. This could indicate that a significant part of the motion along the trench occurs aseismically.

2.8.4 Effect of catalogue length

To assess how much $\dot{M}_0^{cat}$ might differ from the long-term rate $\dot{M}_0^{seis}$ (and thereby also m_{max}^{cat} from m_{max}^{seis}), for our catalogue length, we perform a statistical test. As before,

we do this for the case that $\dot{M}_0^{seis}$=$\dot{M}_0^{tec}$. Since m_{max}^{tec} and its recurrence time are upper estimates, the tests will give the maximum possible range for observed/long-term values.

For a catalogue length T_{cat} = 100, 500 and 2550 years, 5000 synthetic catalogues each were made from a magnitude-frequency distribution described by a_3, b_3 and m_{max}^3. Events at all magnitudes are assumed to have a Poissonian distribution in time. The synthetic $\dot{M}_0^{cat}$ define a probability density distribution of the ratio $[\dot{M}_0^{cat}/\dot{M}_0^{seis}]$ for a given T_{cat}. Fig. 2.10 compares the modeled ratios $[\dot{M}_0^{cat}/\dot{M}_0^{seis}]_{mod}$ with the observed ratios $[\dot{M}_0^{cat}/\dot{M}_0^{tec}]_{obs}$. Error ranges for the observed ratios include the factor 2 uncertainty that was estimated by comparing our two catalogues, CAT1 and CAT2, along the NAFZ and within the Marmara Sea where the data in the catalogues differs the most. The much smaller uncertainties in $\dot{M}_0^{tec}$ are ignored.

In all areas except in areas 8, 9 and 10, the statistical test yields a normal probability distribution of $[\dot{M}_0^{cat}/\dot{M}_0^{seis}]_{mod}$ with a mean value equal to 1 and a small standard deviation (sd) up to 0.08-0.18 (for T_{cat} = 100 years). In area 8, the large m_{max}^3=8.4, which has a recurrence time of about 10'000 years, yields most likely ratios of $[\dot{M}_0^{cat}/\dot{M}_0^{seis}]$ below 1, with a value of 0.6 and 0.9 for a catalogue length of 100 and 500 year, respectively. However, even here, the chance of observing ratios larger than 1 is $\geq$ 40 %. In areas 9 and 10, where m_{max}^3 (=10.4 and 9, respectively) are larger than we think reasonable, the mean values range between 0.3 and 0.9. But still, for T_{cat} = 100 years, there is a probability to observe ratios larger than 1 of 15 % in zone 9 and 28 % in zone 10. Thus, except in areas 9 and 10, the a_3, b_3 seismicity distributions should, even for a 100-year catalogue, reflect the long-term seismic deformation, and there is an equal likelihood that $\dot{M}_0^{cat}$ exceeds or underestimates $\dot{M}_0^{seis}$. Even for the a_3, b_3, m_{max}^3 parameters for areas 9 and 10, the probability that a catalogue of 500 years or longer reflects long-term seismic deformation is up to 39 %.

For the San Andreas fault in California, which has similarly high strain rates and maximum magnitudes as our study region and a catalogue that covers about 150 years, $\dot{M}_0^{cat}$ is comparable to the geodetic moment rate $\dot{M}_0^{tec}$ [*Ward*, 1998b], that is, geodetic strain is completely released seismically over the time span of the catalogue. By contrast, for the Eastern Mediterranean, we find that the short-term catalogue moment rates are always less than the long-term tectonic moment rates ($[\dot{M}_0^{cat}/\dot{M}_0^{tec}]_{obs}$ in Fig. 2.10), although the statistical tests show that in most areas the probability of

$\dot{M}_0^{cat}$ exceeding or lagging behind $\dot{M}_0^{seis}$ is equal. There are three possible explanations for the low $[\dot{M}_0^{cat}/\dot{M}_0^{tec}]_{obs}$: 1) the long-term seismic deformation is not equal to the long-term tectonic deformation, that is, a large part of the tectonic deformation is released aseismically, 2) the seismic historical catalogues systematically underestimate the moment rates, that is, the completeness length for one or several magnitude intervals is overestimated and/or 3) the moment rate over the catalogues happened to be low, that is lacking seismicity will be released in future. Explanation 3) is unlikely to apply to all regions at the same time. We hold a combination of 1) and 2) responsible for the low $[\dot{M}_0^{cat}/\dot{M}_0^{tec}]_{obs}$.

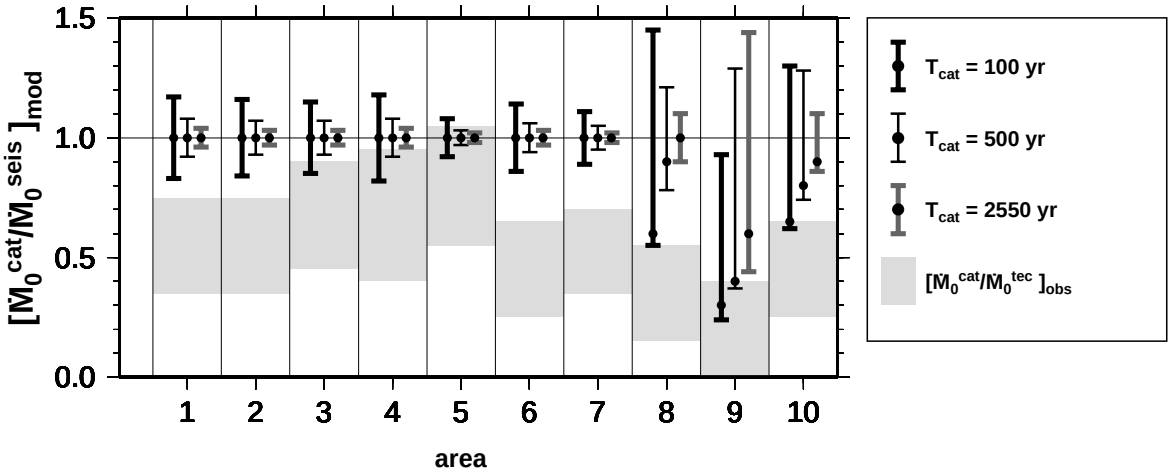

Figure 2.10: Distribution of ratios $[\dot{M}_0^{cat}/\dot{M}_0^{seis}]_{mod}$ obtained for a synthetic catalogues produced using a Poissonian recurrence distribution and a magnitude-frequency distribution characterized by a_3, b_3 and m_{max}^3, for a catalogue length of 100 yr (solid line), 500 yr (dotted line) and 2550 yr (gray line). Black dots represent the mean value. 2/3 of the modeled ratios lie within the error bars. Low $[\dot{M}_0^{cat}/\dot{M}_0^{seis}]_{mod}$ are for a and b implying that a significant part of the strain is released by large infrequent events with recurrence times that are often longer than 2550 years. In most areas, the observed ratios $[\dot{M}_0^{cat}/\dot{M}_0^{tec}]_{obs}$ (in gray) are less than the expected ratios $[\dot{M}_0^{cat}/\dot{M}_0^{seis}]_{mod}$.

2.8.5 Estimating long-term seismic deformation $\dot{M}_0^{seis}$

Based on the results of section 2.8.3 and 2.8.4, we identify 3 types of areas: 1) regions that have fully seismic deformation, 2) regions that have significant aseismic deformation and 3) regions where the data do not allow us to distinguish between fully seismic and

partially aseismic deformation. For a_3 and b_3 we define our best estimates of m_{max}^{seis} (Table 2.3). The corresponding long-term seismic moment rate $\dot{M}_0^{seis}$ is shown in Fig. 2.11.

The low seismic moment rates $\dot{M}_0^{cat}$, and high m_{max}^{tec} required are clear evidence for significant aseismic deformation (that is, shallow coupling widths) in the southern Aegean and along the Hellenic arc in areas 8, 9 and 10. In addition, the largest events in areas 9 and 10 are old and significantly exceed the size of any others recorded in these regions (Fig 2.9), leading us to think that even m_{max}^{cat} may be overestimated. For areas 8, 9, and 10 we consider an m_{max}^{seis} between about 7.5 and 8 most plausible. This yields $\dot{M}_0^{seis}/\dot{M}_0^{tec}$ = 40-50 %, <10 %, and 55-65 %, respectively. In area 10, convergence includes an oblique component. The extensional part of this motion is reflected in the focal mechanisms and seems to be responsible for the larger amount of seismic strain. Fully seismic deformation is likely within the Marmara Sea (area 3), along the NAFZ (area 4) and along the Kephalonian fault (area 5). In Fig. 2.10, at least one of the estimates of $[\dot{M}_0^{cat}/\dot{M}_0^{tec}]_{obs}$ is close to 1 and m_{max}^3 is similar to the observed m_{max}^{cat}. m_{max}^{seis} is estimated to be close to M_{max}^3: 7.6-7.8 in area 3, 7.4-7.8 in area 4 and 7.4-7.5 in area 5. The corresponding $\dot{M}_0^{seis}$ amounts to 85-100 % of $\dot{M}_0^{tec}$ in areas 3 and 4 and 95-100 % in area 5. In areas 1, 2, 6 and 7, the data allow a small component of aseismic deformation, especially in zone 2 and 6.

In summary, the strike-slip zones appear to be fully seismic. The trench region is affected by at least 45 % aseismic deformation. The other regions are characterized by 10-60 % aseismic deformation but uncertainties in the catalogues, in the strain rates and in the assignment of magnitudes do not allow us to be conclusive about this. For most regions, $\dot{M}_0^{tec}$ thus gives a reasonable first-order estimate of $\dot{M}_0^{seis}$, but a catalogue that provides tight constraints for a and b values is necessary for better estimates of the aseismic component of deformation.

2.9 Conclusions

In this paper, seismic and geodetic data are combined to estimate earthquake recurrence parameters as used in seismic hazard analyses. We obtain truncated Gutenberg-Richter distribution parameters, a value, b value and m_{max}, and the corresponding long-term seismic moment rates $\dot{M}_0^{seis}$, that are consistent with seismicity data, tectonic informa-

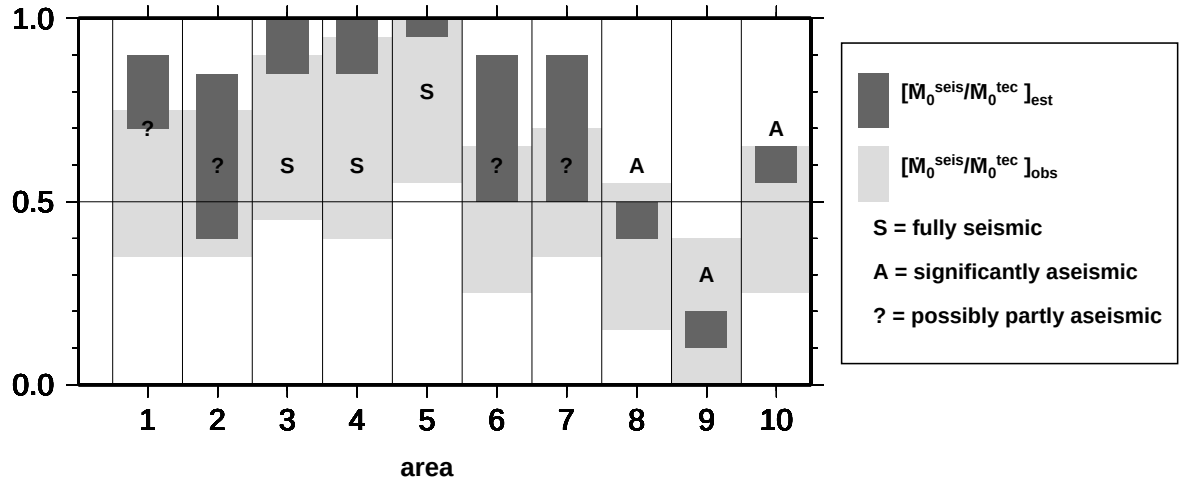

Figure 2.11: Best estimate and observed moment ratios. $[\dot{M}_0^{seis}/\dot{M}_0^{tec}]_{est}$ = ratio of the long-term seismic moment rates and the long-term tectonic moment rates, $[\dot{M}_0^{cat}/\dot{M}_0^{tec}]_{obs}$ = ratio of the short-term seismic moment rate and the long-term tectonic moment rates (in dark gray with error intervals in light gray). We distinguish three types of areas: S = areas with fully seismic deformation, A = areas with significant aseismic deformation, ? = areas where the data do not allow us to distinguish between fully seismic and partially aseismic deformation.

tion and strain rates.

The eastern Mediterranean was chosen as a study region for its dense distribution of data. This density allows for detailed comparison between the short-term seismic strain rate documented by earthquake catalogues and the tectonic strain rate field measured geodetically. For all tectonic regimes, we find that both the seismic strain rate field over several magnitude units and the geodetic strain rate field are very similar in style. Thus, a catalogue which reflects only the long-term rate of small events can reliably illustrate the deformation style.

The ratio of long-term seismic to total strain is estimated by comparing the amplitudes of the seismic catalogue moment rates $\dot{M}_0^{cat}$ with the geodetic moment rates $\dot{M}_0^{tec}$. Our statistical analyses show that, when averaged over a tectonic regime, the moment rates contained in the historical catalogues should estimate (within 10-25 %) the long-term seismic moment rate well. It is as likely to observe an $\dot{M}_0^{cat}$ that exceeds $\dot{M}_0^{seis}$ as one that lags behind it. This applies generally to areas like the eastern Mediterranean and California where strain rates are on the order of 100 nanostrain, m_{max} does not exceed 8-8.5 and the catalogue spans at least 100-200 years. In the

eastern Mediterranean, however, the observed $\dot{M}_0^{cat}$ is systematically lower than $\dot{M}_0^{tec}$. Errors in magnitude or catalogue completeness estimates probably contribute to these low $\dot{M}_0^{cat}$ estimates. Good constraints are also important for small earthquakes since for b values larger than or equal to 1 events with $M_w = 4.5 - 6.5$ can accommodate up to 60 % of the deformation.

From the very large maximum magnitudes required to accommodate the geodetically observed strain along the Hellenic arc, we infer that less than 55 % of the convergence occurs seismically, consistent with previous results [*Main and Burton*, 1989; *Koravos et al.*, 2003]. This implies that the trench is largely uncoupled as has been observed for other trenches with back-arc spreading and/or retreating downgoing plates [*Scholz and Campos*, 1995]. In contrast, the strike-slip zones encompassing the Northern Anatolian Fault Zone (NAFZ) and the Kephalonian fault are fully seismic. A small component of aseismic deformation may characterize the prolongation of the NAFZ into the Northern Aegean Trough (NAT). This aseismic component may be due to the relative immaturity of the plate boundary here. For the extensional zones in central and northern Greece and western Turkey, up to 10-60 % of the deformation is aseismic. In the southern Aegean, deformation occurs mostly aseismically. Very thin lithosphere due to extension and hydration by the subducting slab probably limits the seismogenic thickness.

Averaged over tectonic zones, $\dot{M}_0^{cat}$ should approach $\dot{M}_0^{seis}$. However, on a smaller scale, the seismic strain rate field inferred from the catalogues (Fig. 2.6) is rougher than the long-term tectonic strain rate field (Fig. 2.7). This variability in short-term seismic strain rate field reflects that the largest events lead to deficits or excesses of seismic moment release. For example, along the NAFZ a local lack of seismicity is found in the Marmara Sea. However, when moment rates are averaged over a region also including the strike-slip faults south of the Marmara Sea there is no clear deficiency of seismic strain release in the last 500 years.

2.10 Acknowledgments

We thank Bill Holt and John Haines for making the strain rate mapping program available and Corné Kreemer for his help with the implementation of the method. We thank James Jackson for providing his catalogue. This project benefitted from discussions with

Steven Ward and David Jackson. We also thank the latter for providing a solution to include magnitude uncertainties in the maximum likelihood approach. The SESAME data were obtained from Maria-Jose Jimenez (IGCP n○ 382 project). We are also grateful to John Beavan, Corné Kreemer and an anonymous reviewer for their thoughtful reviews of the manuscript. This research was funded by MunichRe and ETH Zurich. This is contribution n○ 1248 of the Institute of Geophysics, ETH Zurich.

Chapter 3

A recent tectonic reorganization in the South-Central Mediterranean

Saskia Goes, Domenico Giardini, **Sarah Jenny** and Hans-Gert Kahle

Published in Earth and Planetary Science Letters

3.1 Abstract

New geodetic, seismicity, geologic and geochemical data document a major tectonic reorganization in the Central Mediterranean around 0.8-0.5 Myr, when rapid trench migration and consequent Tyrrhenian back-arc extension which dominated the region's evolution since the Tortonian (10-8 Myr) stopped. In response, the African convergence in Sicily was transferred to a back-thrust in the Southern Tyrrhenian. The Ionian region now diverges from the main part of Africa, with northeastward motions that reflect the joint influence of African push and Hellenic slab pull, and are transmitted to Adria. A diffuse transform boundary formed across northeastern Sicily to connect the Sicilian and Calabrian plate boundaries, causing opening of the Messina Straits - home to devastating historical earthquakes - and unusual volcanism in the Aeolian Island arc and the intraplate Mount Etna.

3.2 Introduction

Plate boundary reorganizations give insight in the dynamics of plate tectonics. To understand plate reorganizations, we need to be able to read the complex geologic record they leave, a task made more difficult by the scarcity of present-day analogues where details can be well mapped out. By combining geodetic and seismicity data with geologic, paleomagnetic and geochemical information, we document a recent change in the tectonic character of the South-Central Mediterranean, related to the last stages of subduction under Southern Italy.

The African-European plate boundary zone displays unusual tectonic complexity. In the South-Central Mediterranean, over a length of few hundreds kilometers, it encompasses slowly converging orogenic belts (Apennines, Maghrebides, Alps), rapidly extending oceanic basins (Tyrrhenian, Aegean), active volcanism (Etna, Vesuvius and Campi Flegrei, the Aeolian Arc with Stromboli and Vulcano), devastating seismic activity resulting in over 100'000 casualties per century (Eastern Sicily 1693, Calabria 1783, Messina 1908, Irpinia 1980) and rotating blocks and microplates (Fig. 3.1). Traversing Sicily from south to north, one crosses from the African continental platform (Iblean plateau), through Apenninic nappes, across the Etna volcanic province into the European Alpine front of the Peloritani Mountains. Tectonics during the last 8 to 10 Myr were controlled by the interaction of slow African-European convergence and fast subduction roll-back below the southern Apennines and Sicily accompanied by back-arc extension and sea-floor spreading in the Tyrrhenian Sea [*Faccenna et al.*, 2001a; *Gueguen et al.*, 1998]. Current observations show this changed, 0.8-0.5 Myr ago.

3.3 Tectonic evolution

The recent changes in Central Mediterranean tectonics can only be interpreted in the context of the regional evolution. During the slow and oblique Africa-Europe convergence between 60 and 35 Myr, a 200-300 km long lithospheric downwelling accumulated under the Ibero-European margin [*Faccenna et al.*, 2001a, 2004] (Fig. 3.2a). The gravitational pull of this subducted slab [*Malinverno and Ryan*, 1986] initiated trench retreat around 35 Myr. In a first stage of rapid migration, from 35 to 16 Myr, the Iberian margin rifted and the Corsica-Sardinia-Calabro-Peloritani block migrated counterclockwise

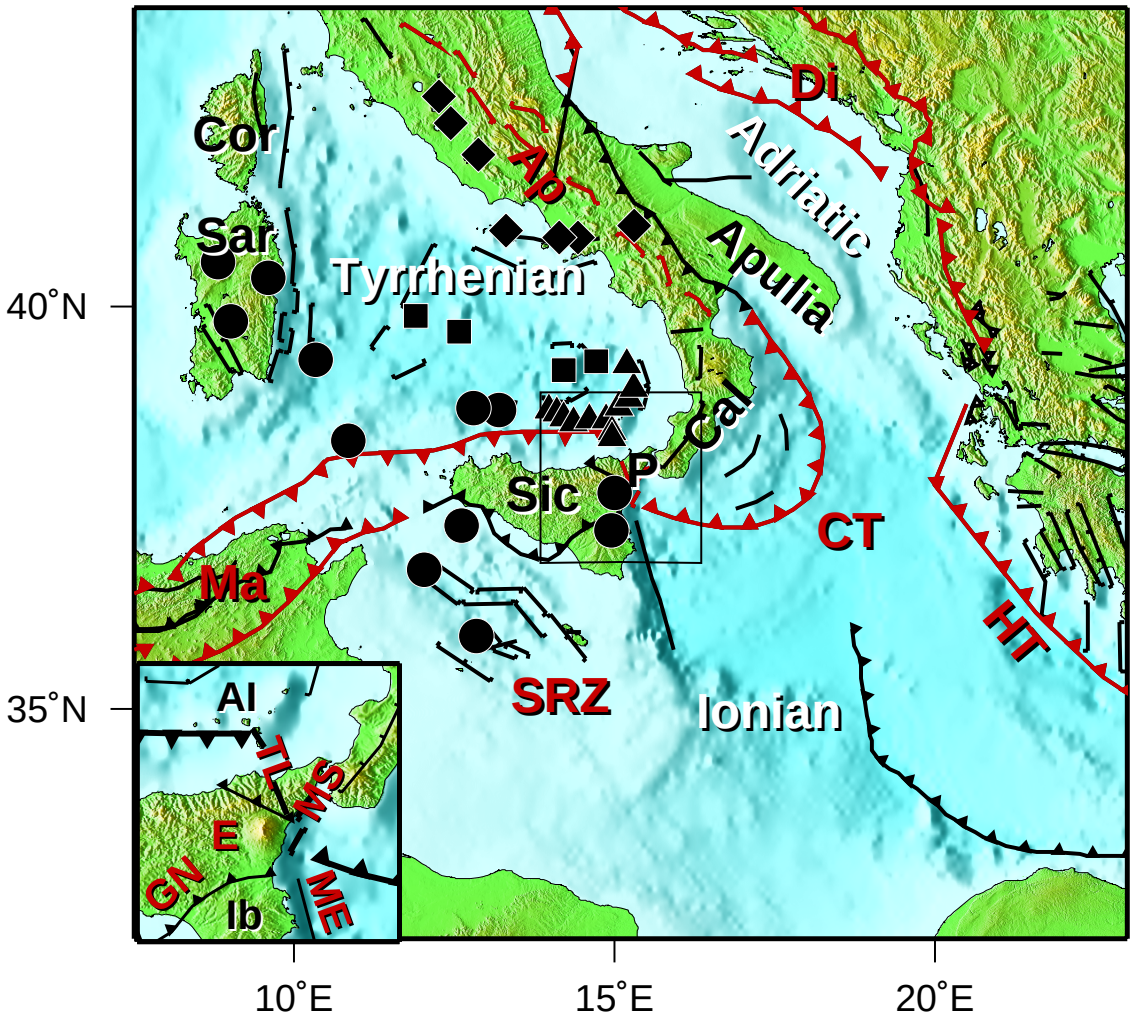

Figure 3.1: Topography (National Geophysical Data Center) with tectonic boundaries, major ones in red lines, others in black. Black symbols mark Pliocene-Quartenary volcanic areas [*Serri*, 1990; *Ambrosetti et al.*, 1987], where circles denote intraplate (alkalic to sub-alkalic) volcanism, squares mid-oceanic ridge (tholeitic) volcanism, and triangles and diamonds subduction related volcanism changing character from oceanic (calc-alkaline-shoshonitic-triangles) to more continental (increasingly potassic-diamonds). Abbreviations used are: Ap - Apennines, AI - Aeolian Islands, Cal - Calabria, Cor - Corsica, CT- Calabrian Trench, Di - Dinarides, E - Etna, GN - Gela Nappe, HT - Hellenic Trench, Ib - Iblean Plateau, Ma - Maghrebides, ME - Malta Escarpment, MS - Messina Straits, P - Peloritani Block, Sar - Sardinia, Sic - Sicily, SRZ - Sicily Rift zone in the Sicily Channel, TL - Tindari-Letojanni Line.

with the Apenninic section of the trench, consuming oceanic floor and leaving in its wake the newly formed Liguro-Provencal Basin [*Faccenna et al.*, 2001a; *Gueguen et al.*, 1998; *Speranza et al.*, 2002]. By 15 Myr, subduction and trench migration had stalled along the whole margin, as the western end of the trench collided with Africa's margin and the subducting lithosphere reached the base of the upper mantle [*Faccenna et al.*, 2001b; *Carminati et al.*, 1998b]. Retreat of the Italian trench section resumed between

8 and 10 Myr (Fig. 3.2b, c) [*Speranza et al.*, 2003; *Mascle et al.*, 1988]. In this second phase of roll-back, the Calabro-Peloritani block rifted from the Corsica-Sardinian block and migrated rapidly, at a rate of 6-8 cm/yr, to its present position between Sicily and Apulia, while the Tyrrhenian basin opened in the back-arc. During this whole period, Africa steadily converged northwestward at a small velocity of 0.5-1 cm/yr [*Faccenna et al.*, 2001a; *Gueguen et al.*, 1998].

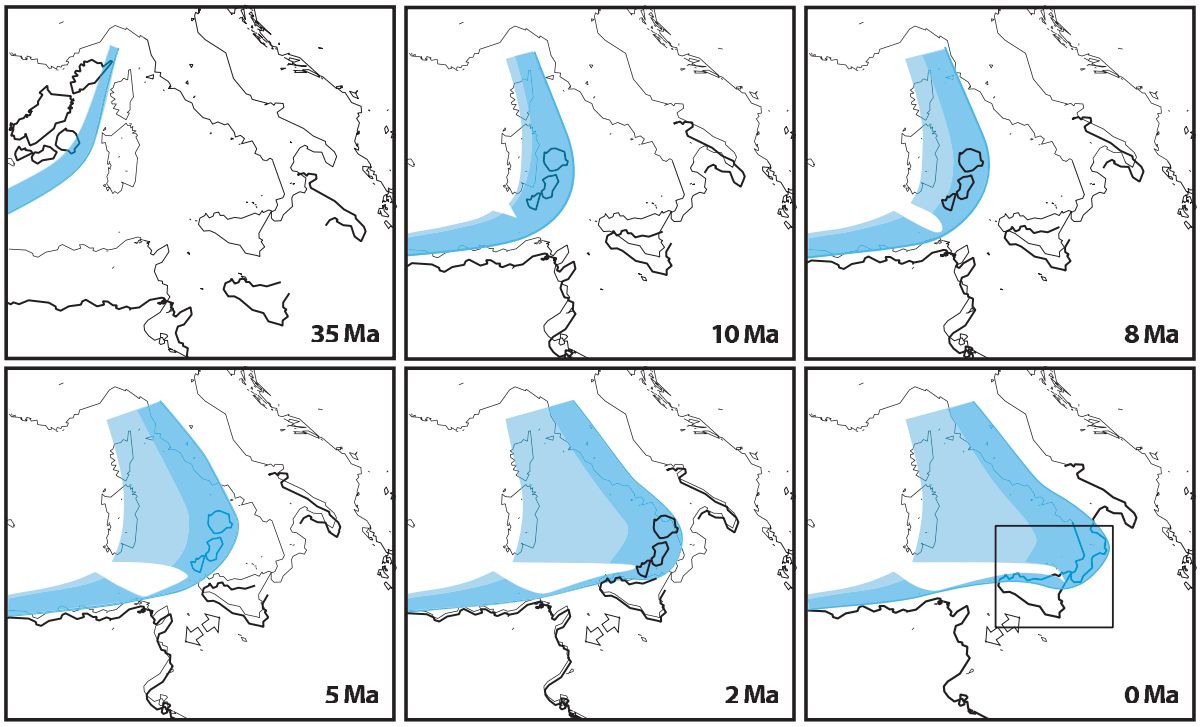

Figure 3.2: Sketch of the tectonic evolution of the Central-Western Mediterranean, based on *Faccenna et al.* [2001a], *Gueguen et al.* [1998], *Faccenna et al.* [2004] and *Carminati et al.* [1998a], with our reconstruction of subducted plate geometry. Bold lines mark the reconstructed paleogeography from 35 Myr to present. For reference, thin lines show current geography in all panels. Dipping part of the slab is shaded in dark blue, the part that lies flat above 660 km in light blue. Extension in the Sicily Channel started around 5-6 Myr. The box in the 0 Myr panel marks the region shown in Fig. 3.4.

In our reconstruction of the subducted slab, the migration of the active subduction front progressively increased trench length, which, to be accommodated at depth, required slab tearing. A gap started developing around 10 Myr and widened toward the east, below the southern Tyrrhenian, allowing transfer of mantle material from the African to the European side of the slab and facilitating further fast roll-back [*Faccenna et al.*, 2001b; *Carminati et al.*, 1998b]. Our gap geometry is compatible in size and shape with tomographic results [*Piromallo and Morelli*, 1997; *Bijwaard et al.*, 1998], and differs from other proposed tears in the slab below Sicily [*Faccenna et al.*, 2004;

Gvirtzman and Nur, 1999; *Doglioni et al.*, 2001]. Furthermore, it is consistent with the volcanic record. Most of the volcanic centers in the southern Tyrrhenian and in Sardinia have (phases of) volcanism with the signature of an intraplate mantle source - which under Europe and northern Africa has a OIB-HIMU geochemical flavor [*Hoernle et al.*, 1995; *Wilson and Patterson*, 2001] -, similar in character to internal African plate volcanism (in the Sicily Rift Zone and southeastern Sicily). No such an intraplate imprint is found in the centers in the northern Tyrrhenian (Fig. 3.1) [*Serri*, 1990; *Ambrosetti et al.*, 1987; *De Astis et al.*, 2000]. This distribution is consistent with flow of mantle from the African back side of the slab, around a migrating slab edge below the southern Tyrrhenian. Between 5 and 2 Myr, the rapidly migrating trench rolled past the Sicilian margin of Africa. The combination of the E-SE migration of the Calabrian trench and of the NW motion of Africa resulted in a small amount of subduction under Sicily, on the order of 100-150 km. Oblique trench roll-back plus African convergence resulted in Plio-Pleistocene dextral strike-slip and southward advancing thrusting in the Sicilian Penninic Nappes, most recently thrusting the Gela Nappe over the carbonate platforms on Sicily's southern margin [*Tortorici et al.*, 2001; *Speranza et al.*, 1999; *Lickorish et al.*, 1999; *Catalano et al.*, 1996].

Recently collected geodetic data [*Hollenstein et al.*, 2003] (Fig. 3.3a and Fig. 3.3b), combined with historical and instrumental seismicity (Fig. 3.3c and Fig. 3.3d) document that the present-day tectonics differ markedly from the pattern that dominated the region's evolution during the last 8-10 Myr in several respects.

3.4 A recent change

3.4.1 Africa-European convergence north of Sicily

Today, most of Sicily moves together with the African plate, as GPS velocities at stations in Sicily (TRAP, NOTO) and the Sicily Channel (LAMP, MLTA, GOZO) match the African plate motion. Internal deformation in Sicily is small (except in the northeastern corner, discussed in Section 3.4.5, and the 5 mm/yr Africa-European convergence is mainly absorbed in a belt located north of Sicily (TRAP) and south of Ustica (USTI) and Stromboli (STRM). This offshore zone is characterized by frequent, moderate-sized thrust earthquakes (Fig. 3.3d), which have largely escaped historical detection. On the

basis of its location at the backside of the accretionary complex, and the shallow dip of the southward-sloping seismic nodal planes (Fig. 3.3d), we interpret the faulting as back-thrusting. As the trench reached the buoyant, continental African lithosphere in Sicily, it progressively sutured. By 1-0.8 Myr, the internal deformation, rotation and overthrusting of the Sicilian nappes ceased [*Tortorici et al.*, 2001; *Speranza et al.*, 1999; *Lickorish et al.*, 1999; *Catalano et al.*, 1996], indicating the end of subduction under Sicily. The continued 0.5 cm/yr advancing of the African continent resisted further northward underthrusting, and convergence was apparently transferred to the northern front of the accretionary complex, to a narrow back-thrust zone in continental lithosphere thinned by back-arc extension

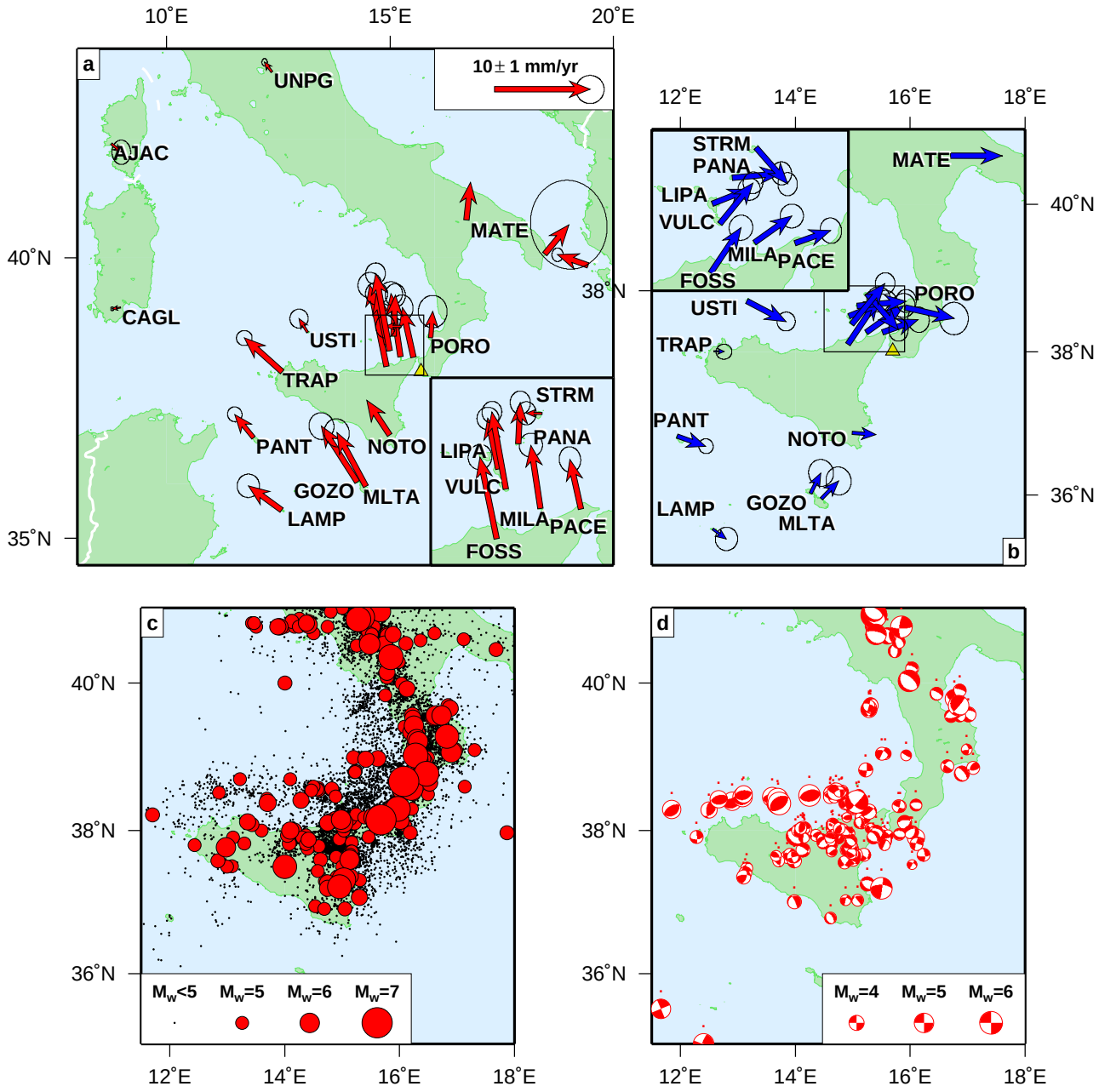

Figure 3.3: Geodetic and seismicity data for the area of interest: GPS velocity vectors [*Hollenstein et al.*, 2003] transformed into a Eurasian (panel a) or African (panel b) reference frame using poles from the REVEL model [*Sella et al.*, 2002], instrumental and historical seismicity (panel c), and focal mechanisms (panel d). The white triangle in a and b marks the position of Reggio Calabria. Insets in a and b show Aeolian Island velocities in more detail. Seismicity data are a compilation from the historical CPTI catalogue for the time interval -217 BC-1981 [*Working Group CPTI*, 1999] and the instrumental CSTI for the period 1981-1996 [*Instrumental Catalog Working Group CSTI*, 2001]. Moment tensor solutions are from the Harvard Centroid Moment Tensor catalogue [http://www.seismology.harvard.edu, *Dziewonski et al.* [1981] (events with Mw $>$ 5.5, between January 1977 and December 2002), from the European-Mediterranean Regional Centroid Moment Tensor catalogue [*Pondrelli et al.*, 2002] and the Swiss Seismological Survey [http://www.seismo.ethz.ch/info/mt.html, *Braunmiller et al.* [2002]] (events with 4.1 $<$ Mw $<$ 5.2), and from *Frepoli and Amato* [2000] (events with 2.5 $<$ Mw $<$ 4.4 in southern Italy and Sicily). Note the different scales used for event size in c and d.

3.4.2 Stalling of Calabrian roll-back and back-arc extension

Roll-back of the Calabrian arc is no longer ongoing. Station PORO on Calabria's western coast moves northwards relative to Europe with a rate of 2.9 ± 1.2 mm/yr; very similar motion is observed in Reggio Calabria [*D'Agostino and Selvaggi*, 2003]. Although large historical earthquakes occurred on the normal faults bordering the Calabrian Alpine province, motions along these faults, inferred from geomorphology, amount to only 1-2 mm/yr [*Tortorici et al.*, 1995; *Monaco and Tortorici*, 2000], i.e., a minor fraction of the 5-6 cm/yr average roll-back velocities observed in the region since Tortonian times [*Faccenna et al.*, 2001a]. At the same time, back-arc extension in the Tyrrhenian is no more observed. Stations located on all borders of the Tyrrhenian basin have motions that are almost indistinguishable from stable Europe (CAGL within 0.4 mm/yr, AJAC and UNPG within 1.4 mm/yr and USTI and STRM within 1.7 mm/yr, uncertainties are $\leq$ 0.9 mm/yr), and, except for AJAC, are in a direction opposite to previous back-arc extension. Trench migration and the accompanying fast subduction probably halted, when the Calabro-Peloritani block reached its present location and became trapped between the Southern Apennines, where the trench had collided with the buoyant Apulian platform, and the advancing African margin in Sicily. The consequent slow-down of mantle flow around the slab edge [*Buiter et al.*, 2002; *Giunchi et al.*, 1996b] induced a rapid uplift of the whole area (including Calabria, the Aeolian Islands and northeastern Sicily) at rates as high as 1-2 mm/yr (possibly aided by slab detachment [*Buiter et al.*, 2002]. This effect should decrease southwards, where indeed lower uplift rates and even subsidence are observed [*Monaco and Tortorici*, 2000; *Westaway*, 1993; *Monaco and Tortorici*, 1995; *Mulargia et al.*, 1985]. Calabrian geology records the change as a transition, 1-0.5 Myr, from strongly compressional to extensional deformation [*Tortorici et al.*, 1995; *Monaco and Tortorici*, 2000].

3.4.3 Transfer zone formation

The different behavior of the Sicilian and Calabrian portions of the African margin since 0.8-0.5 Myr, resulted in the development of a diffuse dextral transfer zone accommodating the 5 mm/yr motions due to the offset between the Sicilian back-thrust and the Calabrian trench (Fig. 3.4). Eastern Sicilian seismicity shows a mix of dextral strike-

slip and extensional mechanisms (Fig. 3.3d). At the northwestern end of the zone, a significant part of the differential motion (around 3 mm/yr) is taken up along the dextral Tindari-Letojanni line, which runs below the Aeolian Islands of Salina, Lipari and Vulcano on to the northern shore of Sicily. While the other Aeolian Islands formed as a subduction arc above the no longer migrating subducted lithosphere, Lipari and Vulcano developed more recently [*De Astis et al.*, 2000; *Mazzuoli et al.*, 1995], on the transfer zone. In the southeastern part of the transfer zone, most of the motion occurs along normal faults oriented perpendicular to the African motion, in the Peloritani, the Messina Straits and near Etna [*Tortorici et al.*, 1995; *Monaco and Tortorici*, 2000; *Hirn et al.*, 1997; *Monaco et al.*, 1997]. Geological estimates allow 3 mm/yr of extension in the Messina Straits, which started opening around 0.5 Myr [*Tortorici et al.*, 1995; *Monaco and Tortorici*, 2000]. Contrary to previous interpretations [*Monaco and Tortorici*, 2000; *Meletti et al.*, 2000], we explain the Messina Straits' extensional faulting as the result of the differential plate motion, rather than as a consequence of regional uplift, and the development of the dextral transfer zone as a result of African motion, rather than an indication of ongoing migration of the Calabrian arc.

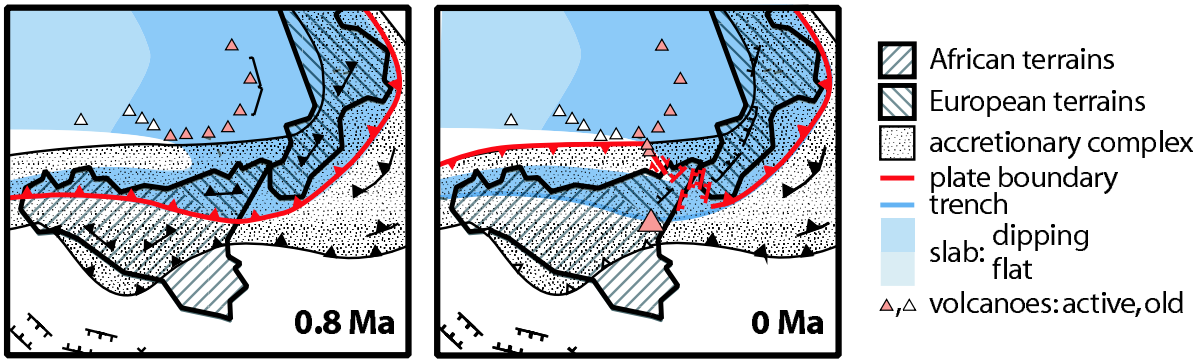

Figure 3.4: Detailed sketch of the consequences of the recent tectonic change on the Sicily-Calabrian area. Lines and fills are explained in the legend.

3.4.4 Ionian-Adria motions

From the Sicily Channel to Calabria to Apulia, motions become less and less African and rotate increasingly northeastwards. Stations MLTA and GOZO move almost like stable Africa, but document (Fig. 3.3b) 2-2.5 mm/yr of active, northeast-directed, rifting in the Sicily Channel, whose opening started around 6 Myr and was thought to have ceased

[*Argnani*, 1990]. Calabria (PORO, Reggio Calabria) is shifting north at 2.9 mm/yr relative to Europe. The Apulian site MATE, documents the north-northeast drift of the Adria block towards the Dinarides, at 4.0 mm/yr. Thus, the region extending from the Sicily Channel (whose young extensional features may continue as far south as Libya, [*Westaway*, 1990; *Argnani and Torelli*, 2001], all the way to Apulia (southern part of the Adria block) now diverges from Africa.

Contrary to the situation in Sicily, the African convergence around Calabria did not transfer to the back of the subduction complex. However, the historical record does also not include any of the large subduction earthquakes that would be required to accommodate the 5 mm/yr African convergence plus the 1-2 mm/yr extension across the Calabrian peninsula; and even small thrust events are almost absent (Fig. 3.3c,d). We infer that the Calabrian trench is locked, and that the Ionian domain is shifting to the north-northeast together with Calabria, at 2-3 mm/yr. Locking of the trench removed the northward pull of the Calabrian slab on Africa's Ionian corner. At the same time, the weak coupling at the Hellenic trench - less than 20% of the total budget is released seismically [*Jenny et al.*, 2004] - allows for the efficient transfer of slab pull to the Ionian surface lithosphere. The combined effect of the overall northwestward advance of Africa, and the northeastward pull of the long subducting Ionian slab under the Hellenic trench, results in the current kinematics. This resulting motion is transferred to Adria, inducing its north-northeastward shift and counterclockwise rotation [*Anderson*, 1987; *Nocquet and Calais*, 2003; *Devoti et al.*, 2002]. The 0.7 Myr onset of the dominant extensional phase in the southern Apennines [*Hippolyte et al.*, 1995] fits well in this interpretation. Stresses induced by the southern Tyrrhenian slab tear probably initiated Pliocene activity in the Sicily Rift Zone [*Faccenna et al.*, 2004], but the pull of the Hellenic slab is held responsible for the rift's continued activity, its orientation and extent.

3.4.5 Europe-Africa-Ionian corner

The largest relative motion occurs in northeastern Sicily and the Aeolian islands, where we observe a striking, north-northwestern movement of all stations relative to Europe (up to 8.7 mm/yr), motions consistent with several other measurements in Sicily [*D'Agostino and Selvaggi*, 2003; *Serpelloni et al.*, 2003]. No significant nearby earthquake occurred

during the campaign period, nor do the time series of motion show any sudden and simultaneous jumps [*Hollenstein et al.*, 2003] that would point to an earthquake-related signal. The large distance from Etna, which was active [*Patane et al.*, 2003] during the observation period, and the absence of a clear decay pattern, as expected for volcanic activity [e.g., *Trasatti et al.*, 2003], from any of the volcanoes in the area rule out a volcanic origin. Instead, the coherent clockwise rotation of the area relative to Africa, indicates a larger-scale tectonic origin. This region escapes from Africa with motions that decrease from a maximum of 5.7 $\pm$ 0.9 mm/yr at FOSS to the almost European motion of Stromboli (STRM) in the north. The rotation of this small region mirrors the larger scale deformation of Africa's Ionian corner, but its velocities are larger than any other observed in the Central Mediterranean.

We interpret these large velocities as the superposition of several effects. First, the clockwise rotation of the region is associated with the dextral transfer zone (see Fig. 3.4). Second, African compression against the Tyrrhenian margin induces local east-northeastward escape (perpendicular to African motion) through the plate boundary offset, facilitated by the weak Aeolian lithosphere. Finally, the very recent cessation of volcanism in the western Aeolian Islands and the changing chemistry of Eastern Aeolian lavas [*De Astis et al.*, 2000] indicate that the slab tear tip is now located below the region. Stresses due to the tear tip enhance the clockwise rotation, as does the remaining mantle flow around the Calabrian slab section. The extensional stress field associated with the plate boundary offset, the escape of northeastern Sicily, and propagation of the slab tear triggered 0.5 Myr, the formation of Etna, Europe's largest active volcano. Whether additionally, the presence of a mantle upwelling [*Schiano et al.*, 2001; *Tanguy et al.*, 1997] is necessary to explain Etna's and earlier Iblean volcanism is an open question.

3.5 Concluding remarks

The last stages of Southern Italian subduction have recently induced several tectonic changes: (1) In Sicily, motion has been transferred to a back-thrust. A similar process seems to be in progress in Costa Rica-Panama and eastern Indonesia (Flores-Timor Islands) in response to hampered continuation of subduction. (2) The slab has started segmenting, creating a large lateral gap under Sicily (Fig. 3.2) (other possible (hori-

zontal) tears have been proposed as well [*Carminati et al.*, 1998b]). (3) As subduction under Calabria locked, the African plate started internally deforming, as evidenced by the motions of Calabria and Apulia and the Sicily Channel, further giving rise to strong deformation in a corner region as plate boundaries are readjusting. These young and changing tectonics of the South-Central Mediterranean are associated with diffuse, strongly time-dependent and sometimes devastating seismicity, which until now defied explanation for lack of a comprehensive tectonic framework.

3.6 Acknowledgments

Discussions with Claudio Faccenna and Fabio A. Capitanio helped shape our ideas. This research was funded by ETH Zurich and MunichRe. Publication number 1367 of the Institute of Geophysics.

Chapter 4

Seismic potential of Southern Italy

Sarah Jenny, Saskia Goes, Domenico Giardini and Hans-Gert Kahle

Tectonophysics, In Review

4.1 Abstract

Recently collected geodetic data together with seismic and neotectonic data completely modify our understanding of the current tectonics and seismic hazard of the relatively slowly-straining South Central Mediterranean plate boundary zone. We estimate long-term average seismic moment rates from a comparison of (tectonic) deformation rates inferred from geodetic and geologic data with strain rates represented by the historical seismicity. We find that north of Sicily, where most of the 5 mm/yr African-European convergence is accommodated, seismic hazard based only on recorded past seismicity is likely an underestimate. By contrast, the series of large earthquakes that hit Calabria in the 18th century released tectonic strain rates accumulated over several thousand years, and the high level of seismicity of the past few centuries cannot be representative for the long-term average. Tectonic deformation rates in central and western Sicily are low, and although occasional damaging earthquakes can occur, their recurrence rates are long. Relatively high tectonic strain rates in northeastern Sicily (including

the Messina Straits), are probably accommodated in part aseismically, but still lead to a significant potential for $M \sim 7$ strike-slip and normal faulting events in this corner region between the European and the internally-deforming African plates. The situation in southeastern Sicily (where large past earthquakes were recorded but their location is uncertain) and the Calabrian trench (where a record of seismicity is almost absent) is less clear. These regions accommodate an Africa-European convergence modified by internal deformation of the Ionian section of the African plate. The two southeastern Sicilian $M \sim 7$ events in the last 1000 years would accommodate the maximum amount of deformation that can be ascribed to this region. Some convergent seismic activity along the trench, including $M \sim 7$ earthquakes cannot be ruled out. Overall, the whole southern Italian region displays strongly time-dependent seismic behavior, with periods of intense activity followed by long quiescence. In such regions, it is essential that hazard analyses not only include traditional seismotectonic data, but all available constraints on total and seismic strain rates.

4.2 Introduction

In the South-Central Mediterranean (Fig. 4.1), many unknowns hamper the assessment of seismic hazard. The deformation rates are low, and historical seismic catalogues are not long enough to encompass a few cycles of the largest events. Records of offshore seismicity for both the island of Sicily and the Calabrian peninsula are almost non-existent. This leads to large uncertainties in earthquake magnitude and location and spatially variable levels of catalogue completeness. Previous seismic hazard assessment of southern Italy is largely based on historical seismicity (e. g., *Slejko et al.* [1998] and *Slejko et al.* [1999]). Besides the Southern Apennines, where a long record of large events exists, Calabria, the Messina Straits and southeastern Sicily have been identified as regions of high seismic hazard. Similarly, the region around the 1968 Belice earthquake in western Sicily is often characterized as an area with seismic potential.

However, new geodetic data [*Hollenstein et al.*, 2003] combined with recent seismicity and geologic and geochemical data document a deformation field [*Goes et al.*, 2004] different from what one would infer from the distribution of historical seismicity. For example, Calabria, which was hit by five $M \geq 6$ events in the year 1783 alone, has had

no event of this magnitude since 1908 and does not show up as a high deformation rate area. On the other hand, in the southern Tyrrhenian, between the north coast of Sicily and the Ustica and Aeolian Islands, the geodetic data document high compressional strain rates, accompanied by many moderate-size earthquakes. However, no historic events in this region have been recorded. Based on all available information on tectonic and seismic strain rates, the paper aims at quantifying the seismic potential of Southern Italy.

Previous work on seismic and/or tectonic strain of Southern Italy has been done on a much coarser scale, using at most the very few geodetic constraints that were available until recently. *Albarello et al.* [1997] and *Mantovani et al.* [2001] predicted an Italian deformation field from a two-dimensional finite-element model driven by horizontal motions only, where variations in strength led to various escape scenarios. Seismic deformation rates have been determined for the Apennines by *Westaway* [1992] (from seismic moments estimated from macroseismic effects of historical earthquakes), for the whole western and central Mediterranean by *Pondrelli* [1999] (using regional moment tensors), and for all of Europe (including the Mediterranean) by *Ward* [1998a] (using the 100-year NEIC earthquake catalogue). *Pondrelli* [1999] found that seismicity accounts for about 30 % of the total deformation, inferred from VLBI data, in Calabria and along the Apennines, and for about 10 % within Sicily. Only in the Sicily Channel, does the ratio reach a higher value (79 %). *Ward* [1998a] obtained similarly low percentages in his comparison of seismic and VLBI strain rates, and attributes them to the short catalogue length compared to the long time scale of deformation in this slowly straining region. Based on seismicity only, *Boschi et al.* [1995a] estimate the 20-year probability of an $M \geq 5.9$ crustal seismic event to be very low in most of Italy, except in northern and southeastern Sicily. They obtain a probability above 65 % in the Capo d'Orlando region, along the northeastern coast of Sicily.

The average level of a region's seismic hazard is determined by long-term seismic strain which translates into seismic moment rates, $\dot{M}_0^{seis}$. $\dot{M}_0^{seis}$ cannot exceed the tectonic loading rate of the area, but if part of the deformation occurs aseismically, i. e., by slow creep rather than in sudden earthquakes, $\dot{M}_0^{seis}$ can be less, even substantially less, than the tectonic deformation rates. At best, seismicity catalogues can give an estimate of the seismic moment rate averaged over the catalogue's duration, $\dot{M}_0^{cat}$. However, even

when not significantly affected by catalogue completeness and uncertainties in magnitude and location, $\dot{M}_0^{cat}$ may not be representative for long-term seismic moment rates, if the recurrence times of the largest events much exceed the catalogue length. In this case, $\dot{M}_0^{cat}$ may be advanced or lag behind $\dot{M}_0^{seis}$, depending on whether large earthquake sequences happened in the time span of the catalogue or not. Consistent with *Ward* [1998a]'s results, *Viti et al.* [2001] - using a statistical analysis based on bootstrap resampling of the Mediterranean catalogue - also conclude that the effect of incomplete sampling of major earthquakes due to catalogue shortness is a dominant source of uncertainty in estimating long-term seismic strain rates. We found [*Jenny et al.*, 2004] that for the strain rates in Greece, a 100-year catalogue should give an approximation of the long-term seismic moment rate within $\pm$ 30 % without a bias towards low or high moment rates. This implies that in Italy, where strain rates are ten times lower, at least a 1000-year long (complete) catalogue is required to achieve such agreement. Shorter catalogue lengths tend to give moment rate estimates biased towards the low side [*Ward*, 1998a; *Jenny et al.*, 2004]. We determine estimates of both catalog-averaged ($\dot{M}_0^{cat}$) and tectonic ($\dot{M}_0^{tect}$), i. e. maximum, moment rates to bracket a plausible range for $\dot{M}_0^{seis}$. We assume that geodetic observations (screened for short-term fluctuations that could be due to earthquake or volcanic movements) document tectonic moment rates. Using a truncated Gutenberg-Richter relationship, we show how uncertainties in $\dot{M}_0^{cat}$ and $\dot{M}_0^{tect}$ affect the estimate of the magnitude-frequency distribution of the seismicity. The seismic potential of the region is given as the recurrence times of $M_w = 7$ within seven tectonic zones.

4.3 South-Central Mediterranean tectonics

Central and western Mediterranean tectonics over the past 30-35 Myr has been controlled by retreating subduction inside the Africa-European convergence zone. Since late Cretaceous-early Paleocene, a subduction zone off the Ibero-European margin accommodated the slow Africa-European convergence. About 30-35 Ma (Myr ago), this trench started retreating [*Dewey et al.*, 1989; *Faccenna et al.*, 2001a], opening first the Liguro-Provencal basin (30-16 Ma), and in a second phase, the Tyrrhenian (8 to 0.5 Ma). During the opening of the Tyrrhenian Sea, the Calabro-Peloritani fragments de-

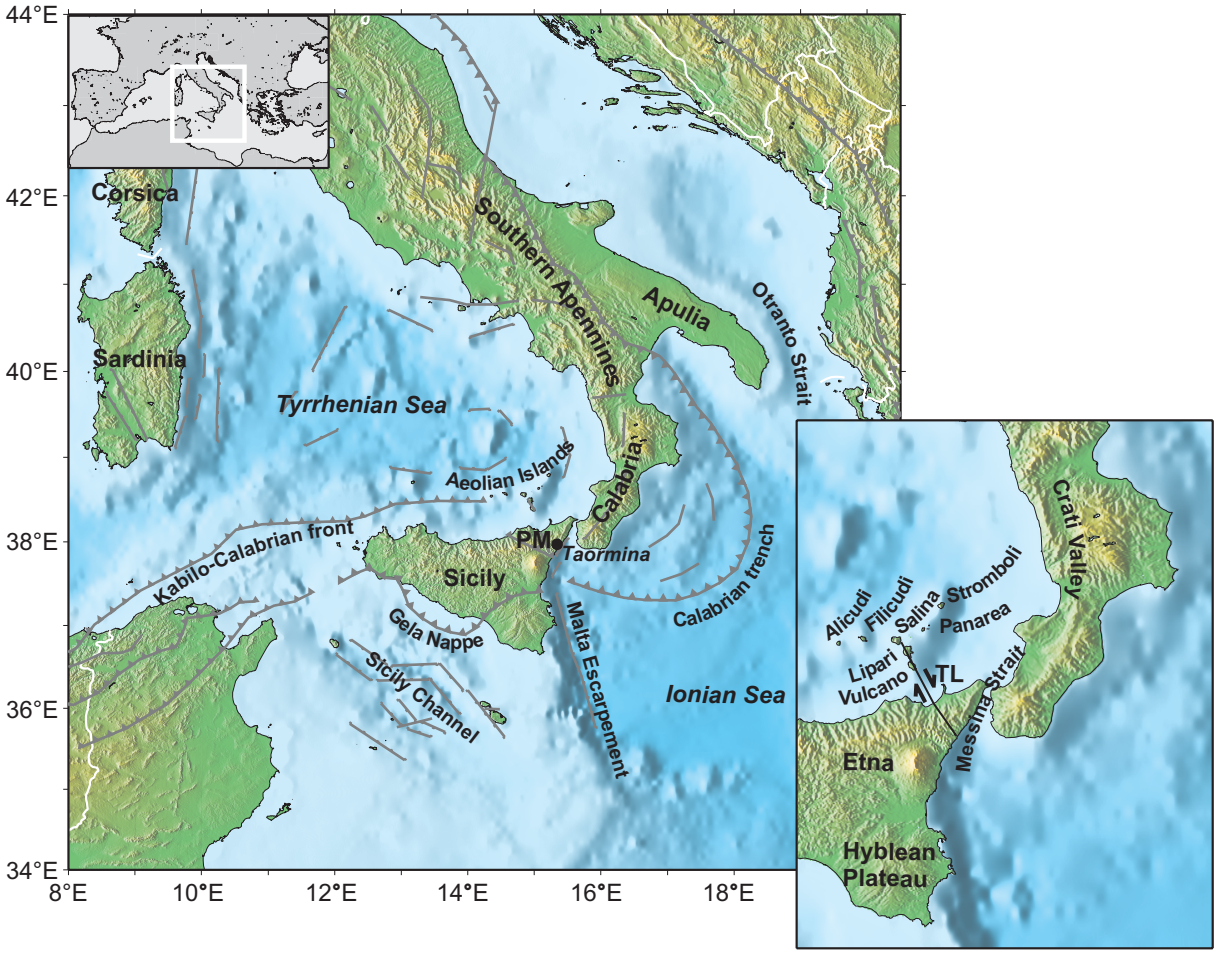

Figure 4.1: Topographic map of the study region with the main tectonic and geographic elements marked

tached from the Corsica-Sardinia block and migrated to their present position where they docked 1-0.5 Ma, to become the toe of Italy and the eastern tip of Sicily. It has been generally assumed that roll-back and the accompanying back-arc extension continue until today. However, our recent GPS observations [*Hollenstein et al.*, 2003] in combination with neotectonic data show that a tectonic reorganization must have occurred 1-0.5 Ma, in response to the progressing collision with the African margins of Sicily and Apulia and the docking of Calabria [*Goes et al.*, 2004].

The GPS data (Fig. 4.2) were collected during four campaigns between 1994 and 2001 at 16 stations in southern Italy, Sicily, on the Aeolian Islands and in the Sicily Channel and merged with data from 8 permanent stations. This constitutes a significant densification of previous strain rate data that was mainly constrained by the permanent stations at Matera (MATE) and Lampedusa (LAMP). The data document the following present-day situation (Fig. 4.3) [*Goes et al.*, 2004]:

1. The Africa-European convergence around Sicily, which caused internal deformation of the Sicilian nappes until 0.8-0.5 Ma, has now transferred off the north coast of Sicily, to what is most likely a back-thrust, where Sicily overthrusts the Tyrrhenian.

2. Calabria moves northwards at 2.5-3 mm/yr documented by stations at Monte Poro [*Hollenstein et al.*, 2003] and Reggio Calabria [*D'Agostino and Selvaggi*, 2003]. Thus the south-eastward roll-back at rates of 5-8 cm/yr, which characterized the previous 8-10 Myr, has basically ceased. At about 0.8-0.5 Ma, compression in Calabria stopped, to be replaced by fast uplift (at $\sim$ 1 mm/yr) and extension in arc-parallel as well as perpendicular grabens [*Moretti and Guerra*, 1997; *Monaco and Tortorici*, 2000].

3. The Tyrrhenian moves (within about 1.5 mm/yr) with stable Europe, and shows no evidence of active back-arc extension.

4. Unfortunately, there is no data that directly constrain the kinematics of the Ionian. For our seismic potential assessment we consider two scenarios: In T1 the trench accommodates the few mm/yr convergence of a rigid African plate. Scenario T2 [*Goes et al.*, 2004] assumes the trench is locked and continued pull of the long Hellenic slab causes internal deformation of the Ionian corner of Africa.

5. The northwestern Sicilian-Aeolian Island region forms a corner region where the deformation between Europe, Calabria, Africa and Africa's Ionian corner concentrates, resulting in a transfer zone which contains both dextral strike-slip faults and normal faults. The main strike-slip structure is the Tindari-Letojanni fault system in northeastern Sicily. Onshore, more than one active dextral fault branch has been mapped. Offshore, the location of the Aeolian islands Salina, Lipari and Vulcano is controlled by releasing steps in the fault system [*Gioncada et al.*, 2003; *De Rosa et al.*, 2003; *Ventura et al.*, 1999]. We also associate the well-documented (and seismogenic) extensional structures in the Messina Straits [*Monaco and Tortorici*, 2000] with this transfer zone and do not see it as an offshore continuation of the internal Calabrian faults, in contrast to what is often assumed [*Monaco and Tortorici*, 2000; *Tortorici et al.*, 1995; *Westaway*, 1993; *Monaco et al.*, 1997; *Stewart et al.*, 1997]. The Malta Escarpment further south has also been associated with this "Siculo-Calabrian Rift Zone". In spite of large historical earthquakes

in southeastern Sicily that are sometimes attributed to this escarpment [*Monaco and Tortorici*, 2000; *Anderson and Jackson*, 1987], seismic lines show no evidence that it has recently been active south of Siracusa [*Argnani and Bonazzi*, 2003]. Recent activity on structures east of the Malta Escarpment can however not be ruled out [*Argnani and Bonazzi*, 2003]. Active extensional structures have been mapped just offshore from Etna [*Bianca et al.*, 1999].

6. At around 0.7 Ma, thrusting in and around the southern Apennines ceased and today, the southern Apennines are characterized by extension [*Amato and Montone*, 1997; *Hippolyte et al.*, 1995], which differs from the back-arc extension that affected Italy's western coast before 0.7 Ma. East of the Apennines, a combination of extension perpendicular to the belt and compression in northwest direction results in strike-slip faulting [*Amato and Montone*, 1997].

Based on this reevaluation of the seismotectonics, the southern Italian region can be divided into seven zones: (1) the back-thrust north of Sicily, (2) central and western Sicily, (3) the Aeolian Island region and northeastern Sicily, including the Messina Straits, (4) southeastern Sicily and its offshore region, (5) Calabria, (6) the Calabrian Trench, (7) the Southern Apennines. Our subsequent discussion will be organized according to these regions.

4.4 Tectonic strain rates

The southern Italian GPS data give us new quantitative constraints on tectonic strain rates. We combine our geodetic data with published geodetic and geologic slip rate data. For our comparison with seismic strain rates, we calculate maps of (1) fully distributed strain and (2) strain concentrated along prescribed faults. The first approach provides a good overview of the regional style of deformation, while the second provides estimates of fault slip rates, under the assumption that the dominant faults are known.

4.4.1 Deformation modeling methods

The continuous strain rate field is derived using the method of Haines and Holt [*Haines and Holt*, 1993; *Holt and Haines*, 1995; *Haines et al.*, 1998; *Beavan and Haines*, 2001],

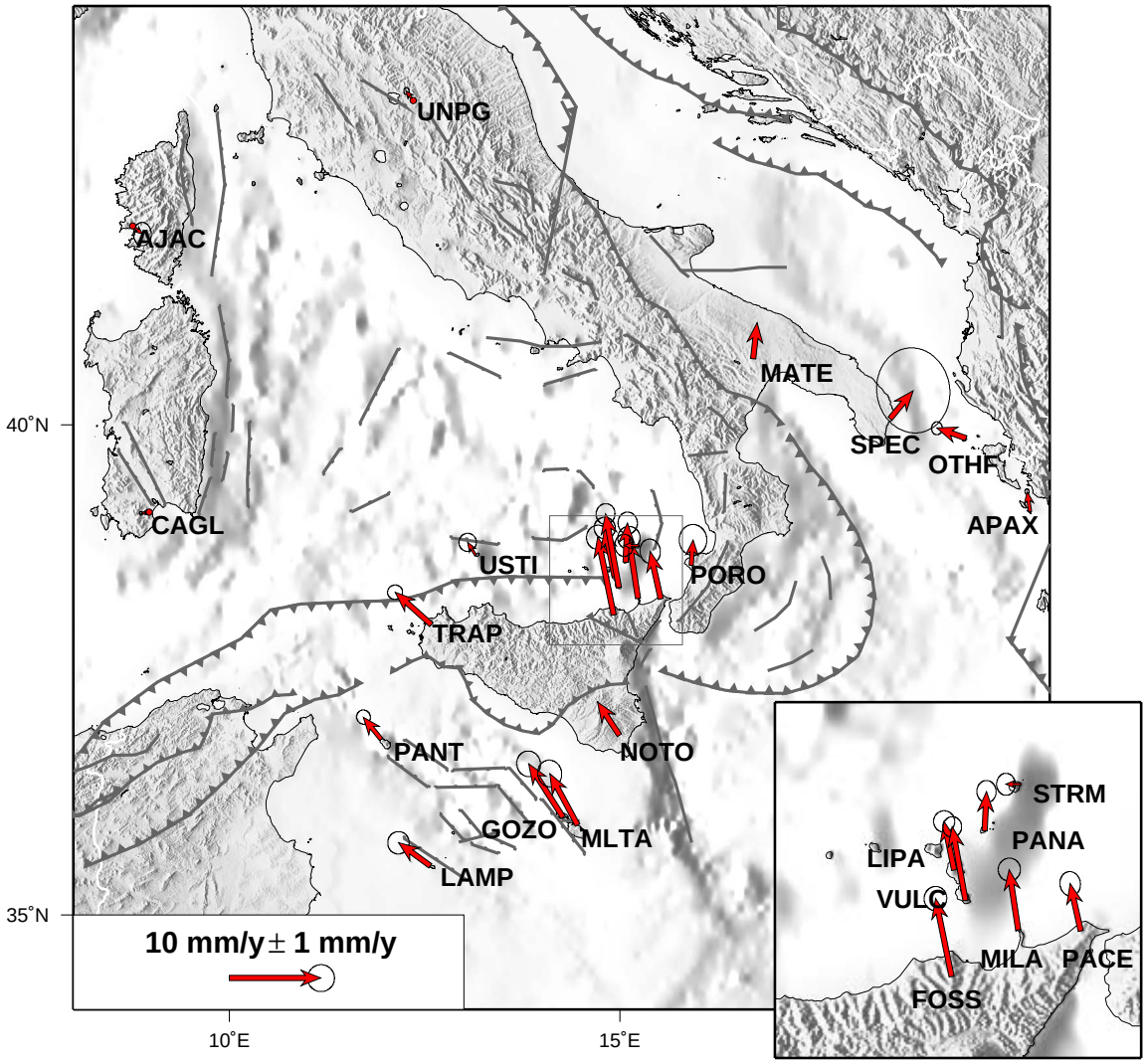

Figure 4.2: GPS velocities from *Hollenstein et al.* [2003] relative to an Eurasian reference frame using rotation poles from *Sella et al.* [2002]. The error ellipses correspond to formal statistical errors, scaled by 21.25 and 42.5 for campaign stations and permanent stations, respectively [*Hollenstein et al.*, 2003]. Although this region moves at rates of only a few mm to 1 cm/yr relative to stable Europe, most velocities exceed their estimated uncertainties, except at station SPEC, which was re-monumented during the observation period.

which minimizes the difference between a self-consistent horizontal velocity gradient field, on a curvilinear grid with variable knot point spacing, and strain observations, that can include geodetic velocities, plate motions, seismic moment tensors and fault slip rates. The uneven spacing of the GPS stations leads to very smoothed strain rates in areas with few stations and concentrated strain rates only where the distribution of stations is dense (Fig. 4.4). During the inversion, the continuous strain rate field was smoothed over one neighboring grid cell. In scenario T1 (shown in Fig. 4.4), the Ionian

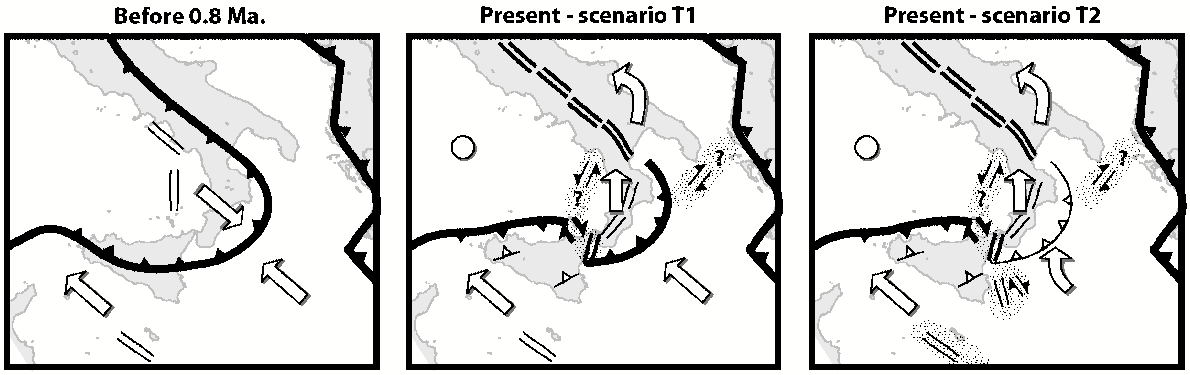

Figure 4.3: Tectonic interpretation based on a combination of the recent geodetic observations [*Hollenstein et al.*, 2003] with neotectonic and recent seismicity data [*Goes et al.*, 2004]. The main plate boundaries are marked with bold lines, other faults with thin lines. Bold white arrows indicate the main direction of motion of the plates and blocks relative to stable Europe, where the dot in the present-day Tyrrhenian denotes the region's fixity w.r.t. Europe. Until around 0.8 Ma, the tectonics were characterized by roll-back of the Calabrian trench and back-arc extension in the Tyrrhenian (left panel). Two alternative scenarios for the present-day tectonics are shown (center and right panels). The geodetic data constrain the current motion of most of Sicily with stable Africa, the northward motion of Calabria and the counterclockwise rotation of Adria. These motions require the existence of two additional deformation zones, in the Strait of Otranto and the Tyrrhenian offshore of Calabria, which do not have any well-defined expression and may be very diffuse. There are no observations in the Ionian basin, which leaves open whether it moves with Africa (T1), leading to continued although much slowed down convergence along the Calabrian trench, or the region is internally deforming (T2), with motion changing from African in the south to Calabria/Adria-like in the north. As discussed in the text, other observations make us prefer the second interpretation.

Basin is prescribed to move rigidly with the rest of Africa, according to the African pole of *Sella et al.* [2002]. In T2, the Ionian Basin moves in the same direction as Calabria, as defined by the GPS velocity at the station of PORO (and Reggio Calabria). Uncertainties in the continuous strain rates are of the order of 20 nanostrain/yr (10^{-9}/yr).

The second method, developed by Lundgren [*Lundgren et al.*, 1995, 1998], computes crustal motions in an elastic spherical shell cut by faults, using a finite element approach. Calculated motions are the result of prescribed nodal displacements and/or relative displacements across faults. Motion along the faults can be unconstrained, prescribed only in style, or also in magnitude. The faults are frictionless, and overlaps or gaps are allowed in response to perpendicular motions. To estimate the slip expected on major fault structures in the region as a result of the geodetically measured velocities, we prescribe GPS motions (as displacements) at the station locations and plate motions at the model boundaries. Motion along all other faults in the area is unconstrained and purely a response to the boundary conditions. The model domain is the same

as was used for studying the eastern Mediterranean [*Lundgren et al.*, 1998]. It spans the entire Mediterranean and extends from the Azores to Iran, in order to include the stable interiors of the main plates. In the central Mediterranean, we updated the major fault structures to match current information. Material properties in the central and western Mediterranean are constant (Young's modulus of 70 GPa, Poisson's ration of 0.25). Changing these properties laterally did not affect results in our region of interest. Here too, we calculate two cases where the Ionian is prescribed to move with Africa or with Calabria (Fig. 4.5). Uncertainties in the fault slip rates from the finite element model, due to uncertainties in the geodetic constraints, are about 1 mm/yr.

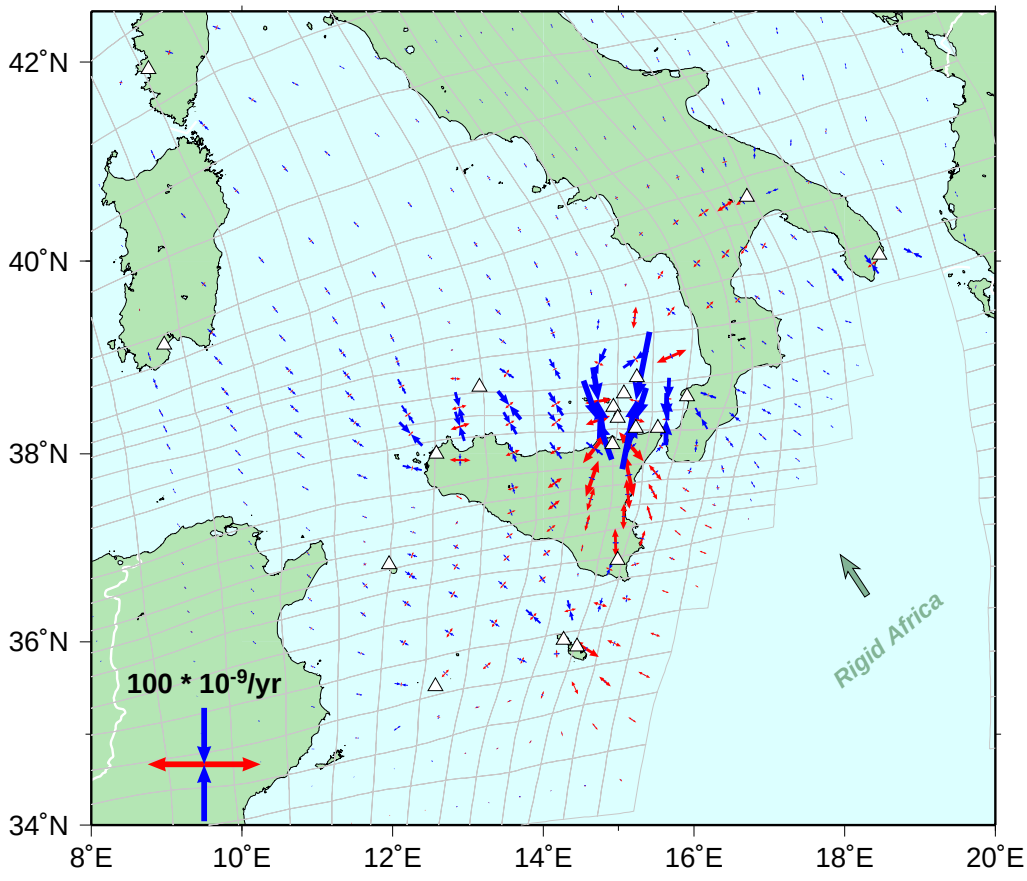

Figure 4.4: Continuous strain rate field derived from the GPS velocities in Fig. 4.2 with the method of *Haines and Holt* [1993]. Shown are directions of minimum and maximum horizontal strain in each cell of the model grid, for Ionian motions according to scenario T1 (Fig. 4.3). Strains for a model where the Ionian is constrained to move as in T2 are almost indistinguishable.

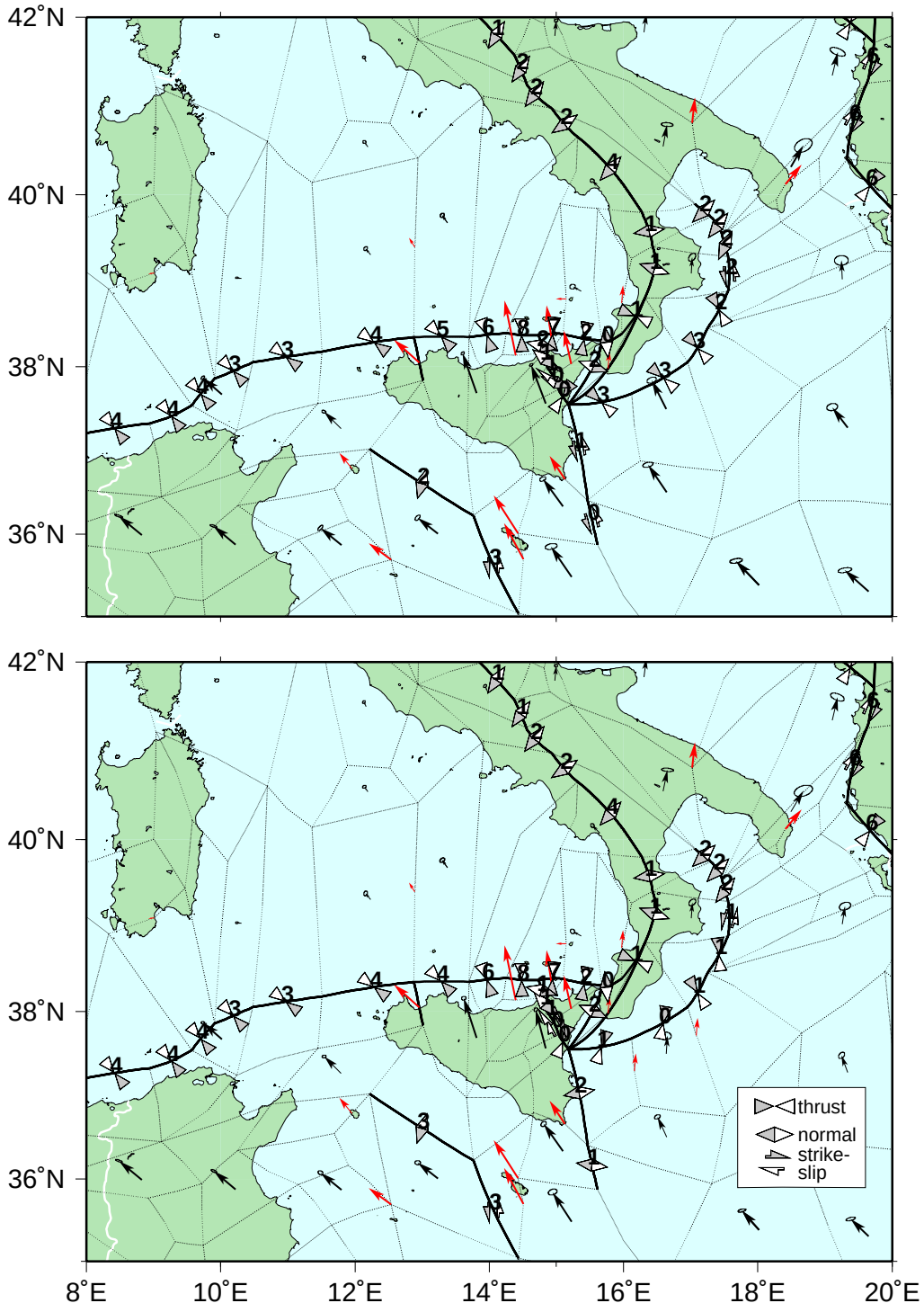

Figure 4.5: Fault-localized slip rates computed with an elastic finite-element model [*Lundgren et al.*, 1995, 1998] driven by the GPS observations (in red, assigned to close-by nodal points of the grid shown by thin dotted lines) and African plate motion. The resulting finite element displacements with uncertainties are shown by the black arrows, the fault slips by the double white (hanging wall) and grey (foot wall) arrows with numbers that show the slip rates in mm/yr. The model covers the whole Mediterranean, but only the part covering our region of interest is shown. The rest is unchanged from [*Lundgren et al.*, 1998]. Two representative models are shown: (a) with Ionian motions according to scenario T1, (b) with Ionian motions according to scenario T2 prescribed by adding two arrows with PORO motions south of the Calabrian trench.

4.4.2 Tectonic strain and slip rates from geodetic data

The strain rate field is dominated by compression around the Aeolian Islands with strain rates reaching 120 nanostrain/yr (Fig. 4.4). If localized along one thrust fault this implies slip rates of up to 7-8 mm/yr (Fig. 4.5). Because this compression exceeds the African motions of the other Sicilian stations, extension between northeastern Sicily and Noto is required. If distributed, this extension is on the order of 50 nanostrain/yr. When localized along the faults in the elastic plate model, the Aeolian velocities can add 1-2 mm/yr of transtension along a fault oriented like the Tindari-Letojanni system and rotate the extension along a fault oriented like the Messina Straits. Geological data indicate uplift rates in the Messina Straits of 0.9-1.1 mm/yr [*Bordoni and Valensise*, 1998; *Westaway*, 1993; *Catalano and De Guidi*, 2003]. To what extent these reflect the local extension is unclear. There is no information available for slip rates along the Tindari-Letojanni fault or others in the region. The geodetic data do not constrain the deformation to be limited to these two faults and distribution of the motions across more faults is likely.

Aside from the unusual strain rates associated with the Aeolian velocities, the geodetic velocities imply a zone of higher strain rates in the southern Tyrrhenian between the northern coast of Sicily (TRAP) and Ustica (USTI) and Stromboli (STRM). Strain rates here are 30-60 nanostrain/yr depending on the width of the zone over which they are accommodated. Equivalent fault slip rates are 3-4 mm/yr. Together with faults further south inside Sicily, slip rates amount to full Africa-Europe convergence. The African motion of Trapani localizes most of the convergence between Africa and Europe north of Sicily. Even without the large Aeolian velocities, 2 ± 1 mm/yr of extension occurs in the Messina Straits due to the jump in the convergent boundary from south of Calabria to north of Sicily. The rest of the Tyrrhenian Sea is a low strain rate area (<10-20 nanostrain/yr). Strain rates along the southern margin are at the higher end of this range, due to the small velocities of the stations USTI, PORO and STRM relative to Europe.

The geodetic data imply some low strain-rate intraplate deformation (about 20 nanostrain/yr, or slip rates of 1-3 mm/yr if localized) in Sicily and its Strait. Between Malta-Gozo and Lampedusa there is a small amount of extension, consistent with NW-SE striking extensional faults within the Strait [*Boccaletti et al.*, 1987; *Argnani*,

1990]. Strain around Pantelleria may be influenced by caldera deflation [*Bonaccorso and Mattia*, 2000]. A small amount of compression is observed between southeastern Sicily and Malta-Gozo. The curved elastic model fault along the front of the Gela nappe accommodates up to 3 mm/yr deformation of various styles. Motion of several faults in Sicily will be projected onto this single model fault south of the Kabilo-Calabrian front, and its continuity in the elastic model will lead to high estimates of motion along it. Given the geologic information on the cessation of most thrusting and rotation inside the Gela Nappes by about 0.8-0.5 Ma, it is likely that Sicily's internal strain is on the low side of the range. We use tectonic slip rates of 0.5-1 mm/yr for the seismic potential analysis.

The Calabrian stations Monte Poro and Reggio Calabria move northwards, rather than southeast as would be expected for roll-back of the Calabrian trench. In the continuous strain rate model, Calabria is dominated by compression due to the converging Aegean and African plates. Only the differential motion between the Apulian stations MATE and SPEC and the Calabrian stations requires some more or less east-west oriented extension. Combining geological, geomorphological and structural evidence, *Tortorici et al.* [1995] and *Monaco and Tortorici* [2000] inferred vertical slip-rates as a result of arc-perpendicular extension of 0.6-1.5 mm/yr in Calabria. If in the elastic model any extension is prescribed within Calabria, it is compensated by extra compression along the trench.

A lack of stations south of the trench leads to poor geodetic constraints on the localization of strain in this region, but we test two cases. In the continuous strain rate model the two cases are hardly distinguishable because of the smoothing that occurs in areas of low data distribution. Thus only case T1 is shown in Fig. 4.4. In the elastic model with faults (Fig. 4.5), scenario T1 gives 2-4 mm/yr of convergence along the trench where oriented perpendicular to the African motion. Along the north-south to northwest-southeast oriented eastern end of the trench 2.5-3.5 mm/yr of strike-slip and extension is projected (motion between Calabria and Adria). The internal deformation scenario T2 results in a more north-south directed trench convergence of 0.5-1 mm/yr, depending on how much of the area south of the trench is constrained to move with Calabria. In addition to some motion along the trench, case T2 would localize 1-2 mm/yr of extension between Calabria and Noto on faults that parallel the southeastern

Sicilian coast. Without explicitly prescribed internal deformation, the difference in motion between rigid Africa and Noto results in 0-1 mm/yr of left-lateral motion along faults of this orientation.

The relative motion between Matera and the Sicilian and Tyrrhenian stations is consistent with the Apenninic triangulation strain rates of up to $100 \pm 30 \times 10^{-9}$/yr [*Hunstad et al.*, 2003], or a slip rate of 3-4 mm/yr in the southern Apennines. The westward convergence of the Aegean stations and NE motion of MATE (and SPEC) imply compression of up to 40 nanostrain/yr in the Strait of Otranto. No fault in this location was introduced in the finite element model, because none has been clearly recognized. As a result, it shows up as one of the very few regions with internal strain in the elastic model.

4.5 Seismicity

Many structures in the southern central Mediterranean generate seismicity (Fig. 4.6). The most prominent is the Apenninic belt that is responsible for the events up to $M = 6.9$. Between 99 A.D. and today, 19 events with $M \geq 6$ have been recorded. The largest occurred in 1456 and 1857 with $M = 6.9$, and in 1694 and 1980 with $M = 6.8$. Apenninic events predominantly reflect extension perpendicular to the orogen. Smaller strike-slip events occur in the southern Apenninic foreland, including the destructive $M = 5.6$ and $M = 5.7$ events of 2002 (Fig. 4.7).

Several moderate historical earthquakes have affected the northern coast of Sicily. Based on intensity maps, the largest event, in 1823, has been assigned a $M = 5.9$. Other moderate events were the 1726 $M = 5.6$ and the 1940 $M = 5.4$ earthquakes. Since a better coverage of seismic stations was achieved, a zone about 40 km offshore has been recognized as seismically highly active. Since 1979, at least 9 events with $M \geq 5.0$ have occurred. The RCMT Catalogue [*Pondrelli et al.*, 2002] contains 9 events with $M \geq 4.5$ for the year 1998 alone. The Harvard CMT Catalogue locates the 2002 $M = 6.0$ within this zone. The high current levels of seismicity and geodetic strain accumulation together with the isoseismals of some of the historic events (e. g., the 1823 event, DOM4.1 intensity data base, http://emidius.mi.ingv.it/DOM/, *Monachesi and Stucchi* [1997]) that span the entire coastal region, suggest to us that at least some of the

moderate historical earthquakes may have occurred in this offshore active zone instead of along the coast (See Section 4.7.1). Such a shift in location would also increase the size of these historic events.

Central and western Sicily have a relatively low level of activity, but are not free of damaging earthquakes. In 361, a $M = 6.6$ shook central Sicily. In 1968, the western Sicilian Belice sequence contained besides the main $M = 6.1$ event, six other shocks with $5 < M < 5.4$. No surface rupture has been mapped, but the hypocentres of these events are distributed between 36 and 1 km depth along the roughly N-dipping plane defining a buried thrust. The pure and oblique thrusting mechanisms all relate to approximate N-S shortening [*Monaco et al.*, 1996].

Most of northeastern Sicily and its offshore region are seismically active. Offshore, west of the Tindari-Letojanni fault system, crustal earthquakes with depths < 40 km are associated with the back-thrust. East of it, offshore crustal seismicity is almost absent and intermediate and deep events within the Benioff zone are recorded. The largest events recorded around the Aeolian Islands are the dextral $M = 6.1$ event in 1978 and the $M = 5.7$ thrust event in 1980. Onshore, a strong concentration of events is associated with the Etna. The non-volcanic events display a range of mechanisms [*Frepoli and Amato*, 2000] (Fig. 4.7). In northeastern Sicily, *Guidi et al.* [2003] carried out a leveling survey of dated Holocene marine notches along the coast of Taormina, at the southern termination of the Taormina Fault. Their survey suggests the occurrence of three major seismic events in the past 5000 years with $M = 6.5 - 7.0$, at about 5000 years B.P., at 3200 years B.P. and possibly the 853 A.D. They interpret the Taormina fault as a prolongation of the extensional zones in Calabria and the Messina Straits, producing earthquakes with a recurrence of more than 1500 years. The largest event recorded in the seismically strongly active Messina Straits was a $M = 7.2$ in 1908. This event caused 70 cm subsidence along coastline of Sicily and 50 cm in Calabria and is thought to have had an east-west extensional mechanism [*Monaco and Tortorici*, 2000].

In southeastern Sicily, several historical seismic events, e.g., the 1169 and 1693 earthquakes, reached $M \sim 7$. The 1693 event was felt in southern Italy and as far south as Malta, and along the coastal region of Tunisia. It devastated the entire southeastern part of Sicily and killed about 54000 people [*Boccone*, 1697; *Baratta*, 1901]. A responsible fault structure for this event has not been identified. It has been located either

on land, along the northern boundary of the Hyblean Plateau [*Mulargia et al.*, 1985; *Boschi et al.*, 1995b], which would make it a thrust event, or offshore along the Malta Escarpment [*Postpischl*, 1985; *Piatanesi and Tinti*, 1998], supposedly with a normal faulting mechanism. *Bianca et al.* [1999] relate the 1693 event to normal faulting activity in the Ionian, in response to approximately ESE-striking extension. They estimate a recurrence interval of 550 ± 50 yr, based on events that occurred in 122 B.C., 363, 1169 and possibly in 797 A.D. All these events severely damaged all of eastern Sicily, generating large tsunamis recorded along the entire Ionian coast of the island. In the recent catalogue (Fig. 4.7) only one $M \geq 5$ strike-slip event is recorded in this area.

Calabria has been struck in the past by some of the most catastrophic earthquakes in the Mediterranean region. Between 1600 and 1900, 19 events with $M \geq 6$ have been recorded, five of them during the year 1783 alone, the largest with $M = 6.9$. The largest events occurred in western Calabria in March 1638, in the Crati Basin [*Galli and Bosi*, 2003], and in 1905, at Mt Poro with $M = 7$. Almost all the Calabrian events recorded are concentrated in less than three centuries between 1638 and 1908, and they often occurred within a few months or years of one another (e. g., March and June 1638, February-March 1783, and 1905-1908) or within one century (southward migrating sequence of Crati Valley of 1767 $M = 5.9$, 1835 $M = 6.0$, 1854 $M = 6.2$ and 1870 $M = 6.2$). In southern Calabria, all major earthquakes have been related to primary NE-SW normal faults [*Tortorici et al.*, 1995; *Jacques et al.*, 2001; *Galli and Bosi*, 2003]. The tectonic regime of northern Calabria is still poorly constrained. In eastern Calabria, a few strong earthquakes have been recorded: the 1638 (June), $M = 6.6$, 1832 $M = 6.5$ and the 1836 $M = 6.2$ event. No causative faults for these events have been identified. Based on palaeo-seismological studies, *Galli and Bosi* [2003] shifted the epicenter of the 1638 event westward. Since 1908, Calabria is seismically quiet. Under Calabria, a 200 km wide, 40-50 km thick Benioff zone starts, which dips with about 70° beneath the Tyrrhenian and reaches a depth of 450 km [*Selvaggi and Chiarabba*, 1995]. We will not consider these intraplate subduction events further in this paper.

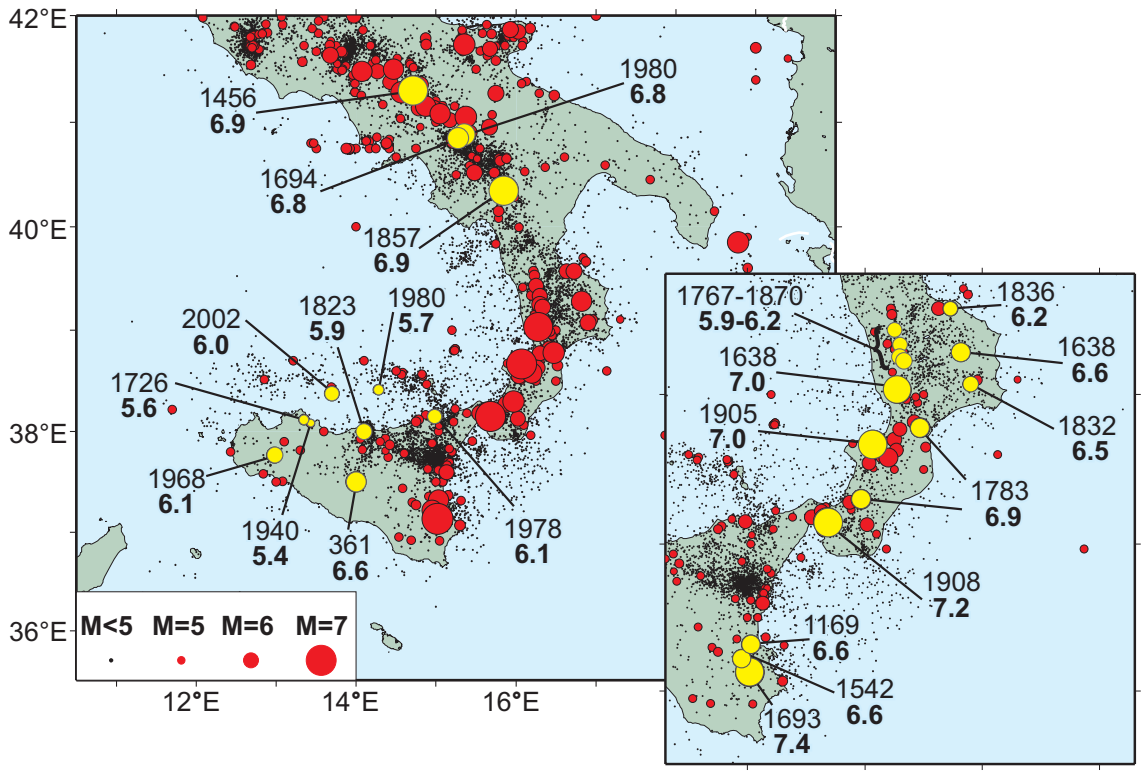

Figure 4.6: The distribution of southern Italian seismicity with the largest events in dark grey, and the significant events discussed in the text in light grey and marked with their date and estimated moment magnitude. The seismicity data are a compilation from the historical CPTI catalogue (217 BC - 1981) [*Working Group CPTI*, 1999] and the instrumental CSTI (1981-1996) [*Instrumental Catalog Working Group CSTI*, 2001].

4.6 Seismic strain

4.6.1 Style of seismic and tectonic strain

The deformation styles from the focal mechanisms are more easily compared with the geodetic strain rates when converted to directions of maximum and minimum horizontal strain. This is done by a Kostrov summation of the moment tensor data (Fig. 4.7) on the same grid used in the continuous geodetic strain model (Fig. 4.4). Fig. 4.8 shows the resulting seismic deformation styles (not amplitude). In spite of the brevity of the moment tensor catalogues and the predominantly small events, seismic and geodetic strain rate directions are very similar in much of the region.

Geodetic strain rate patterns are consistent with seismic extension perpendicular to the Apennines and some strike-slip faulting east of the chain. The Africa-European convergence north of Sicily is consistent with the compressional mechanisms in the offshore belt. These mechanisms mostly have a shallower southward dipping nodal plane

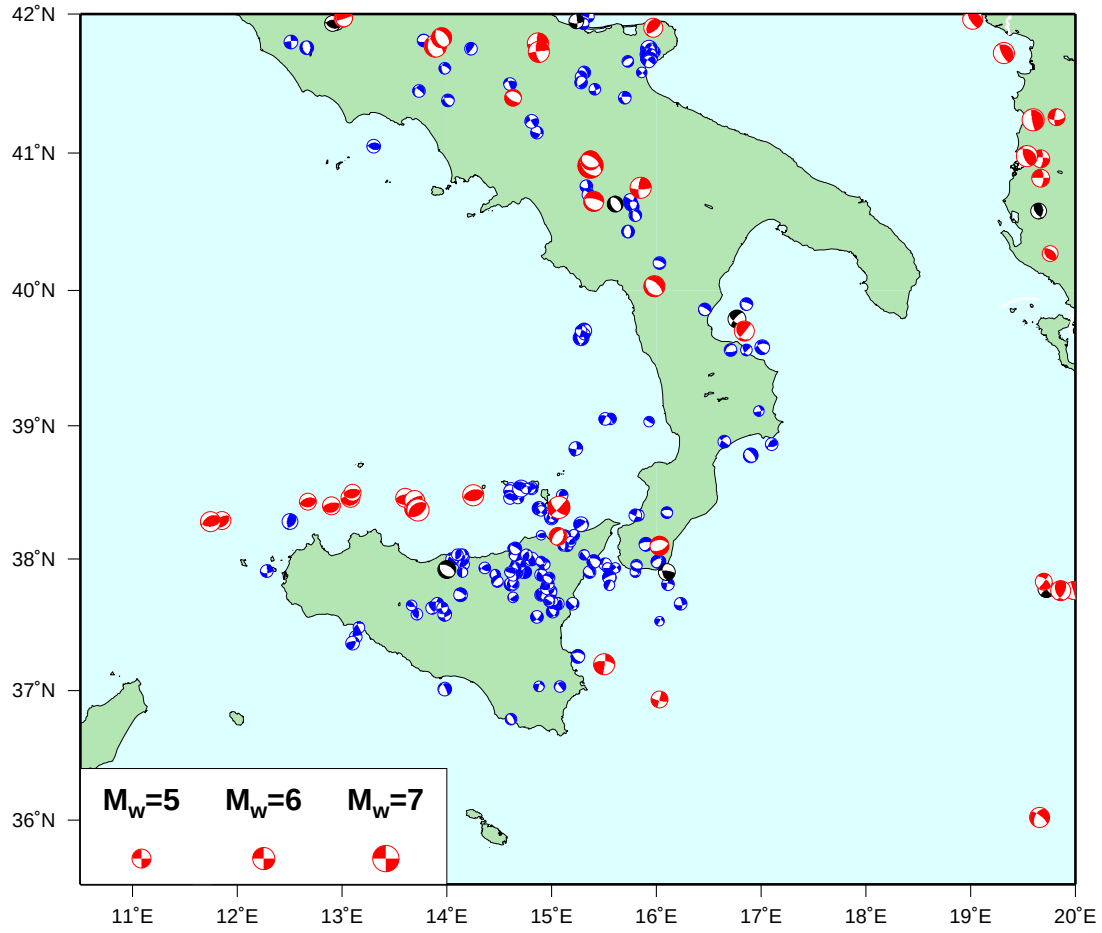

Figure 4.7: Southern Italian focal mechanisms for events since 1977. Moment tensor solutions are from the Harvard Centroid Moment Tensor (CMT) catalogue (http://www.seismology.harvard.edu, *Dziewonski et al.* [1981]) between January 1977 and September 2003 for events with $M_w > 5.5$, supplemented by mechanisms for smaller events ($4.1 < M_w < 5.2$) from the European-Mediterranean Regional Centroid Moment Tensor (RCMT) catalogue [*Pondrelli et al.*, 2002] and moment tensors from the Swiss Seismological Survey (*Braunmiller et al.* [2002] and http://www.seismo.ethz.ch/info/mt.html)and 173 focal mechanisms compiled by *Frepoli and Amato* [2000] for small earthquakes ($2.5 <$ Mw < 4.4) in southern Italy and Sicily.

compatible with our interpretation of this zone as a back-thrust. Seismic and geodetic directions of compression and strike slip faulting in central and western Sicily as well as in the Sicily Channel are the same. Focal mechanisms in the Aeolian Islands east of Alicudi and Filicudi reflect both the dextral character of the Tindari-Letojanni system and north-south compression consistent with the geodetic deformation. Such agreement between seismic and tectonic styles of deformation has also been found in several other regions around the world [*Amelung and King*, 1997; *Kreemer et al.*, 2000; *Jenny et al.*, 2004].

Discrepancies between seismic and geodetic styles of deformation may indicate slip partitioning in which one component of deformation is mostly aseismic [*Jenny et al.*, 2004]. The very strong geodetic compression with a small strike-slip component around the Aeolian Islands is not clearly represented in the seismicity (Fig. 4.8). Instead, seismic strains mainly reflect strike-slip, consistent with NNW-SSE striking faults in the area. The low strength of the warm and thin southeastern Tyrrhenian may cause most of the compressional strain to be released aseismically. More difficult to interpret is the discrepancy in style in northeastern Sicily, where a few focal mechanisms have north-south axes of tension as the geodetic strain rates, but many reflect east-west extension. Of the events to the southwest of Calabria, some have strike-slip mechanisms with compressional axes approximately parallel to African motion, while a few mechanisms in northeastern Calabria show east-west compression more consistent with influence from the advancing Aegean.

4.6.2 Estimating catalogue moment rates

To estimate $\dot{M}_0^{cat}$ we use the historical CPTI (Parametric catalogue of Italian earthquakes, http://emidius.mi.ingv.it/CPTI/, *Working Group CPTI* [1999]) for the time 217 BC - 1981 and instrumental CSTI (Instrumental catalogue of Italian earthquakes, *Instrumental Catalog Working Group CSTI* [2001]) for the period 1981-1996. Completeness intervals for different magnitude ranges were defined using the method of *Mulargia et al.* [1987]. The data does not allow unequivocal assessment of completeness, especially for the large magnitudes. Therefore, we give a range of completeness intervals for each magnitude window (Table 4.1). Although completeness levels probably vary regionally, the data do not permit defining spatially varying intervals. The estimated uncertainties include those associated with possible regional variation. In addition to completeness uncertainties, we use magnitude uncertainties of ± 0.2 for the time period 1981-1996, ± 0.25 for 1911-1981, ± 0.35 for 1500-1911 and ± 0.5 for pre 1500 events. We convert the apparent magnitude M_a of the CPTI and CSTI catalogues into moment rate $\dot{M}_0$ in Nm/yr, using the following equation [*Working Group CPTI*, 1999]:

$$log_{10}\dot{M}_0 = 22.9 - 0.47 \times M_a + 0.14 \times M_a^2 \tag{4.1}$$

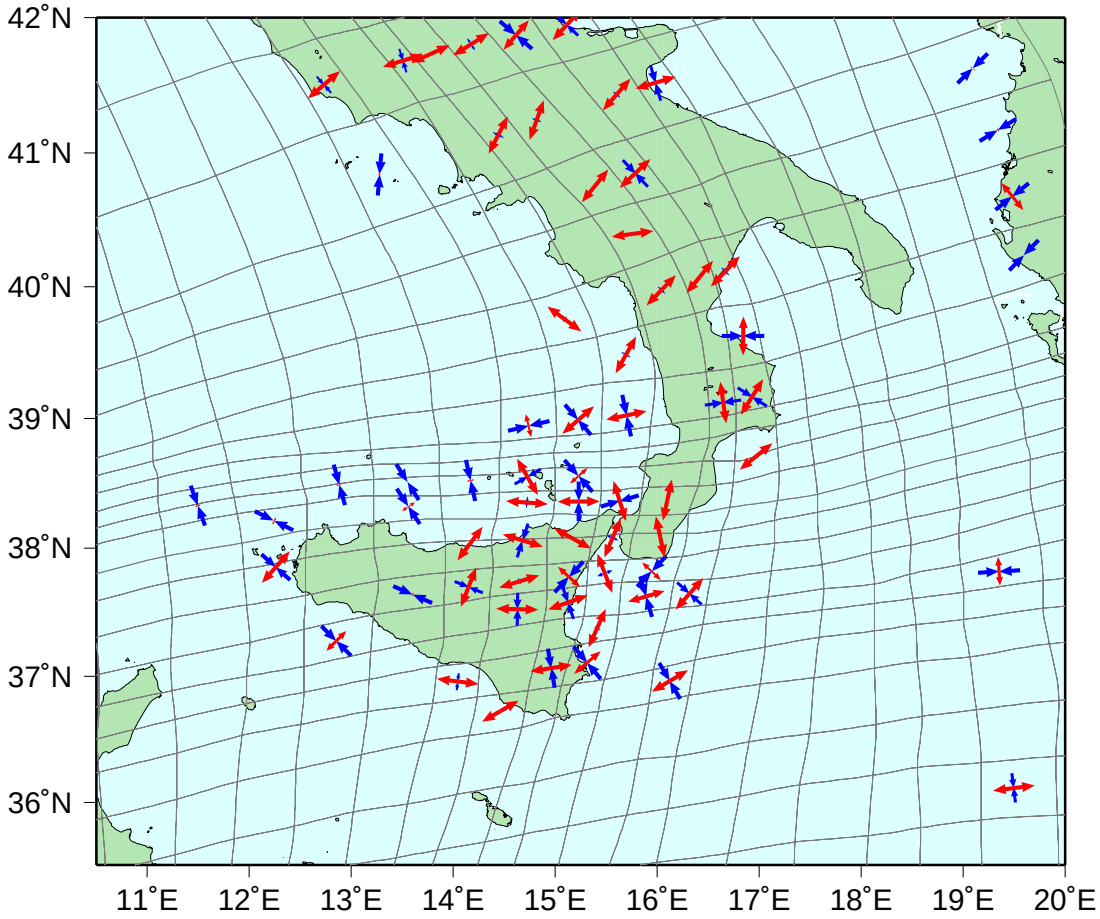

Figure 4.8: Seismic strain rate style (not amplitudes) shown as the directions of maximum and minimum horizontal strain rate. The styles are obtained by a Kostrov summation of the moment tensors in Fig. 4.7 within the same grid cells as those used for the continuous GPS strain rate field (Fig. 4.4), to facilitate a comparison.

The moment magnitude M_w (in Nm)is determined as [*Hanks and Kanamori*, 1979]

$$M_w = \frac{2 \times log_{10}\dot{M}_0}{3} - 6.03 \tag{4.2}$$

All magnitudes mentioned in this paper corresponds to M_w, unless noted otherwise.

The largest uncertainties in the southern Italian catalogue moment rate $\dot{M}_0^{cat}$ are due to the uncertainties in earthquake location. For northern Sicily and its offshore area and southeastern Calabria and its offshore region, we determine several alternative $\dot{M}_0^{cat}$, based on different assumptions of whether certain events were on- or offshore. When we shift ambiguous epicenters of events offshore, the magnitude of these events is increased using published intensity attenuation relationships for Italy. The intensity distribution of historical earthquakes is taken from the intensity database of damaging earthquakes

in the Italian area (DOM4.1, http://emidius.mi.ingv.it/DOM/,*Monachesi and Stucchi* [1997]). *Gasperini* [2001] computed the average intensity attenuation relation for all of Italy using the following formula:

$$I_0 - I = 0.52 + 0.56 \times min(D, 45) + 0.0217 \times max(0, D - 45) \tag{4.3}$$

where I_0 is the epicentral intensity, I is the intensity at site, $D = sqrt(R^2 2 + 10^2)$, the hypocentral distance (the source is kept fixed at 10 km of depth) and R the epicentral distance. Attenuation may vary laterally [*Carletti and Gasperini*, 2003]. If we extrapolate the attenuation properties of the shorelines, which appear less attenuating to the offshore regions (which are not well covered by source-receiver paths), the regionalized equation is:

$$I_0 - I = 0.445 + 0.530 \times min(D, 45) + 0.0176 \times max(0, D - 45) \tag{4.4}$$

This means that for events located about 40 km north of the coast, the observed intensities along the coast would underestimate the epicentral intensity by about 2.5-3. The moment magnitude would be underestimated by about 1.1-1.3 units, when computed from epicentral intensity only. If the macroseismic magnitude is computed using the extent of felt areas [*Gasperini and Ferrari*, 2000], the underestimate of magnitude is less, for geometrical reasons. Based on these considerations, we estimate the magnitude correction for relocating an event about 40 km off the coast to be 0.6-1.2 magnitude units.

A range of $\dot{M}_0^{cat}$ is calculated from the historical catalogue taking into account the uncertainties in magnitude, location and completeness length (Table 4.1). Magnitude and completeness length are randomly chosen within the uncertainty range. In areas 1 and 6, the effect of the uncertainty in whether events were on- or offshore is also included. Then $\dot{M}_0^{cat}$ is calculated 10000 times. The resulting distributions are close to Gaussian. The listed uncertainty bounds for $\dot{M}_0^{cat}$ (Table 4.2) encompass 2/3 of the distributions (i. e., approximately one standard deviation).

Table 4.1: Completeness intervals.

date (year)	M_w range
$\geq 0 \pm 500$	≥ 7.5
$\geq 1000 \pm 200$	≥ 7.0
$\geq 1475 \pm 125$	≥ 6.5
$\geq 1625 \pm 100$	≥ 6.0
$\geq 1780 \pm 80$	≥ 5.5
$\geq 1870 \pm 40$	≥ 5.0
$\geq 1885 \pm 20$	≥ 4.5
$\geq 1983 \pm 5$	≥ 3.5

4.7 Estimating seismic potential

We estimate the ratio between seismic and geodetic (tectonic) deformation for the seven main seismotectonic regions (Fig. 4.9). From this ratio, we define the corresponding seismic potential, expressed in terms of the recurrence time of $M_w \sim 7$, within each source zone. Although source zones used in hazard studies are often smaller than the zones used here, this is the maximum level of detail that we can achieve with the available data. Each of the seven areas is characterized by a uniform style of deformation as described in Section 4.3. The southern Apennines have been studied in detail by other authors [*Pantosti and Schwartz*, 1993; *Frepoli and Amato*, 2000; *Ghisetti and Vezzani*, 2002] and we only discuss this region for reference here.

We compare the catalogue and geodetic deformation rates in either zone in the distributed form of moment rates, or in the localized form of slip rates. For the summary in Table 4.2 and Fig. 4.10, the ratio of seismic catalogue deformation and tectonic deformation rates is expressed as the ratio of the seismic versus tectonic slip rates, $\dot{D}^{cat}/\dot{D}^{tect}$. To obtain the average slip rates from $\dot{M}_0^{cat}$, we use a shear modulus $\mu = 3.5 \times 10^{10} Nm^{-2}$, an average 15 km for the thickness of the seismogenic zone, equivalent to the depth above which most of the seismicity is concentrated, and an estimated length of the assumed main fault within the source zone (Table 4.2, Fig. 4.9). The elastic shell model directly gives estimates of the tectonic slip rates $\dot{D}^{tect}$. Continuous strain rates are converted to moment rates using the formula of *Savage and Simpson* [1997] to the estimate scalar moment rates from the horizontal strain rates within each grid cell of the model.

$$\dot{M}_0^{tect} = 2\mu A dMax(\mid \dot{\epsilon}_1 \mid, \mid \dot{\epsilon}_2 \mid, \mid \dot{\epsilon}_1 + \dot{\epsilon}_2 \mid) \tag{4.5}$$

where A is the considered deformation zone's area, d is the seismogenic thickness and $\dot{\epsilon}_1$ and $\dot{\epsilon}_2$ are the principal horizontal strain rates. We use their formula because in some zones the styles are ambiguous. Assuming homogeneous $\dot{M}_0$ in each small grid cell, $\dot{M}_0^{tect}$ in the larger source zones are determined by summing the geodetic moment rates of all grid cells contained in them.

The seismic and geodetic strain rates together with the magnitude-frequency distribution of the seismicity are used to define, for the set of source zones, the $a-$, $b-$value and M_{max} of the truncated Gutenberg-Richter (TGR) distribution. The magnitude-frequency data is shown in Fig. 4.11 (black dots). The grey area represents the corresponding uncertainty range, that is defined by simulating 10'000 catalogues, as described above. Events with $M_w < 4.5$ and with $M_w > 4.5$ are from the CSTI and CPTI catalogues, respectively. In several zones, the magnitude-frequency distribution of the data shows a dip for $M_w = 4.5 - 5$. Although uncertainties in converting macroseismic intensity to magnitude may contribute to an irregular magnitude-frequency distribution, this dip suggests that the CPTI catalogue is more incomplete for small magnitudes than accounted for by our uncertainties in completeness length. The black curves in Fig.4.11 represent TGR distributions for three different amounts of seismic deformation, $\dot{D}_{seis}$, as a fraction of the upper bound tectonic deformation, $\dot{D}_{tect}$ (Table 4.2). For example, for the southern Tyrrhenian back-thrust zone, TGR curves are shown for seismic deformation that amounts to 10 %, 30 % and 100 % of 4 mm/yr of tectonic deformation. For areas 4 and 6, $\dot{D}^{tect}$ for tectonic scenario T2 is used. The $a-$value is adjusted to accommodate the different amounts of seismic deformation. In all curves, the $b-$value is set equal to 1, as the data uncertainties are too large to constrain it better. M_{max} is also fixed, to a value between within the range M_{max}^{obs} and $M_{max}^{obs} + 0.5$. The variations in $a-$value for a range of M_{max} are summarized in Fig. 4.12. For a few areas (1,5 and 6) an additional red curve is shown, where the $a-$value is chosen to be compatible with the data and the M_{max} required for $\dot{D}_{seis} = \dot{D}_{tect}$ is determined. The various cases are discussed in more detail below. The seismic potential estimates for our best estimates of $\dot{D}_{seis}$ are shown in Fig. 4.13.

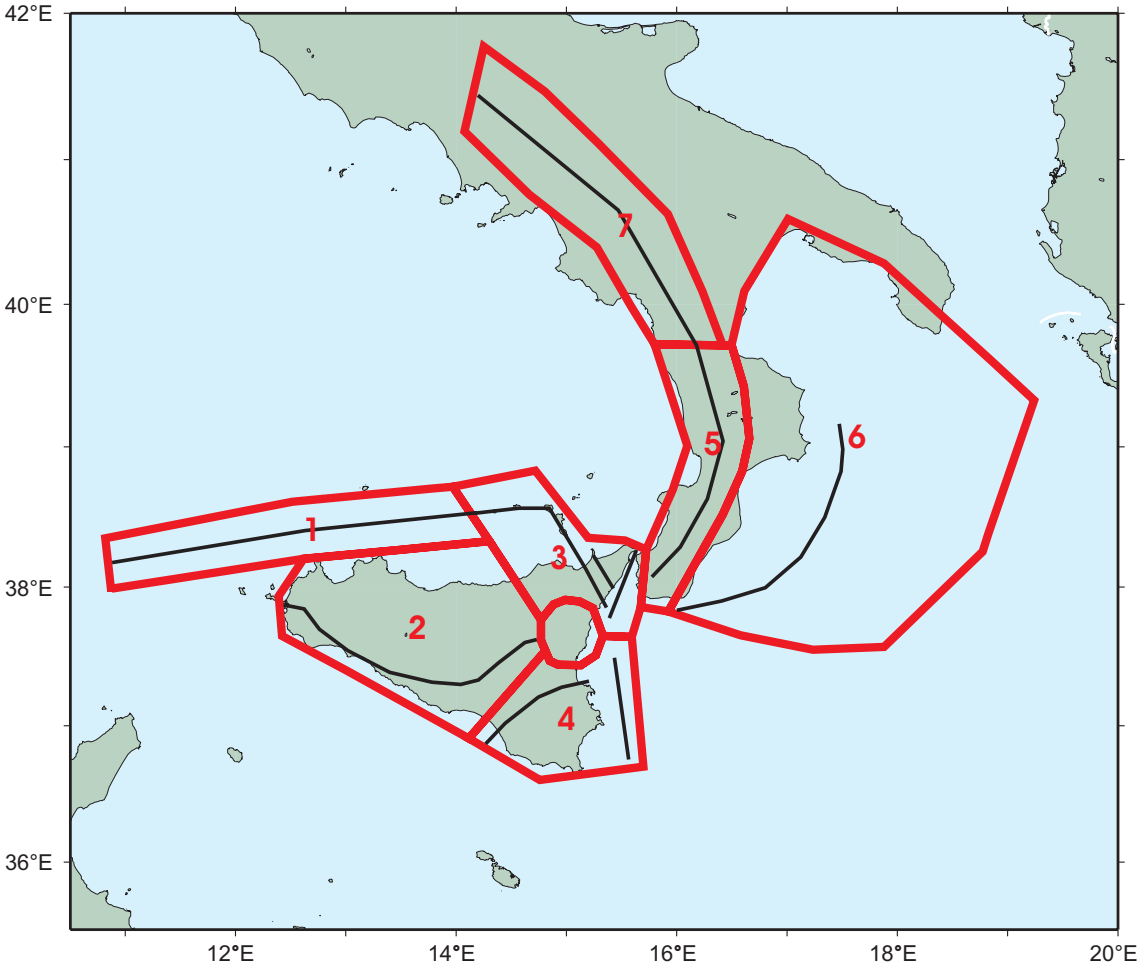

Figure 4.9: For our estimates of seismic potential we use seven large-scale source zones that span different tectonic regimes. The lines in the zones mark the faults assumed to convert moment rates into slip rates.

4.7.1 Back-thrust north of Sicily

The tectonic slip rate $\dot{D}^{tect}$ in the zone just north of Sicily is 3-4 mm/yr (Fig. 4.5). For $\dot{D}^{cat}$, three different cases are considered that give end-member estimates of $\dot{M}_0^{cat}$: S1) all the largest events along the northern coast of Sicily are attributed to the active Southern Tyrrhenian zone offshore (1726 $M = 5.6$, 1823 $M = 5.9$ and 1940 $M = 5.4$) and their magnitudes are increased accordingly, S2) only the oldest and less well localized event of 1726 $M = 5.6$ is attributed to the active zone offshore, and S3) only events within the actual southern Tyrrhenian source zone # 1 are taken into account. For the 1726 event, the DOM4.1 intensity database contains only one value, for the city of Palermo. The 1823 event was felt along the whole northern coast of Sicily. Although, the intensity database spreads the event over two different locations (for hazard calculations that need onshore sources), an location offshore would better fit these data. No damage

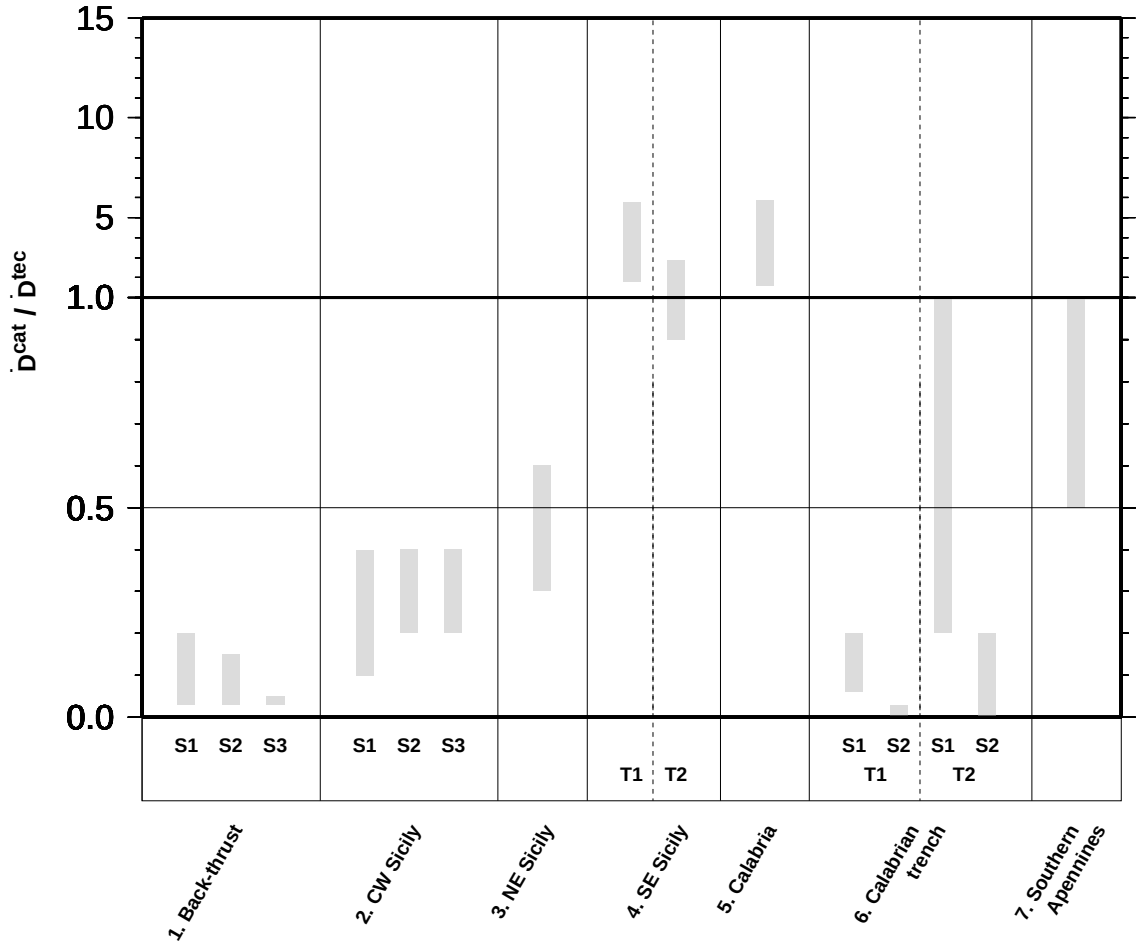

Figure 4.10: A comparison of slip rates estimated from the seismic catalogues ($\dot{D}^{cat}$) and the geodetic data ($\dot{D}^{tect}$) (see also Table 4.2) for the seven source zones in Fig 4.9. For some zones several scenarios are shown (Table 4.2). The results and implications for seismic potential are discussed further in the text.

from the 1823 event is reported on the islands of Alicudi, Filicudi and Ustica, where an offshore $M \sim 7$ event should have been felt. However, the intensity catalogue for these islands contains no records before 1892, while since then about ten events were felt, suggesting the database may be incomplete. The 1940 event has been located close to Palermo. According to the intensity database, it was felt only in areas close to the city and not on Alicudi and Filicudi. For none of these events have on-land faults been identified. Many moderate events have been recorded within the offshore active zone during the past twenty years (Fig. 4.7). Thus, we consider it likely that at least some of the northern Sicilian events, especially the 1823 earthquake, were located offshore.

Even with all larger events shifted offshore (case S1), the seismic historical catalogue reflects only up to 20 % of the tectonic deformation (Table 4.2). There are three possible interpretations of the discrepancy between seismic and geodetic deformation rates: 1)

the geodetically measured deformation occurs mainly through aseismic creeping, 2) the catalogue is not long (and/or complete) enough to contain the largest rarest event and/or 3) in the near future, the seismic hazard has to be considered high within this source zone. The recent seismic activity within this source zone suggests that at least part of the tectonic deformation is released seismically. The Gutenberg-Richter curve for a seismic deformation that amounts 10 % of the tectonic deformation ($\dot{D}^{seis}/\dot{D}^{tect} = 0.1$) underestimates the recurrence rate of $M_w < 4$ and $M_w > 6$. The curve for $\dot{D}^{seis}/\dot{D}^{tect} = 0.2$, fits the data better, although it implies that events smaller than $M_w 6$ are missing in the catalogue. An incomplete record is probably due to the offshore location of the source zone and the low density of seismic stations available to record activity within the southern Tyrrhenian. If all tectonic deformation is released seismically ($\dot{D}^{seis}/\dot{D}^{tect} = 1$), the catalogue significantly underestimates the seismic activity for the whole range of magnitudes. For $\dot{D}^{seis}/\dot{D}^{tect} = 1$ and an a-value representing the observed seismic activity (red curve in Fig. 4.11), a M_{max} up to 9.3 is needed. Such a large magnitude is not realistic. Therefore, we infer that a considerable part of the deformation is released aseismically.

We estimate the long-term seismic deformation rates to be around 30-40 % of the tectonic rates (Fig. 4.13). The seismic deformation is likely to lead to earthquakes with maximum magnitudes as large as 7.5. For a smooth magnitude-frequency distribution with a typical $b-$value=1, about 45 % of the total moment is released in events $\geq M_{max} - 0.5$. Taking a seismic slip rate $\dot{D}^{seis}$=0.2-2.5 mm/yr of which 45 % is released in M7 events, the expected recurrence time T_{rec}^{M7} would be 300-1200 yrs (Fig. 4.13). The occurrence of such large offshore events significantly increases the level of seismic hazard along the northern coast of Sicily compared to previous estimates (e. g., *Slejko et al.* [1998] and *Slejko et al.* [1999]). One can argue that the length of the catalogue is not sufficient to represent the long-term seismic activity and that a period of low seismic activity has been observed, which may be followed with a period of higher seismicity. If over the long-term, 100 % of the tectonic deformation would be released in earthquakes, the recurrence interval of $M_w \sim 7$ decreases to 100-250 years.

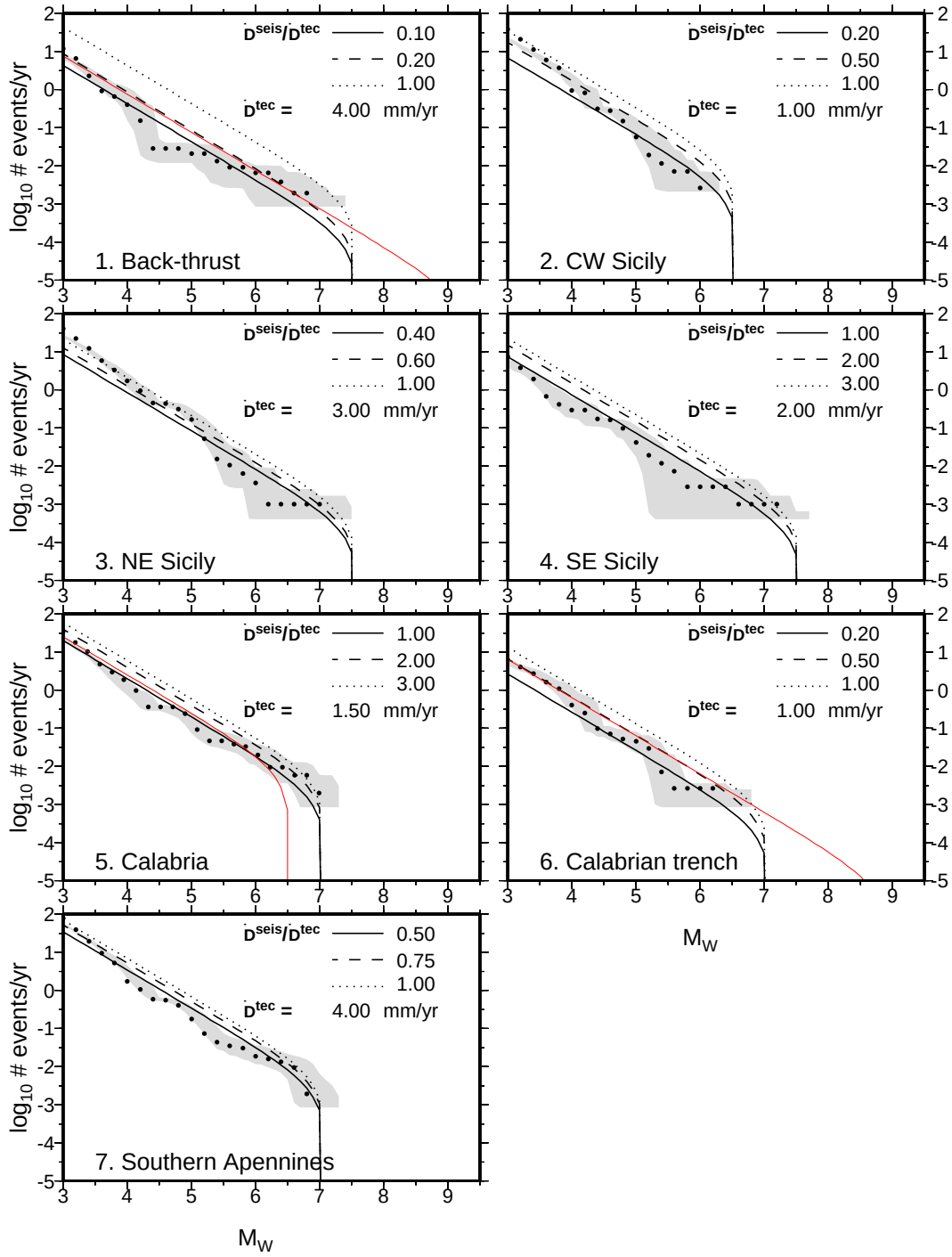

Figure 4.11: The log_{10} of the cumulative number of events versus magnitude for the historical (CPTI) and instrumental (CSTI) seismic catalogues (black dots). The grey area represents the uncertainty in event magnitude, location and completeness length of the catalogues. The lines represent truncated Gutenberg-Richter distributions with b=1 for different amounts of seismic deformation, $\dot{D}^{seis}$, given as a fraction of $\dot{D}^{tect}$. For the black curves, M_{max} was fixed to a value close to the maximum size observed and a was varied. For the red curves in areas 1, 5 and 6, a was fixed to be compatible with the data, $\dot{D}^{seis}$=$\dot{D}^{tect}$, and the required M_{max} is calculated.

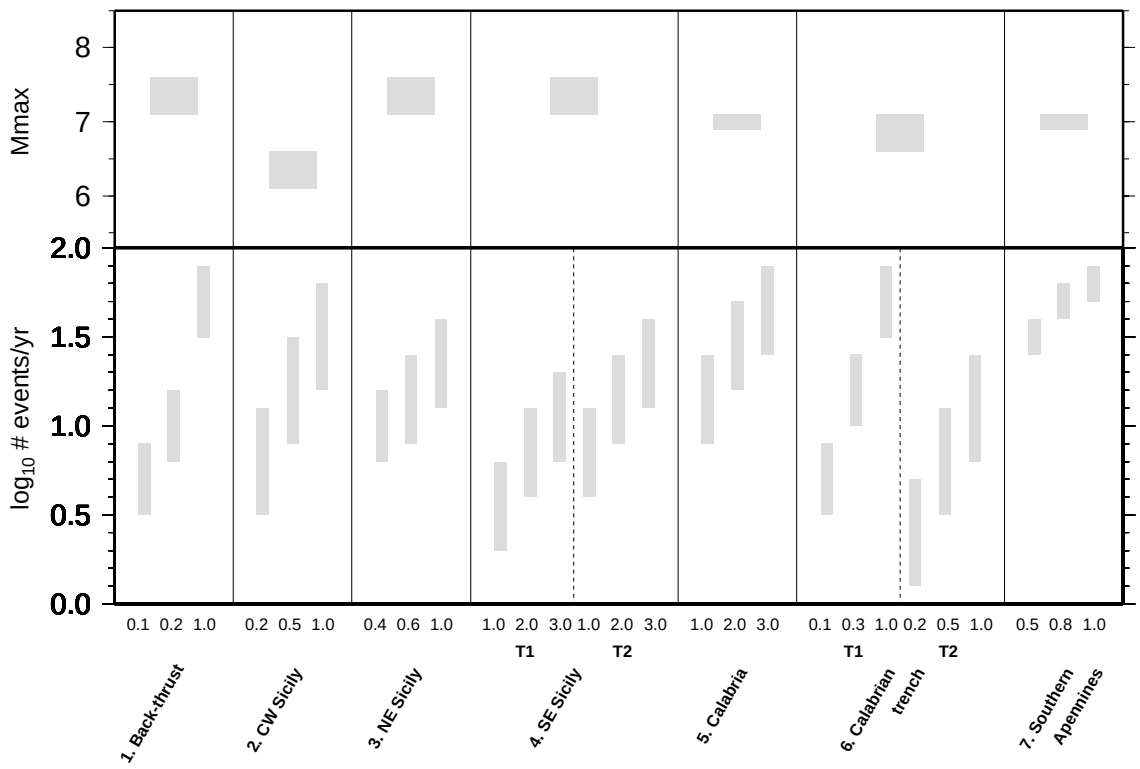

Figure 4.12: The log_{10} of the cumulative number of events at $M_w = 3$ ($a-$value). The $a-$values are determined for the M_{max} range shown in the upper panel and the same $\dot{D}^{seis}/\dot{D}^{tect}$ ratios as in Fig. 4.11 (marked along the horizontal axis). The tectonic scenarios T1 and T2 yield a different range of $a-$values in areas 4 and 6.

4.7.2 Central-Western Sicily

Consistent with our assignment of several of Sicily's historical earthquakes to offshore zone 1, three scenarios of central and western Sicilian seismicity are tested: in S1) the coastal 1726, 1823 and 1940 are not included within the source zone, in S2) only the 1726 event is not included, in S3) all events comprised within the source zone are used. Only between 10 and 40 % of the maximum tectonic deformation is reflected in the catalogue. In Fig. 4.11, the Gutenberg-Richter curve for $\dot{D}^{seis}/\dot{D}^{tect} = 0.5$ ($\dot{D}_{seis}$ =0.5 mm/yr) fits the magnitude-frequency distribution within the uncertainties of the data. The curve for $\dot{D}^{seis} = \dot{D}^{tect} = 1$ mm/yr would imply that the catalogue is largely incomplete, even for the largest magnitudes. This is improbable and suggests that, in this case, about half of the deformation is occurring aseismically. Alternatively, tectonic deformation rates are on the low end (< 0.5 mm/yr) of the estimates and are mostly accommodated seismically. In either case, we do not expect earthquakes much larger than those recorded to date, $M_{max} = 6.5$ may be up to 7, along distributed faults in central and western Sicily. We estimate that 20 to 100 % of the tectonic deformation is released seismically.

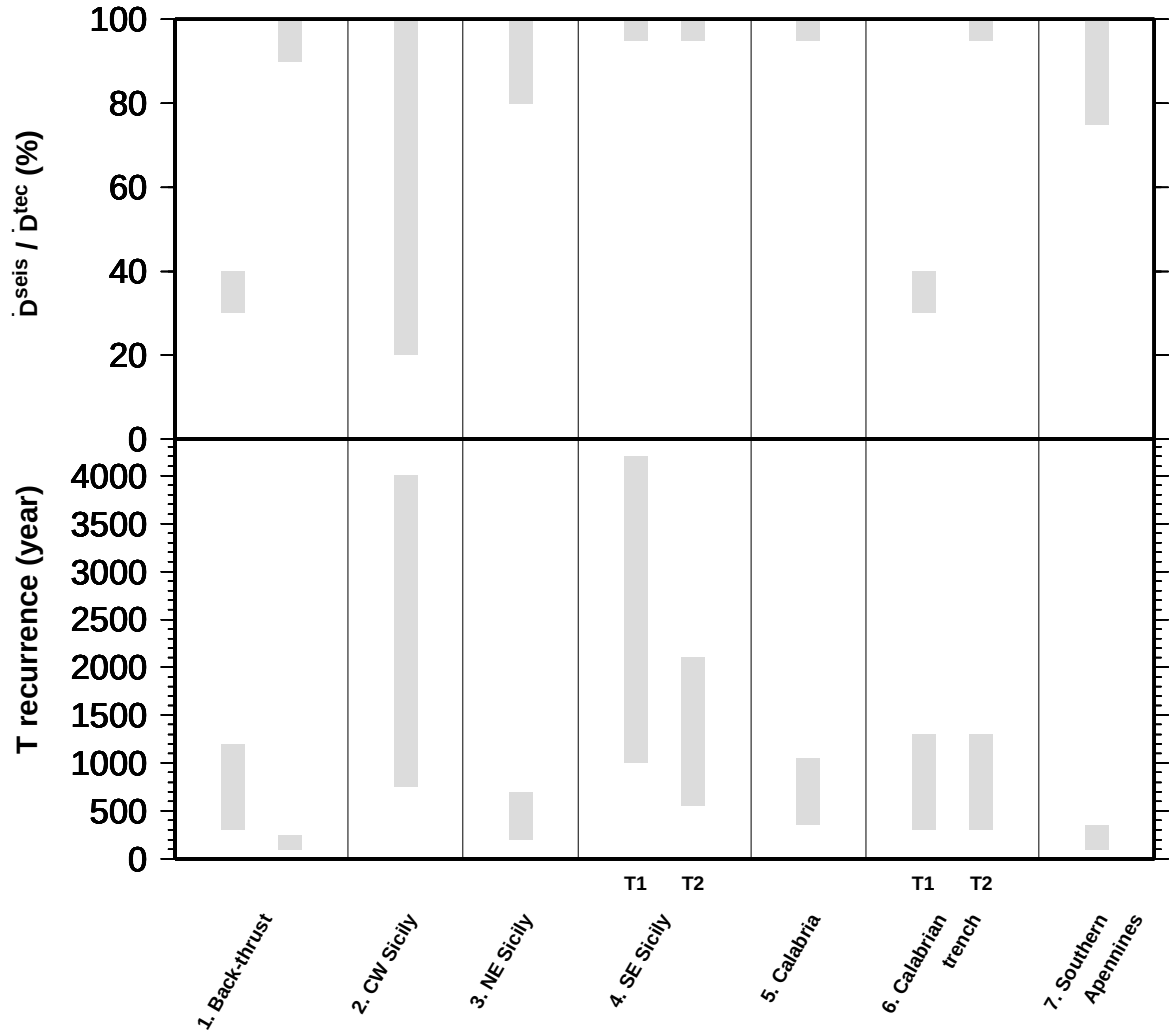

Figure 4.13: Seismic potential expressed as the recurrence time of $M_w \sim 7$ within each source zone (Fig. 4.9). Recurrence times are determined for our best estimates of $\dot{D}^{seis}/\dot{D}^{tect}$ (upper panel). $\dot{D}^{tect}$ are given in Table 4.2.

T_{rec}^{M7} would be long: 750 and 4000 years for $\dot{D}^{seis}$ = 0.2-0.5 mm/yr.

4.7.3 Aeolian Islands region and Northeastern Sicily

According to the geodetic data, this area is characterized by relatively high strain rates, translating into slip rates of up to 7-8 mm/yr along the Alicudi-Filicudi-Salina alignment. Along faults oriented like the Tindari-Letojanni fault system, 1 ± 1 mm/yr dextral to extensional motion is possible. Faults oriented like the Messina Straits can accommodate 2 ± 1 mm/yr of mostly extensional deformation. The $\dot{M}_0^{cat}$ in zone 3 reaches a maximum of $1.92 \cdot 10^{17}$ Nm/yr. When localized along the Tindari-Letojanni fault system (120 km length) and Messina Straits (75 km) only, this corresponds to $\dot{D}^{cat}$ =0.9-1.2 mm/yr. If we take the added tectonic slip rates for the two fault systems to be 2-3

mm/yr, the catalogue rates correspond to 30-60 % of the tectonic deformation. For the region overall, however, only a small amount of the total deformation is reflected in the seismic catalogue. Together with the observed discrepancy between the style of seismic and geodetic deformation, we take this as evidence that much of the deformation is, also on the long-term, released aseismically. In the warm and thin lithosphere around the Aeolian Islands long-term seismic deformation may be comparable to the current seismicity levels, i. e. very low. The expected levels of on-land seismic deformation may be up to 1 mm/yr along the Tindari-Letojanni fault system and up to 2 mm/yr in the Messina Straits region. Such seismic deformation rates are compatible with the magnitude frequency data (Fig.4.11). Thus, we estimate that most of the deformation (80-100 %) is released seismically along the Tindari-Letojanni fault system and the Messina Strait. This gives the region an overall seismic potential to generate $M_w \sim 7$ events every 250-700 years, with recurrence times of 900-1800 years along the dextral fault systems and 700-1000 years in the Messina Straits.

4.7.4 Southeastern Sicily

The large historical earthquakes recorded in southeastern Sicily add up to moment rates that equal or exceed those expected tectonically. Internal deformation of the African plate leads to $0 - 2$ mm/yr of motion on faults that parallel the southeastern Sicilian coast. Somewhat larger motions of a few mm/yr could be accommodated along thrust faults bounding the Hyblean block to the northwest. However, neither are the isoseismals of the historic events very consistent with buried thrust faults of such an orientation, nor is an onshore location consistent with the generation of tsunamis. Furthermore, there is no geologic evidence of recent fault activity within the Sicilian nappes. Assuming a fault length of 100 km, the catalogue moment rate corresponds to $\dot{D}^{cat} = 1.8 - 2.9$ mm/yr, resulting in a $\dot{D}^{cat}/\dot{D}^{tect} = 180 - 580$ % for scenario T1, and 90-290 % for T2. Thus, most of the tectonic deformation in this region appears to be seismic. A higher tectonic rate of 2 mm/yr, as in internal deformation scenario T2, is most consistent with the level of seismicity and consistent with the magnitude-frequency data (Fig. 4.11). In the absence of evidence of recent activity along the Malta Escarpment, the historic events would need to have ruptured other offshore faults. Recent focal mechanisms are consistent with a combination of extension in approximately east-west direction, as predicted for a N-S

oriented fault, and compression more-or-less in the direction of African convergence. This convergence may increase the overall tectonic slip rates for the area. Thus, we cannot conclude that the recorded seismicity released more than its share of tectonic deformation, although the excess of $M_w < 7$ compared to the $\dot{D}^{seis}/\dot{D}^{tect} = 1$ curve may suggest some clustering of seismic activity. Lower tectonic deformation rates than 2 mm/yr would require clustering. It can be expected that future activity levels of the offshore area will be at a similar level as $\dot{M}_0^{cat}$, with maximum events of up to M7.0-7.5 and T_{rec}^{M7} of 550-2100 years (Fig. 4.13).

4.7.5 Calabria

In Calabria, the geodetic data do not reflect the geologically and seismically observed extension. The velocities at Monte Poro and Reggio Calabria do not indicate any extension between the Tyrrhenian and Calabria, nor between the two Calabrian stations. Thus, any extension needs to occur south of the stations and given the range of plausible directions of motion of the Ionian, this extension needs to be compensated by compression further south. The geologically estimated vertical slip-rates [*Tortorici et al.*, 1995; *Monaco and Tortorici*, 2000] give extension rates of 0.6-1.5 mm/yr. $\dot{M}_0^{cat}$ yields average slip-rates of 2.4-3.5 mm/yr for an assumed fault length of 200 km (Table 4.2). Thus, the observed seismic deformation is 1.6 to 5.8 times larger than the tectonic deformation. This can explain the low level of seismicity observed in Calabria since 1905, as the past seismicity released strain accumulated in several times the span of the catalogue. In Fig. 4.11, the TGR curve is shown for seismic deformation that amounts to 100 %, 200 % and 300 % of the tectonic deformation. The curve for $\dot{D}^{seis}/\dot{D}^{tect} = 1$ underestimates the observed recurrence rate of the largest events. For an $a-$value consistent with the catalogue seismicity and $\dot{D}^{seis}/\dot{D}^{tect} = 1$, $M_{max} = 6.5$ (red curve), i.e., smaller than the $M_{max}^{obs} = 7$. This too suggests that the seismicity is clustered. Since all tectonic deformation has been accommodated seismically, it is unlikely that significantly larger magnitude earthquakes than already observed are to be expected. We estimate $M_{max} = 7.0$ with a recurrence time of 350-1050 years. Large variations in seismic activity level as observed in Calabria are predicted from physical earthquake models with heterogeneous faults, where periods of strong activity, including large earthquakes and spanning several recurrence cycles, alternate with periods of low activity with only

small events [*Ben-Zion et al.*, 2003]. Another prediction of these models is a switch from a characteristic magnitude frequency distribution in the high-activity periods to a smooth Gutenberg-Richter distribution. The magnitude-frequency distribution of the earthquakes in the catalogue (using the completeness intervals in Table 4.1), approximates a smooth Gutenberg-Richter distribution quite well. However, in the case of a mode switch during the catalogue, it may not be appropriate to merge the recent level of seismicity of small events with the older record of larger earthquakes.

4.7.6 Calabrian trench

$\dot{D}^{tect}$ along the Calabrian trench covers the range of nearly completely locked to unlocked (0.5-3.5 mm/yr), depending on the tectonic scenario used. As in northern Sicily, locations of the older Calabrian events are not certain enough to discriminate offshore from onshore events. Therefore we test two possibilities: S1) the 1947 $M = 5.8$ event is shifted 40 km offshore, S2) only events that the catalogues locate within the trench source zone are taken into account.

The seismic deformation estimates are relatively low, with slip-rates of up to 0.5 mm/yr, suggesting the motion along the trench is almost absent. This is consistent with tectonic scenario T2, which gives a 0.5-1.0 mm/yr tectonic slip-rate. However, uncertainty in catalogue completeness does not allow us to rule out tectonic scenario T1. Offshore events may have remained undetected or may occur in the future. But given the very low level of recent seismicity ($a-$value) and $b = 1$, a M_{max} up to 8.9 would be needed to accommodate the maximum tectonic deformation of 3.5 mm/yr for T1. Such a M_{max} is too high for the size of the trench and a large part of the tectonic deformation is probably accommodated aseismically, in this case.

Thus, we infer that seismic motion along the trench is at most 1 mm/yr, allowing for a few offshore historic events to have remained undetected. This interpretation leads to maximum event sizes of up to $M \sim 7$ with recurrence times between 300 and 1300 years.

4.7.7 Southern Apennines

In the elastic plate model, the difference in velocity between Matera and the Tyrrhenian translates into $3 - 4$ mm/yr extension perpendicular to the southern Apennines. This

estimate is compatible with the geodetic strain rates *Hunstad et al.* [2003] measured across the orogenic chain. $\dot{M}_0^{cat}$ corresponds to $\dot{D}^{cat} = 2-3$ mm/yr for an assumed fault length of 350 km. Thus, seismic and geodetic slip rates are compatible, indicating that all southern Apennic strain is released seismically, in earthquakes with magnitude up to 7, and recurrence times of 100-350 year. The full range of $\dot{D}^{cat}/\dot{D}^{tect} = 50-100$ %, i. e., the uncertainties in the moment rates are too large to infer whether catalogue strains are behind the long-term accumulation rate or not. The magnitude-frequency data are reasonably well constrained and define a smooth trend (Fig. 4.11). Thus, we define a ratio $\dot{D}^{seis}/\dot{D}^{tect} = 75-100$. We estimate that M_{max} is similar to the M_{max}^{obs} of 6.9, with a recurrence interval of 100-350 years.

4.8 Conclusions

By combining (geodetically measured) long-term tectonic and historical seismic deformation rates, one can better quantify the seismic potential of regions where strain rates are low, and historical records are not long enough to record a few cycles of the largest events. In Southern Italy, this combined method allows estimating long-term seismic deformation rates in offshore areas where seismic observations are lacking and location uncertainties are large. It also identifies clustered seismicity that cannot be representative of the long-term average level of seismic activity, because it exceeds the tectonic rates of strain accumulation.

The highest levels of tectonic deformation are found north of Sicily, in the Aeolian Island - Peloritani region, and in the southern Apennines. North of Sicily, a back thrust accommodates the up to 4 mm/yr Africa-European convergence. In the Aeolian Island - Peloritani region, the offset between the Sicilian back-thrust and the Calabrian trench is accommodated and a concentration of deformation in this corner region would give slip rates up to 8 mm/yr if localized along a single fault. Along the southern Apennines 3 to 4 mm/yr of extension have been well-documented [*Hunstad et al.*, 2003]. In the rest of southern Italy, the deformation is more diffuse with rates of motion around 1 mm/yr in Calabria, along the Calabrian trench and in the Sicily Rift zone and the Ionian Sea southeast of Sicily. By contrast, the strongest historical seismic activity forms a band from the Apennines through Calabria and the Messina Straits continuing along the

eastern margin of Sicily, and thus does not coincide with the highest tectonic strain rates.

Our analysis indicates that the Apennines, where most of the deformation appears to be released in earthquakes, has the highest seismic potential (an M_{max} around 7 is to be expected on average every 100-350 years), consistent with previous hazard assessment [*Slejko et al.*, 1999]. The seismic potential of the southern Tyrrhenian high strain rate zone is larger than previously estimated, significantly raising seismic and tsunami hazard along the northern Sicilian coast. Although historical catalogues do not identify this area as being seismically active, offshore events have probably been wrongly assigned coastal locations. Recently, this zone has been the most active in Italy south of the Apennines. Still, it is likely that a significant part of the back-thrusting occurs by aseismic creep, giving the region a seismic potential lower than that of the Apennines (an M_{max} around 7, recurring every 300-1200 years). The northeastern corner of Sicily (with faults like the dextral Tindari-Letojanni system and the extending Messina Straits) has a seismic potential slightly larger than the Sicilian back-thrust (T_{rec}^{M7} 200-700 years). Much of the large geodetic strain around the Aeolian Islands appears to induce only slow creep in the warm and thin lithosphere around the volcanic arc. The seismic potential of Calabria and the Calabrian trench is lower than previously estimated from the historical catalogue and African-European convergence rates, respectively. The string of large events recorded in Calabria corresponds to an amount of strain that would take 1.5 to 6 times the length of the catalogue to accumulate, and thus cannot reflect a long-term average level of activity. The combined seismicity data and tectonic evidence is most consistent with a tectonic scenario (T2) with a low level of convergence along the trench and internal deformation in the Ionian corner of the African plate, in part localized off Sicily's eastern coast. We attribute the large southeastern Sicilian 1169 and 1693 events to this offshore deformation. These large events fully accommodate the 1-2 mm/yr of internal deformation (T_{rec}^{M7} 550-2100 years). The Calabrian trench then accommodates only around 1 mm/yr of motion, which nevertheless still allows the occurrence of one magnitude up to 7 event about every 300-1300 years. The lowest strains and seismicity levels are found in western and central Sicily, where only a small part of the plate convergence is currently accommodated. But even here, infrequent M 6.5-7 events (every 750-4000 years) may cause considerable damage. Overall, Southern

Italy displays a strongly time-variable and very diffuse pattern of seismicity in response to relatively low tectonic deformation rates and reorganizing plate boundaries.

4.9 Acknowledgments

We thank Bill Holt and Paul Lundgren for making their codes available, and Corné Kreemer and Paul Lundgren for their help in running them. Further, we thank David Jackson, Steven Ward, and Stefan Wiemer for discussions on determining seismic potential and seismicity characteristics, Max Stucchi for comments on the manuscript and P. Gasparini for information on magnitude-intensity relations. The work was funded by ETH Zurich and MunichRe. This is contribution number 1365 of the Institute of Geophysics.

Source zone		$\dot{M}_0^{cat}$ (Nm)	Equiv. fault length L (km)	$\dot{D}^{cat}$ (mm/yr)		$\dot{D}^{tect}$ (mm/yr)	$\dot{D}^{cat}/\dot{D}^{tect}$ %
1. Sicilian backthrust	(S1)	$2.27 \cdot 10^{16} - 8.93 \cdot 10^{16}$	290	$0.1 - 0.6$		$3.0 - 4.0$	3 – 20
	(S2)	$8.19 \cdot 10^{15} - 3.93 \cdot 10^{16}$	290	$0.1 - 0.3$		$3.0 - 4.0$	3 – 15
	(S3)	$7.76 \cdot 10^{15} - 1.04 \cdot 10^{16}$	290	0.1		$3.0 - 4.0$	3 – 3
2. CW Sicily	(S1)	$2.14 \cdot 10^{16} - 2.67 \cdot 10^{16}$	290	$0.1 - 0.2$		$0.5 - 1.0$	10 – 40
	(S2)	$2.48 \cdot 10^{16} - 3.12 \cdot 10^{16}$	290	0.2		$0.5 - 1.0$	20 – 40
	(S3)	$2.48 \cdot 10^{16} - 3.14 \cdot 10^{16}$	290	0.2		$0.5 - 1.0$	20 – 40
3. NE Sicily		$\leq 1.92 \cdot 10^{17}$	120+75	$0.9 - 1.2$		$2.0 - 3.0$	30 – 60
4. SE Sicily		$9.60 \cdot 10^{16} - 2.23 \cdot 10^{17}$	100	$1.8 - 2.9$	(T1)	$0.5 - 1.0$	180 – 580
					(T2)	$1.0 - 2.0$	90 – 290
5. Calabria		$2.57 \cdot 10^{17} - 3.69 \cdot 10^{17}$	200	$2.4 - 3.5$		$0.6 - 1.5$	160 – 585
6. Calabrian Trench	(S1)	$2.16 \cdot 10^{16} - 5.65 \cdot 10^{16}$	200	$0.2 - 0.5$	(T1)	$2.5 - 3.5$	6 – 20
					(T2)	$0.5 - 1.0$	20 – 100
	(S2)	$7.75 \cdot 10^{15} - 9.65 \cdot 10^{15}$	200	$0.0 - 0.1$	(T1)	$3.0 - 5.0$	0 – 3
					(T2)	$0.5 - 1.0$	0 – 20
7. Southern Apennines		$2.77 \cdot 10^{17} - 4.09 \cdot 10^{17}$	350	$2.0 - 3.0$		$3.0 - 4.0$	50 – 100

Table 4.2: Seismic catalogue and geodetic moment and equivalent slip rates for a fault length L in each source zone.

Chapter 5

Seismic risk assessment of Beijing and surrounding area

Sarah Jenny, Anselm Smolka, Dirk Hollnack and Alexander Allmann

Internal report, Munich Re Group, Munich, Germany

5.1 Introduction

The Munich Reinsurance company (MunichRe) has developed a model to determine the seismic risk of a given area. This report describes how this model is constructed and how it is applied to the city of Beijing and the surrounding area. The city of Beijing with 14 million residents is the largest city of the region. The second largest city is Tianjin with a population of 3.7 million. Beijing and the surrounding area are densely populated and because they are situated in a tectonically very active region, they may represent a high threat for its population. This model aims at quantifying seismic hazard and at translating it into a level of damage that might be expected in the near future.

Seismic hazard describes the probability in time and space that dangerous, earthquake-related natural phenomena such as ground shaking, fault rupture, soil liquefaction, landslides or tsunamis occur. These phenomena result in adverse consequences to society

such as the destruction of buildings and/or the loss of life. The severity of these consequences is a function of the *vulnerability*, which defines the degree of loss resulting from a given level of hazard. *Seismic risk* is a probabilistic expression of the combined effects of seismic hazard and vulnerability. Seismic risk is expressed in terms of PML (Probable Maximum Loss) for different return periods and AAL (Annual Average Loss). Note that the severity of damage and the resulting costs are not only dependent on the strength of an earthquake. There are many factors that can significantly affect the risk, e. g., attenuation of ground shaking with increasing distance from the epicenter, soil conditions at specific sites, earthquake resistance of buildings, population density, and distribution and amount of insured values (liabilities). This model allows to include these elements using the most recent information and data available.

The MunichRe model consists of three steps: 1) seismic hazard assessment of the study area, 2) vulnerability assessment, and 3) seismic risk assessment. Each of these steps is explained in the paragraphs below. Finally, worst-case scenarios are evaluated. These scenarios determine which possible future earthquakes would cause the highest seismic risk within the region.

5.2 Tectonic setting of northeastern China

The present tectonic evolution of northeastern China is driven by the collision of the Indian plate with the Eurasian plate. This collision started about 40 million years ago and is still ongoing. The Indian plate has been penetrating the Eurasian plate resulting in considerable vertical deformation that formed the high Himalayas and the Tibetan plateau. In this process, the Indian plate pushes Eurasian sideways in the way an icebreaker pushes ice away to the sides. This mechanism is called extrusion. Extrusion occurs directed at the Pacific subduction zones and is accommodated by diffuse deformation within China and southeastern Asia.

The study area lies between the relatively stable Amurian block in the north and the strongly deforming South China block in the south (Fig. 5.1), which is being extruded into ESE direction relative to Eurasia [*Flesch et al.*, 2001]. The regional stress field is characterized mainly by EW-trending compression and NS-trending extension [*Xu et al.*, 1993]. The increase in tectonic velocity from the Amurian block (3-7 mm/yr relative

to Eurasia between the latitudes of 50 ° N to 40 ° N, with rates increasing gradually to the south) to the South China block (9 mm/yr relative to Eurasia at 30 ° N, 110 ° E, *Holt et al.* [2000]) is accommodated, in part, by extension south and east of the Ordos plateau (e. g., Weihe Shanxi graben system), as well as by left-lateral shear (e. g., along the Qinling fault system). The Weihe Shanxi graben system extends over 1200 km and reaches a maximum width of 400 km. It is characterized by half-grabens resulting from transtensional deformation that begun in early Pliocene [*Liu*, 1987; *Zhang et al.*, 1998]. During the Pliocene, the maximum thickness of sediments reached up to 3000m. The Weihe Shanxi graben system is active today as demonstrated by the occurrence of strong destructive historical earthquakes of magnitudes 7-8 and horizontal slip rates of 1.8 up to 6.4 mm/yr [*Tapponnier and Molnar*, 1977; *Xu and Ma*, 1992; *Xu et al.*, 1993; *Zhang et al.*, 1994; *Gao et al.*, 1995]. The North China fault system is a northward continuation of the Weihe Shanxi rift system. Whether the North China fault system is also accommodating left-lateral displacement is still a matter of debate [*Pavlides et al.*, 1999; *Davis et al.*, 2001]. The Qinling E-W oriented fault system bounds extensional domains on the south and displays left-lateral slip decreasing in magnitude from west to east [*Chen and Nabelek*, 1988; *Zhang and Vergely*, 1995]. Although the overall deformation of Northern China is left-lateral, NNE directed right-lateral faults play an important role in accommodating the motion between the Amurian plateau and the South China block. These faults have been mapped over a width of $\sim$ 500 km both onshore and offshore and have produced large earthquakes in the past [*Ding et al.*, 1989]. The best known is the Tan-Lu fault. This fault extends NNE-SSW for more than 3000 km and bounds the extensional domains to the east. The Tan-Lu fault has caused the largest historical earthquake observed in the region, the 1668 M_w 8.5 event. An other major right-lateral fault is the Tangshan fault striking NE-SW in the North China plain. This fault caused the more recent 1977 M_w 7.9 event.

5.3 Seismicity of northeastern China

Fig. 5.2 shows the seismicity of northeastern China. The data are from the official historical catalogue of the State Seismological Bureau of China. The catalogue contains 7155 events covering all of China, with $M \geq 4.5$ from -2300 BC to 1999. The magnitude

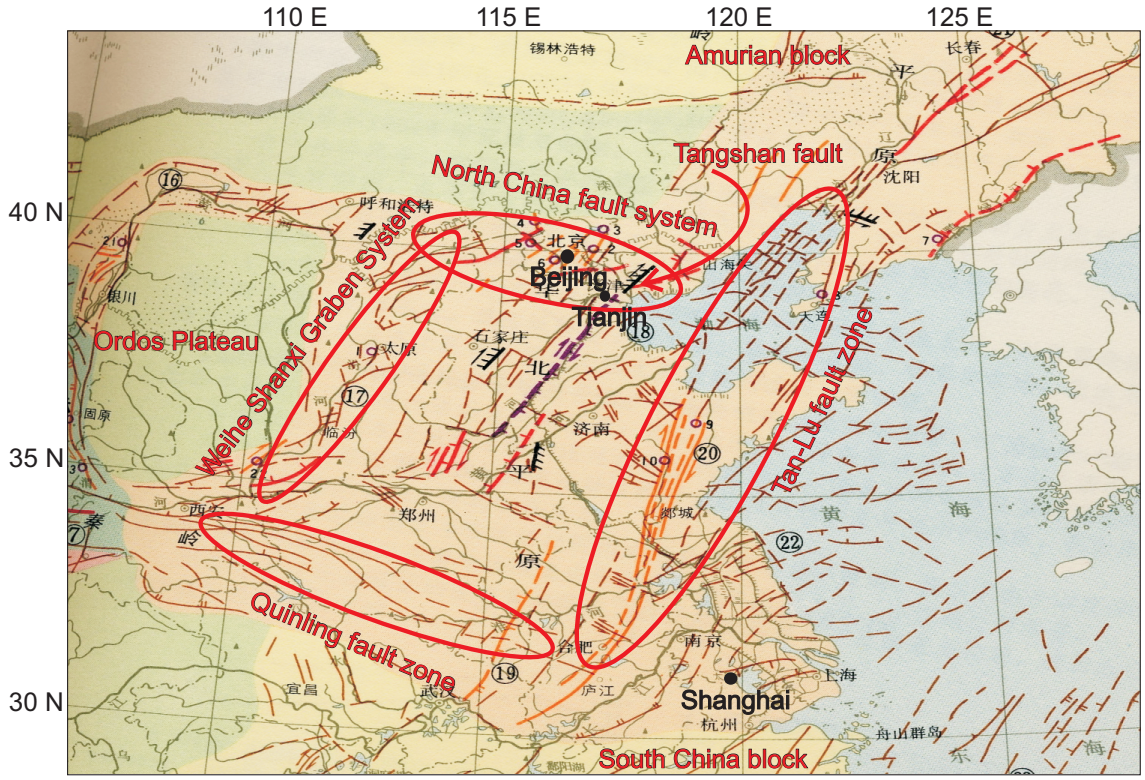

Figure 5.1: Tectonic setting of northeastern China. The map is adapted from *Ding et al.* [1989].

type is not mentioned in the catalogue. Nevertheless, for the instrumental period, comparison with other catalogues like the NEIC-PDE catalogue from the USGS suggests that the magnitude is similar to the moment magnitude M_w for the whole magnitude range. Seventeen events with $7 < M < 8$ and 5 events with $M \geq 8$ have been recorded in the study area.

The aftershock sequence of the 1977 M_w 7.9 Tangshan event causes a significant increase of the seismicity rate of M_w=4.5-6.0 events. Because we are interested in the long-term seismicity rate, this local rate increase is smoothed out by declustering the catalogue. However, note that although this procedure reduces the transient seismicity increase that would immoderately raise the hazard in this area, it underestimates the long-term average rate of smaller events.

The completeness of the historical seismic catalogue is defined by analysing the rate of seismicity versus time within different magnitude intervals [*Mulargia et al.*, 1987] for all of the study area. The obtained completeness lengths are listed in Table 5.1.

Date	Magnitude range (M_w)
$\geq$ **1977-1999**	≥ 4.5
$\geq$ **1950-1999**	≥ 5.0
$\geq$ **1940-1999**	≥ 5.5
$\geq$ **1915-1999**	≥ 6.0
$\geq$ **1900-1999**	≥ 6.5
$\geq$ **1550-1999**	≥ 8.0
$\geq$ **0-1999**	≥ 8.5

Table 5.1: Completeness of the seismic historical catalogue.

5.4 Seismic hazard assessment

The MunichRe model uses a probabilistic seismic hazard analysis that incorporates the effects of all the earthquakes believed to be capable of affecting a site in question, i. e. in this case, the liability locations. The methodology consists of four steps: 1) definition of seismic source zones, 2) evaluation of magnitude-frequency relationships, 3) estimation of earthquake effects at a specific site and, 4) determination of seismic hazard at the liability locations.

5.4.1 Seismic source zones

A seismic source zone defines an area with a similar style of deformation and a homogeneous seismicity. It means that anywhere in that source zone, the average period of time between the occurrence of earthquakes of a given size (recurrence interval or return period) is similar. Source zones are defined based on information about active faults, observed seismicity from historical and instrumental seismic catalogues, tectonic and geological data. Tectonic motion measured geodetically, like GPS, also allows distinguishing between fast and low straining areas. Palaoseismological studies, based on direct evidence of fault rupture and on indirect geologic evidence such as buried sand deposits which indicate that liquefaction due to intense ground motion occurred, is very useful to determine the recurrence interval of large earthquakes back in time where historical seismic records are lacking. Based on all available information, we defined four source zones in our study area. Source zones and major active faults are shown in Fig 5.3. These source zones delimit four main tectonic features of the area. The first source zone demarcates the area around the Weihe Shanxi graben system, the second

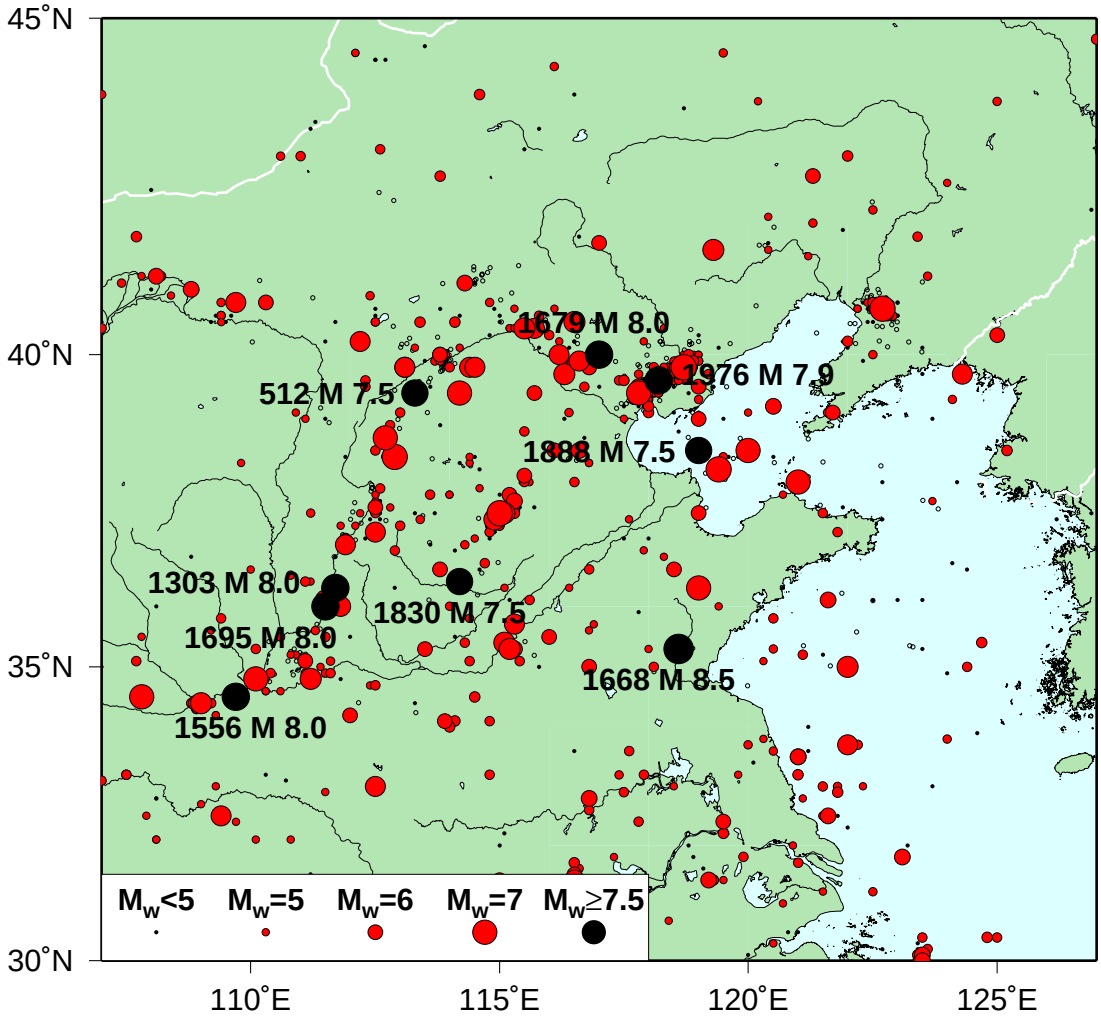

Figure 5.2: Seismicity of northeastern China. Data are from the seismic historical catalogue of the State Seismological Bureau in Beijing.

source zone encompasses right-lateral faults in the center part, the third source zone marks out the Tanlu fault zone and finally, the fourth source zone defines the North China fault system. Although large events have occurred along the Quinling fault, the epicenters are too far away from Beijing and the surrounding area to affect the seismic hazard.

5.4.2 Seismicity space-time distribution

Using the completeness lengths listed in Table 5.1, we calculate the log_{10} of the cumulative number of earthquakes N versus magnitude M for the historical catalogue

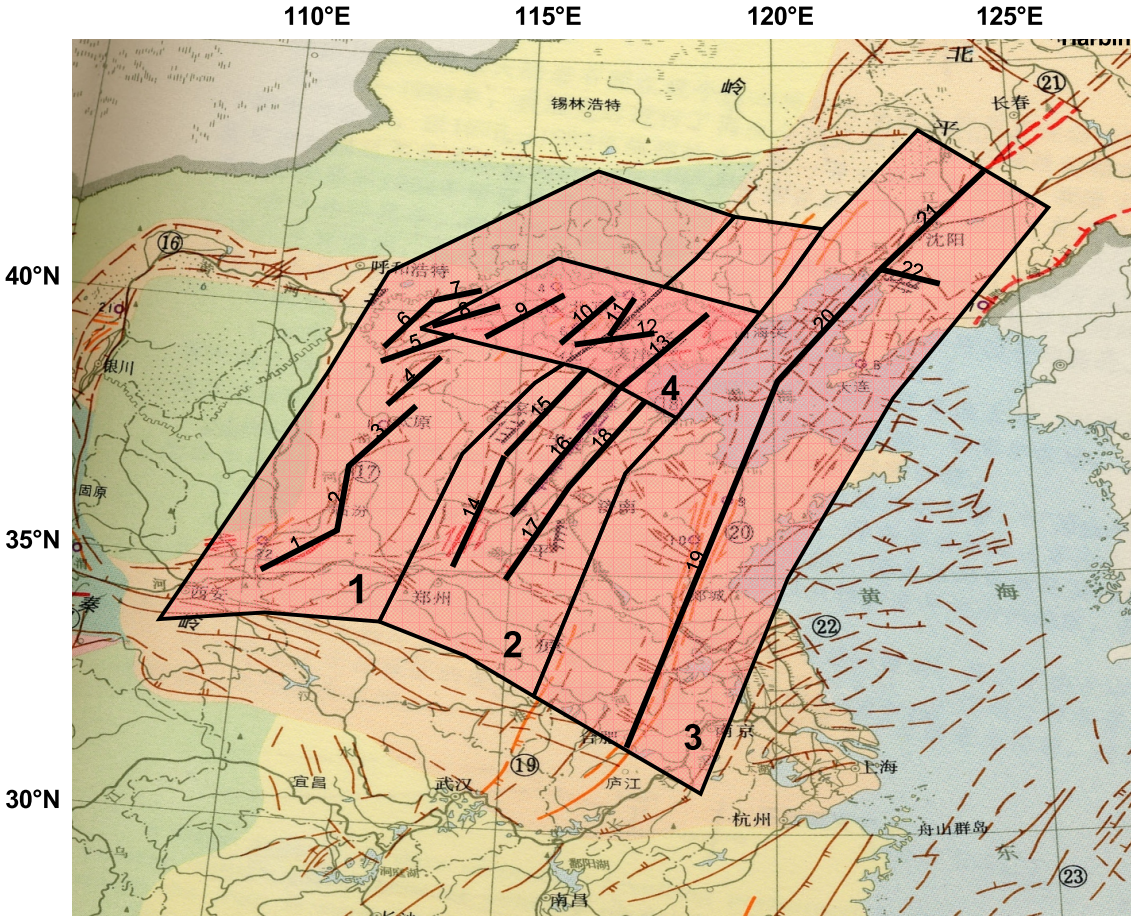

Figure 5.3: The four seismic source zones and 22 major active faults (black lines).

within each source zone, i. e. the magnitude-frequency data (Fig. 5.4, circles). The magnitude-frequency distribution is then approximated by a linear relationship between the logarithm of the number of earthquakes N and magnitude M up to a maximum magnitude M_{max}: $Log(N) = a - bM$ (Fig. 5.4, curves). This relation, also called the truncated Gutenberg-Richter relationship, is described by three parameters: 1) the a-value, the logarithm of the number of events, i. e. the seismicity rate, 2) the b-value, -1 times the slope of the line, i. e. the relative frequency of small versus large events and 3) M_{max}, the maximum event size expected. The a- and b-values are determined by a maximum likelihood fit to the magnitude-frequency data. M_{max} is estimated from the seismic historical catalogue and from the slip rates and lengths of the active faults [*Ding et al.*, 1989]. The a-, b-values, M_{max} and their corresponding return periods are listed in Table 5.2.

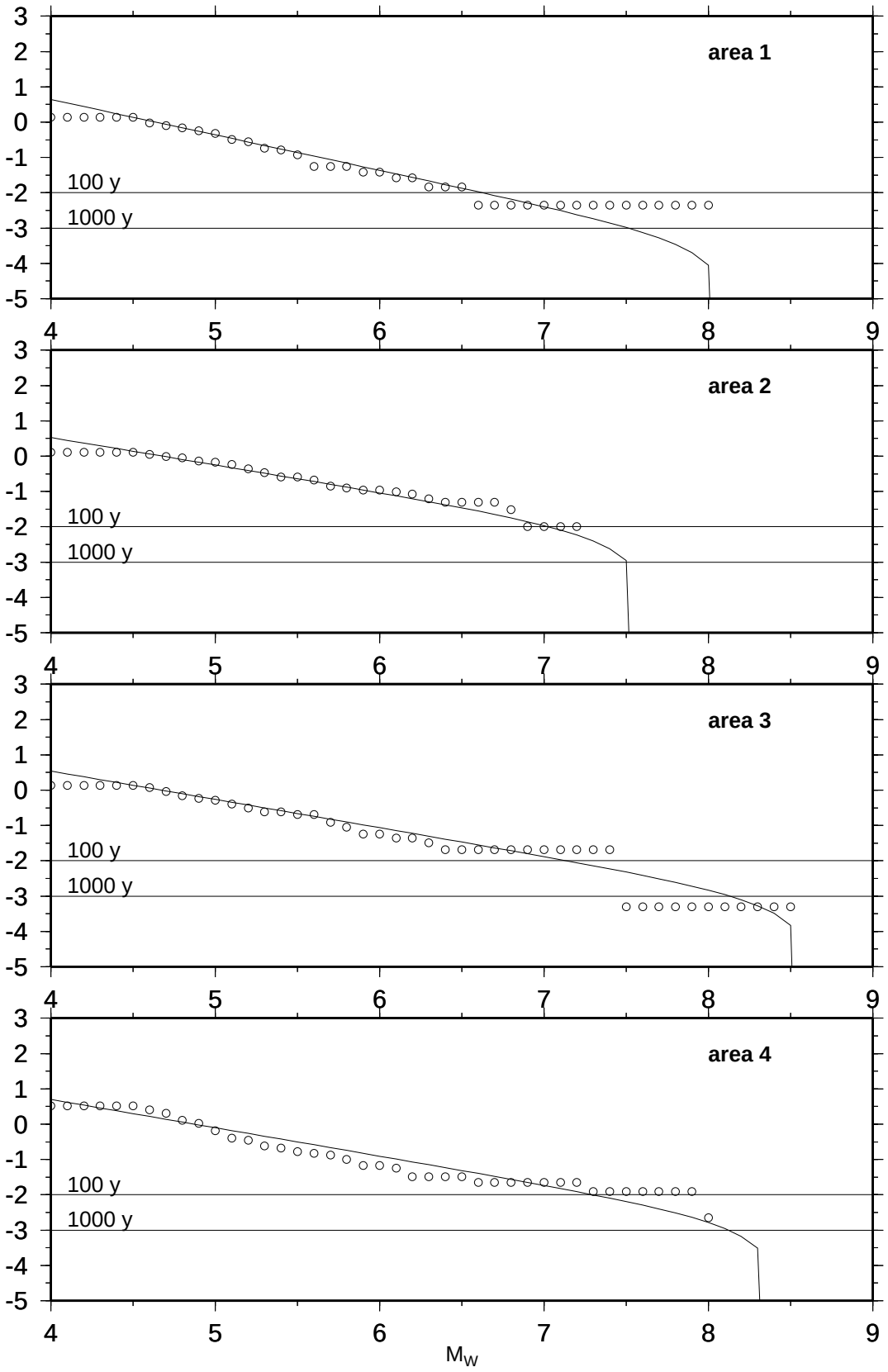

Figure 5.4: The log_{10} of the cumulative number of events versus magnitude for the seismic historical catalogue (circles) in each of the areas shown in Fig. 5.3. The curves represent the truncated Gutenberg-Richter approximations to the magnitude-frequency data.

Source zone	a-value at $M_w = 4.5$	b-value	M_{max}	Recurrence interval of M_{max} (years)
1	0.14	1.00	8.0	10000
2	0.14	0.77	7.5	1000
3	0.14	0.80	8.5	7800
4	0.30	0.80	8.3	3000

Table 5.2: Earthquake recurrence parameters for each source zone.

Earthquakes occur along zones of weakness (faults) in the crust. The main active faults in the region have been mapped based on surface expression and seismicity (see Fig. 5.1 and Fig. 5.2). To account for the concentration of seismicity on the main faults, we attribute a percentage of the total seismicity within the source zone to active faults (Table 5.3). Then, the seismicity rates attributed to active faults are redistributed within all mapped active faults in that source zone (Table 5.4). These seismicity ratios are determined from the seismic activity and the slip rate along the faults. The MunichRe model ascribes only events with $M \geq 6$ to faults. The remaining seismicity is then equally distributed on an equidistant grid within the source zone. The distance between node points of the equidistant grid is chosen between 10 and 30 km (see Table 5.3). A denser grid is assigned to areas with higher liability concentration, e. g., within large urban areas.

Note that faults are not treated as fault lines but as fault zones. This is done by defining a buffer zone on each side of the faults. This buffer zone allows to take into account uncertainties in fault and earthquake location. Thus, in the MunichRe model, earthquakes are assigned either to fault zones or to grid points. In areas where a relatively higher level of seismicity is observed but no active fault is known, "virtual faults"may be assigned. This is the case for the faults 15 and 18 in source zone 2 (Fig. 5.3). These faults concentrate the seismicity in the northern part of the source zone.

5.4.3 Ground motion

The ground motion at any site is the principal cause of damage. Ground motion at a particular site depends on three main factors: 1) source effects, 2) propagation effects and 3) local site effects. The first element describes how the size and nature of the

Source zone	Distance between grid points (km)	Magnitude	%	Seismicity
1	30	M=4.0-5.9	100 %	onto the grid
		M=6.0-6.9	20 %	onto the grid
			80 %	onto the faults
		M=7.0-8.0	100 %	onto the faults
2	30	M=4.0-5.9	100 %	onto the grid
		M=6.0-6.9	20 %	onto the grid
			80 %	onto the faults
		M=7.0-7.5	100 %	onto the faults
3	30	M=4.0-6.4	100 %	onto the grid
		M=6.5-7.4	20 %	onto the grid
			80 %	onto the faults
		M=7.5-8.5	100 %	onto the faults
4	10	M=4.0-7.2	100 %	onto the grid
		M=7.3-8.3	100 %	onto the faults

Table 5.3: Distribution of the seismicity rates on the equidistant grid and the faults versus magnitude within each seismic source zone.

earthquake source controls the generation of earthquake waves. The second element describes the effect of the Earth's structure on these waves as they travel from the source to a particular location. Finally, the third element describes the effect of the uppermost several hundred meters of rock and soil at that location.

Source effects

When an earthquake occurs, the rupture propagates away from the hypocenter along the fault. The MunichRe modell takes this into account for events with $M_w \geq 6$ and considers them as line source whereas smaller events can be treated as point sources. Fault segment lengths are defined using known relationships between earthquake magnitude and rupture fault length (Table 5.5) available from MunichRe database. Over the whole segment length, the ground motion is taken as constant and corresponds to the magnitude of the event. If an event is simulated within a fault zone, the azimuth of the rupture fault is equal to the azimuth of that fault zone. If an event with $M_w \geq 6$ occurs outside a fault zone, the rupture is assumed to propagate in a direction similar to the average azimuth of the known faults in that source zone.

Source zone	Fault	Buffer width	% Seismicity
1	1	20	20
1	2	20	20
1	3	20	20
1	4	20	10
1	5	20	10
1	6	20	12
1	7	20	8
2	14	10	25
2	15	10	10
2	16	10	30
2	17	10	25
2	18	10	10
3	19	25	40
3	20	25	20
3	21	25	20
3	22	5	20
4	8	5	15
4	9	5	15
4	10	5	20
4	11	5	15
4	12	5	15
4	13	5	20

Table 5.4: For each source zone, ratios of the seismicity rate of each fault and the total seismicity rate along faults. The buffer width defines the extent of the fault zone on each side of the fault. The buffer width is defined based on observed seismicity and mapped secondary faults sideways of the main faults.

Propagation effects (ground motion attenuation)

The effects of the travel path on earthquake ground motion are related to attenuation of the propagating seismic waves with increasing distance from the hypocenter.

In our model, ground motion can be described by three different parameters: 1) intensity, 2) peak ground acceleration or 3) peak ground velocity. Because the intensity levels are partly defined by means of building damage data, intensity attenuation relationships are preferred, when available, to peak ground acceleration or velocity attenuation relationships. We did some tests using three different intensity attenuation functions: one by of *Zhang and Chen* [1982]:

$$ln(I) = 1.1473 + 0.1722M - 0.1386ln(D) \tag{5.1}$$

Magnitude	Fault rupture length (in km)
6.0	8
6.1	10
6.2	12
6.3	14
6.4	17
6.5	21
6.6	25
6.7	30
6.8	36
6.9	43
7.0	52
7.1	62
7.2	74
7.3	90
7.4	108
7.5	129
7.6	156
7.7	187
7.8	225
7.9	270
8.0	325
8.1	391
8.2	470
8.3	565
8.4	679
8.5	817

Table 5.5: Fault rupture length versus magnitude used for the study area.

and two functions for eastern China that were established by the *State Seismological Bureau of China* [1991]: for the major axis of isoseismals:

$$I = 6.046 + 1.480M - 2.081ln(D + 25) \tag{5.2}$$

for the minor axis of isoseismals:

$$I = 2.617 + 1.435M - 1.441ln(D + 7) \tag{5.3}$$

where I is the earthquake intensity; M is the magnitude and D the shortest distance to the epicenter (in km). These functions are plotted in Fig. 5.5. Some tests are

performed to define which of these three formula adequately represents the intensity attenuation within the study area. PML curves are calculated based on these three formulas. These results shows that Eq. 5.2 and Eq. 5.3 imply a risk much higher than realistically expected for such an area. Therefore, Eq. 5.1 is used for further calculations. Note that at this step, the calculated risk is significantly affected by the rupture fault lenghts. The fault lengths chosen (Table 5.5) are rather large and yield a relatively high risk.

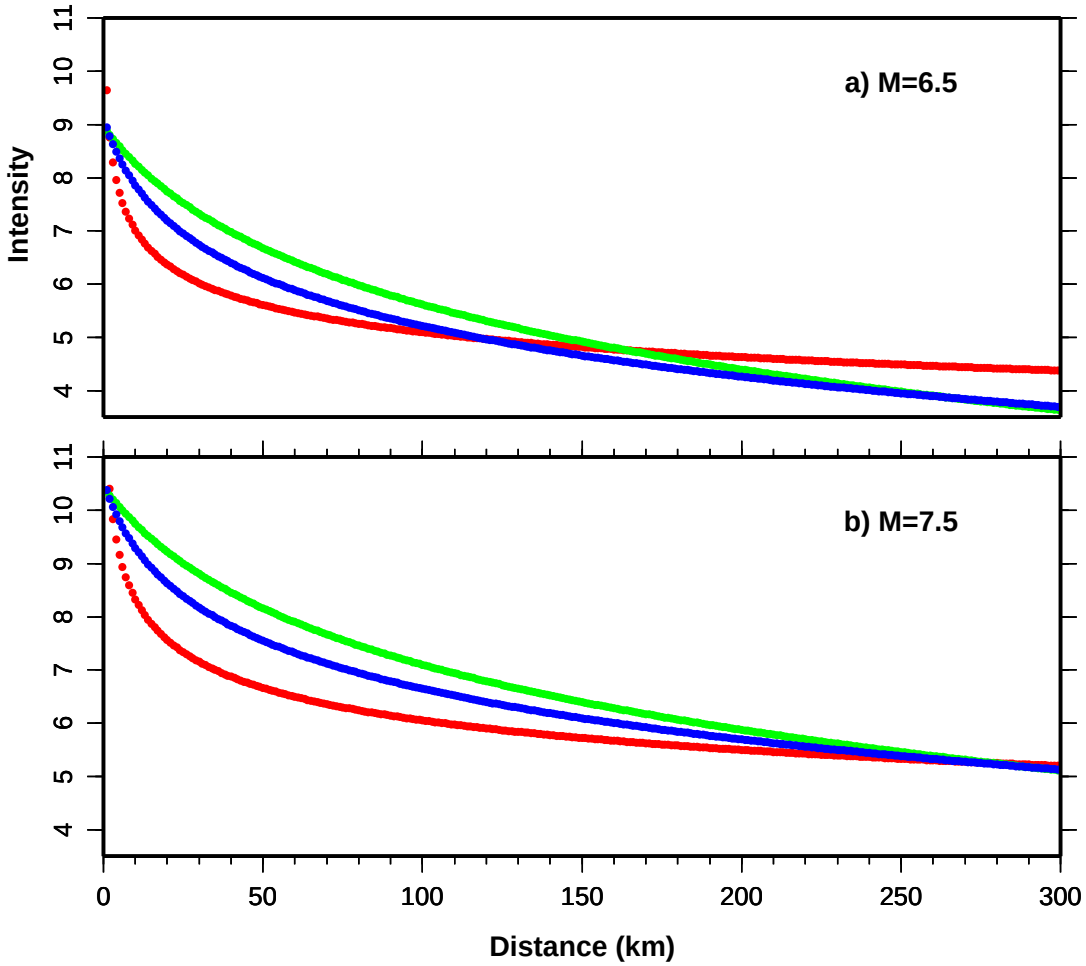

Figure 5.5: Intensity attenuation functions from *Zhang and Chen* [1982] (red) and from the *State Seismological Bureau of China* [1991] for the major (green) and the minor (blue) axis of isoseismals, a) for M = 6.5 and b) for M = 7.5.

Local site effects

Earthquake ground motion can be amplified or damped by the properties of the near surface material through which seismic waves propagate. Earthquake damage at some locations may be much more dependent on these near surface conditions than on the proximity of nearby earthquake sources. Usually, earthquake damage is greater in sites located on soft soils than in those on stiff soils or on rock. Our model takes five different soil conditions into account (Fig. 5.6), from softer to stiffer: 1) Quaternary sediments, 2) Tertiary sediments, 3) young sedimentary rock, 4) old sedimentary rock and 5) igneous rock. The calculated ground motion is assumed to reflect old sedimentary rock soil condition. For stiffer or softer soil condition, the intensity is scaled down or up, respectively (Table 5.6). Fig. 5.6 shows the soil conditions of the study area.

Soil condition	Intensity correction
1 - Quaternary sediments	+1.00
2 - Tertiary sediments	+0.50
3 - Young sedimentary rock	+0.25
4 - Old sedimentary rock	0.00
5 - Igneous rock	-0.25

Table 5.6: Intensity correction for each soil condition

5.4.4 Seismic hazard assessment

According to the probability of occurrence defined by the magnitude-frequency relationships (Section 5.4.2), earthquakes with magnitude up to M_{max} (with a step size of 0.1 unit of magnitude) are simulated within the fault zones and on each node of the equidistant grid. Taking into account ground motion attenuation and local site effects, ground motion at the liability locations is then calculated and defined in terms of Intensity (MMI, Modified Mercalli Intensity), Peak Ground Acceleration (PGA) or Peak Ground Velocity (PGV).

The liability locations are usually defined at the center of the Cresta (Catastrophe Risk Evaluating and Standardising Target Accumulations) zone data. Based primarily on the observed or expected seismic activity within a country, Cresta zones consider the distribution of insured values within a country as well as administrative or political

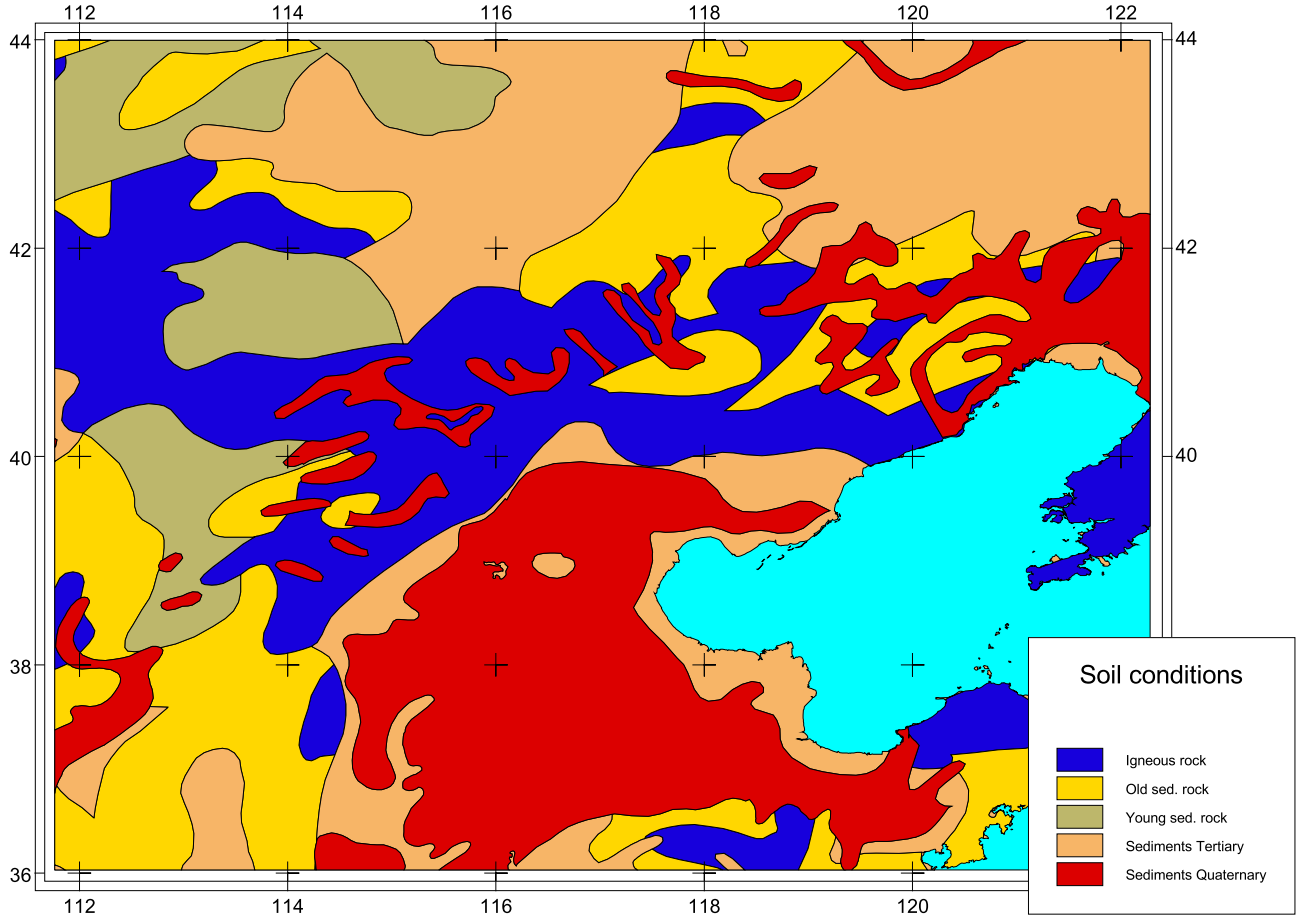

Figure 5.6: Soil conditions

boundaries for easier assessment of risks. Nevertheless, for large Cresta zones, one single location is not sufficient to characterize the intensity within that zone. Based on density population (Fig. 5.7), further liability locations are considered. The denser the population is, the more liability locations are defined. The Cresta zones and the liability locations are shown in Fig. 5.8.

5.5 Vulnerability

Vulnerability is defined as the ratio of the expected average loss to the replacement value of the affected object, on a scale from 0 to 1 (or 0 to 100 %). It depends on the degree of ground motion as well as on the type of the affected item. Fig. 5.9, taken from *Sauter* [1979], shows an example of vulnerability curves for buildings, for different types of construction. The curves show the average expected loss in % (= damage ratio) as a

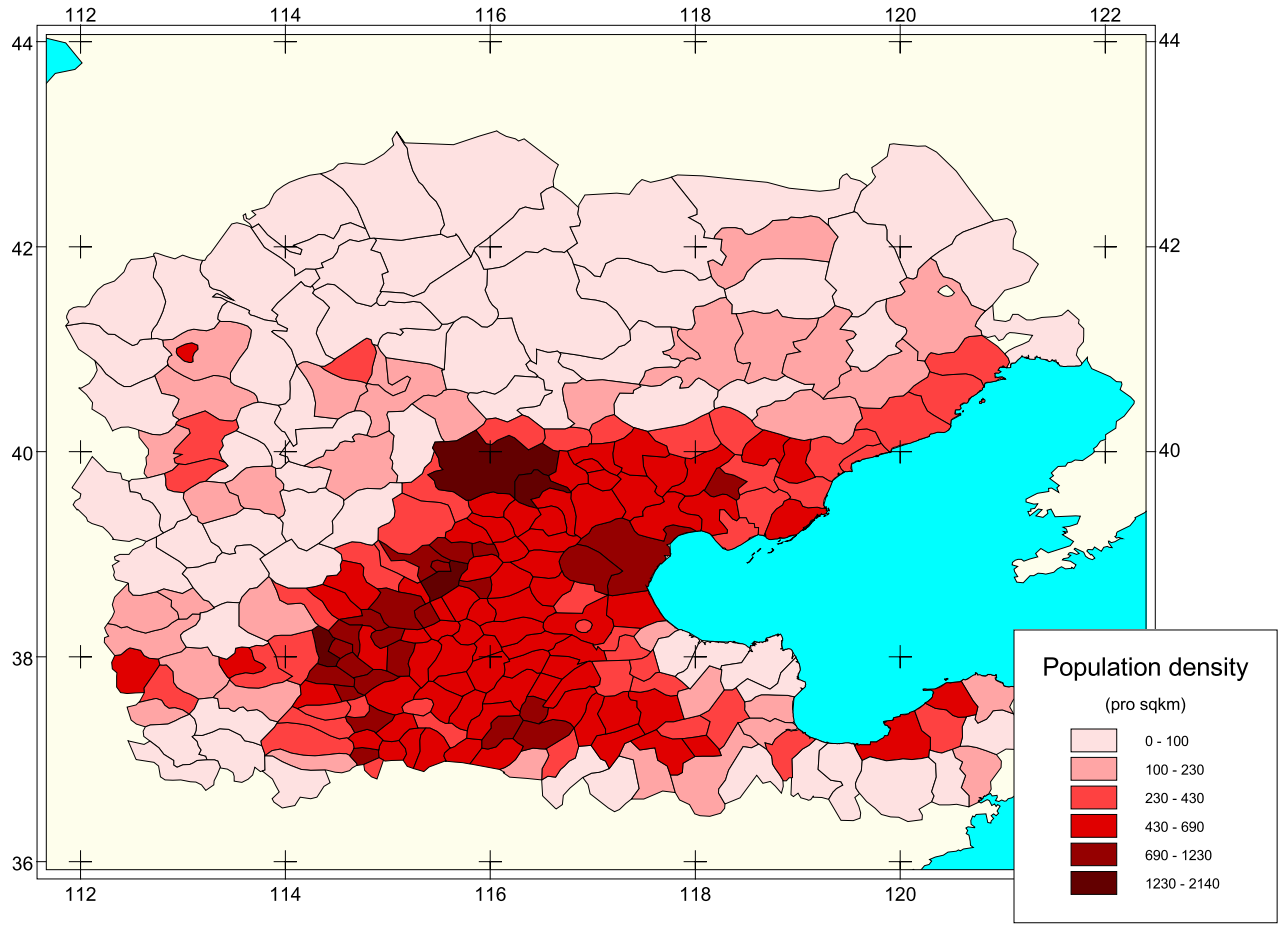

Figure 5.7: Population density.

function of the Modified Mercalli Intensity MMI.

For the Chinese model, similar curves have been developed by making use of loss statistics from Chinese earthquakes [*Research Group for Estimating Losses from Future Earthquakes, State Seismological Bureau*, 1992]. The curves consider the prevailing types of construction and the type of risk, as residential, commercial and industrial objects.

5.6 Seismic risk assessment (PML)

The final goal of a model for seismic risk assessment is the construction of a so-called exceedance probability curve or PML curve (PML = maximum probable loss). The curve is derived from the data base of simulated earthquakes by superimposing the regional distribution of values and the average expected loss as a function of local site intensity. The sites considered are the centroids of the districts (or sub-districts in the

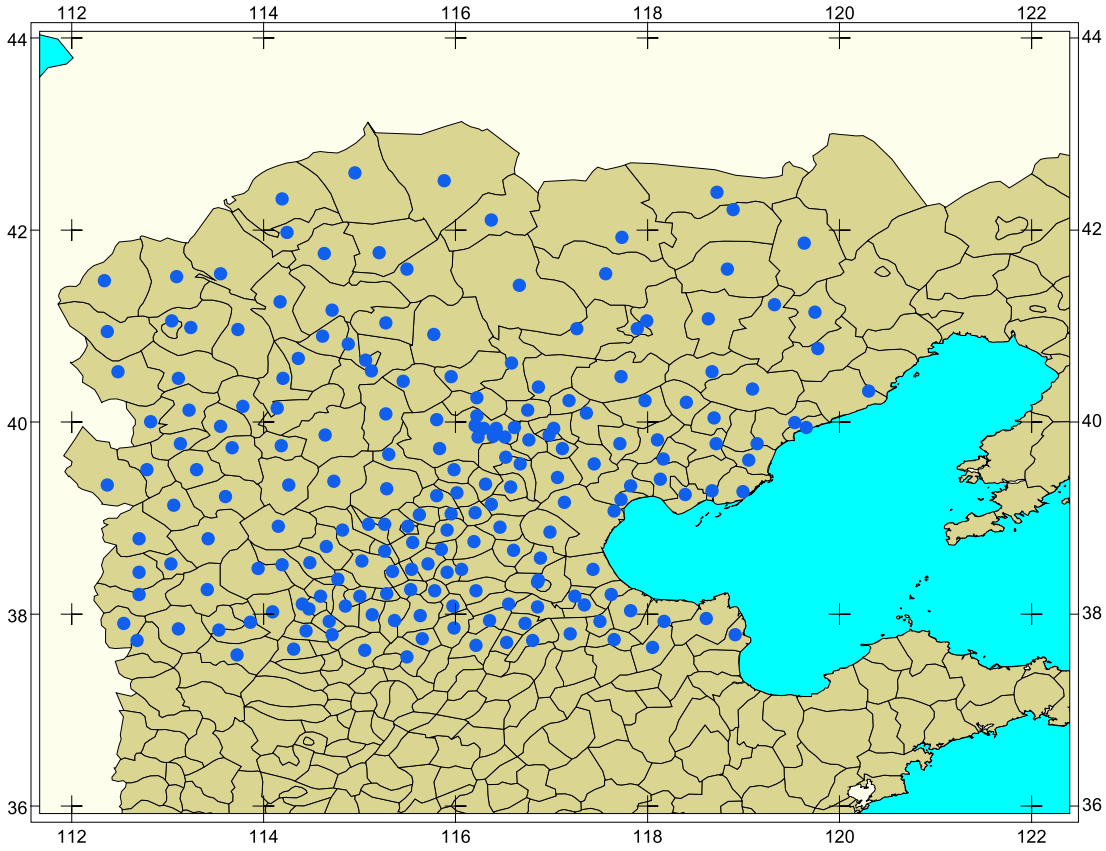

Figure 5.8: Cresta zones and liability locations.

Beijing area). The result of this process is the expected value-weighted loss for each simulated earthquake, together with the corresponding occurrence probability derived from the hazard assessment. An example of such a curve is shown in Fig. 5.10 for residential buildings in Central China. At present, data on insured values do not exist for the simple reason that earthquake insurance for dwellings is not available. Therefore it was assumed that the percentage distribution of values per district is reasonably well approximated by the population distribution. The curve shows the expected percentage loss as a function of the recurrence period. In our example, the expected loss for 100 years would be 1.14 % or greater, the loss for 1000 years 3.71 % or greater. The curve reaches a maximum in the range of 15000 years, and the corresponding 6.25 % represent the worst case scenario. It is determined by seismotectonic considerations, or more precisely by the maximum magnitudes assigned to the different source zones on the one hand, and by the regional distribution of values, on the other hand.

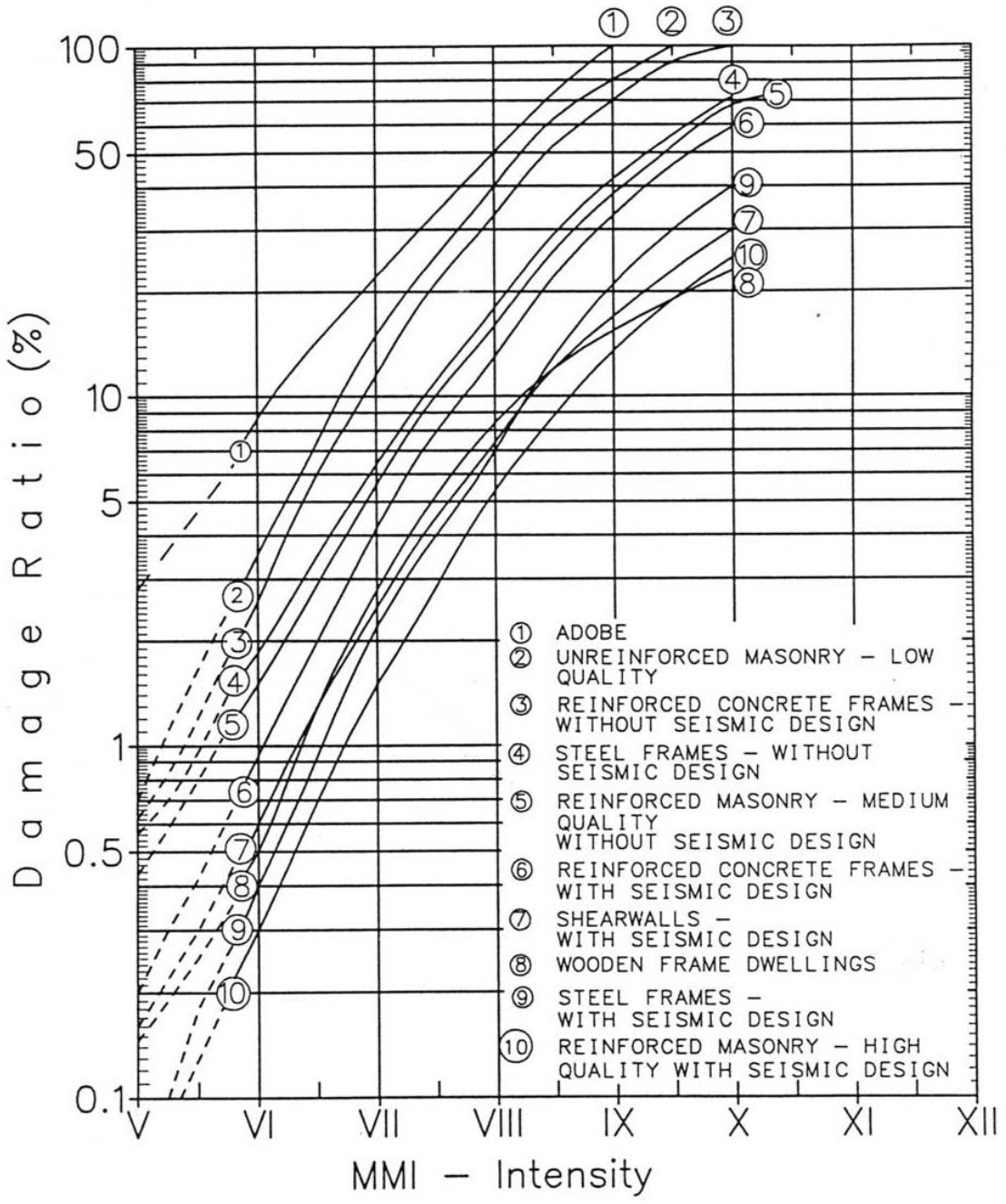

Figure 5.9: Average damage ratio relationships [*Sauter*, 1979].

5.6.1 Worst case scenarios and average annual losses (AAL)

According to our model, the worst case scenarios are produced by earthquakes of magnitude 8.3 located in source 4 on faults 11/12 and 13 respectively. Faults 13 comprises the Tangshan fault, and the high loss is due to the fact that the fault is located directly beneath the city. Faults 11/12 affects the Beijing-Tianjin area where the values-at risk

are much higher than in the Tangshan region, but the fault is farther away from the population centers.

As important as rare high losses are in respect of the ruin probability of insurance companies, the other important risk measure is the average annual loss (AAL). This is the yardstick for the rate that has to be charged to finance the risk which arises from offering earthquake insurance. The contribution of rare high losses to the average annual loss increases with decreasing seismicity, as the relative weight of big events is higher than in areas with more frequent earthquakes. Nevertheless the contribution of worst cases is almost negligible due to their very low occurrence probability. This can be easily seen from our example where (worst case) losses over 6 % contribute 1.36 % and losses over 5 % contribute 13.2 % to the AAL of 0.4690 %.

Program				
	Cedant country:			
	Description:	China		

Treaty						
	Peril:	Earthquake	**Exposure country:**	China	**Zone type:**	Admin3

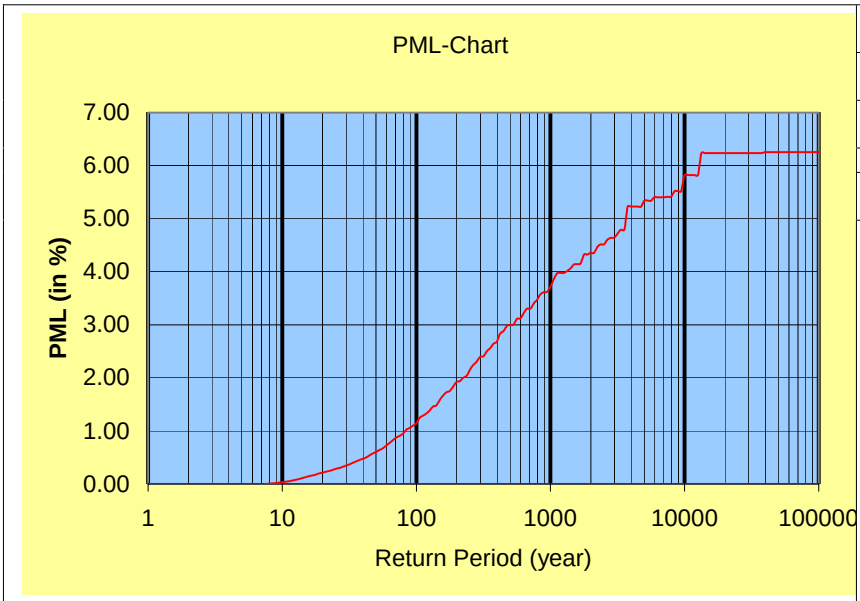

Worstcase: 5,703,778
AAL in ‰: 0.4690
TSI: 91,195,278
Sum ignored:
Currency: EUR
Units: Thousands

Return period	PML (in %)	PML (in value)
10	0.03200	29,100
50	0.60400	550,532
100	1.14400	1,043,594
250	2.15900	1,968,990
500	2.99200	2,728,729
1,000	3.71800	3,391,001

Figure 5.10: Probable Maximum Loss.

Chapter 6

Conclusions

At this moment, combining geodetic and seismic strain rates with geological and tectonic information is the best way to bracket long-term seismic deformation rates. This is true not only for fast straining areas like the Eastern Mediterranean (moving with motions of a few cm/yr and strain rates of 100-500 nanostrain), but also for a slowly straining area like the Central Mediterranean (with velocities of a few mm/yr and strain rates around 30-60 nanostrain).

Important is that the data combined represent the same deformation. In the Eastern Mediterranean, the dense distribution of data allows for a detailed comparison between the short-term seismic strain rate documented by earthquake catalogues and the tectonic strain rate field measured geodetically. Although focal mechanisms from a few decades might not be expected to yield a reliable estimate of long-term seismic strain style, we found a very good agreement between seismic strain patterns inferred from earthquakes over several units of magnitude and regional tectonic strain patterns. This is true in most of our study area, for extensional, compressional and strike-slip regimes. Also, we found that the style of deformation inferred from the small focal mechanisms is very similar to the style inferred from larger events. This suggests self-similarity. *Amelung and King* [1997] obtained similar results for the strike-slip regime of San Andreas fault. Larger events are less frequent. Therefore, it is statistically better to use the more abundant smaller events to define the style of deformation. Agreement between seismic and tectonic styles of deformation has also been found in several other regions around the world [*Amelung and King*, 1997; *Kreemer et al.*, 2000]. Exceptions may indicate an unusual seismotectonic regime. For example, largely aseismic compression along

the eastern Hellenic trench, can explain the discrepancy between the strike-slip seismic styles and geodetic styles that reflect oblique convergence. In Southern Italy, the large north-south geodetic compression in the Southern Tyrrhenian north of Sicily and around the Aeolian Islands is not clearly represented in the seismicity. Instead, seismic strains indicate strike-slip in the Aeolian Islands, consistent with NNW-SSE striking faults in the area. The low strength of the warm and thin southeastern Tyrrhenian may lead to tectonic strain being only in part seismic, apparently with a preference for seismic strike-slip faulting.

If historical catalogues are complete and long enough, the magnitude of the seismic deformation can be defined by summing the moment rates of catalogues. We found that for the strain rates in Greece and maximum magnitudes around 7.5, a 100 to 200-year catalogue should give an approximation of the long-term seismic moment rate within $\pm$ 30 % without a bias towards low or high moment rates. Shorter catalogue lengths tend to give moment rate estimates biased low. Significantly higher maximum magnitudes would require a longer catalog. Similarly, to characterize clustering patterns instead of Poisonian recurrence behavior a longer observation time would be necessary. This implies that in Italy at least a 1000 to 2000-year long (and complete) catalogue is required to achieve reasonable moment rate estimates. The uncertainties in magnitude, location and especially completeness of the catalogues yield uncertainties of up to a factor of 2 in moment rates. By combining long-term tectonic and historical seismic deformation rates, one can better quantify the seismic potential of regions where strain rates are low, and historical records are not long enough to record a few cycles of the largest events.

In Southern Italy, this combined method allows estimating long-term seismic deformation rates in offshore areas where seismic observations are lacking and location uncertainties are large. It also identifies clustered seismicity that cannot be representative of the long-term average level of seismic activity, because it exceeds the tectonic rates of strain accumulation. In the fast straining Eastern Mediterranean, we obtain truncated Gutenberg-Richter distribution parameters, a-value, b-value and M_{max}, and the corresponding long-term seismic moment rates $\dot{M}_0^{seis}$, that are consistent with seismicity data, tectonic information and strain rates. b-values are found to vary around 1. The lowest b-value (0.6) is found along the North Anatolian Fault, where most of the

deformation is released through large events. High b-values are found along the Hellenic trench (1.2-1.3), where very few moderate and large events have been recorded. The uncertainties in the seismic data do not justify a magnitude-frequency distribution different from the truncated Gutenberg-Richter distribution. Also the large uncertainties in the older part of seismic historical catalogues do not allow us to discriminate between a smooth or a characteristic distribution.

The ratio of our best estimates of the long-term seismic deformation and the long-term tectonic deformation measured geodetically allows defining the aseismic part of the strain accumulated. In the Eastern Mediterranean, the strike-slip zones appear to be fully seismic. The trench region is affected by at least 45 % and up to 90 % aseismic deformation. The other regions are characterized by 10-60 % aseismic deformation, where uncertainties in the catalogues and in the geodetic strain rates do not allow us to define any tighter bounds. For most regions, $\dot{M}_0^{tec}$ thus gives a reasonable first-order estimate of $\dot{M}_0^{seis}$, but a catalogue that provides good constraints for a- and b-values is necessary for better estimates of the aseismic component of deformation.

The newly collected geodetic data in Southern Italy document a major tectonic reorganization in the Central Mediterranean around 0.8-0.5 Myr, when rapid trench migration and consequent Tyrrhenian back-arc extension, which dominated the region's evolution since the Tortonian (10-8 Myr), stopped. In response, the African convergence in Sicily was transferred to a back-thrust in the Southern Tyrrhenian. The Ionian region now diverges from the main part of Africa, with northeastward motions that reflect the joint influence of African push and Hellenic slab pull, and are transmitted to Adria. A diffuse transform boundary formed across northeastern Sicily to connect the Sicilian and Calabrian plate boundaries, causing opening of the Messina Straits - home to devastating historical earthquakes - and unusual volcanism in the Aeolian Island arc and the intraplate Mount Etna.

The new geodetic data and their tectonic interpretation significantly influence estimates of the seismic potential of Southern Italy. Interestingly, and different from the situation in the Eastern Mediterranean, regions with high levels of historical seismicity often do not coincide with those with the highest rates of tectonic deformation. This makes using combined information especially critical. The highest seismic potential is estimated for the Southern Apennines, where high seismicity and tectonic rates do co-

incide, and most to all deformation appears to be seismic. Some other fast straining regions (the back-thrust north of Sicily and Sicily's northeastern corner) have a large proportion of aseismic deformation. Still, the seismic potential of these regions is considerably higher than would be estimated from past seismicity only. In other regions, the relatively low level of tectonic deformation appears to be 100 % seismic (Calabria and Southeastern Sicily and its offshore region), and historical seismicity levels may even exceed tectonic strain accumulation rates, indicating the seismic rates are not representative for the long-term. Also in the South-Central Mediterranean, the convergent zones (Sicilian backthrust and Calabrian trench) appear to have relatively low ratios of seismic/total deformation rates. But this area shows no clear relation between the proportion of aseismic deformation and tectonic regime. Overall, Southern Italy displays a strongly time-variable and very diffuse pattern of seismicity in response to relatively low tectonic deformation rates and reorganizing plate boundaries.

The work presented in this thesis shows that an integrated approach involving seismic, geodetic and geologic data results in better constrained estimates of the long-term average seismic potential than those based predominantly on past seismicity, especially in regions that strain slowly compared to the timespan of the available seismic catalogues. Such seismic potential estimates can be incorporated in full hazard or risk analyses (as presented in the Chapter 5), either in the form of a best-estimate set of parameters or in a more statistical hazard approach that incorporates several alternative interpretations with different levels of probability.

Appendix A

New GPS constraints on the Africa-Eurasia plate boundary zone in southern Italy

Christine Hollenstein, Hans-Gert Kahle, Alain Geiger, **Sarah Jenny**, Saskia Goes and Domenico Giardini

Geophysical Research Letters, 30 (18), 1935, 10.1029/2003GL017554, 2003

A.1 Abstract

Southern Italy is a key area for understanding the tectonic processes in the Africa-Eurasia collision zone. We analyze new GPS measurements carried out between 1994 and 2001. The results are presented in terms of time series, trajectories and velocities of crustal motion, as well as a geodetic strain rate field. While central Italy, Corsica, Sardinia and the Tyrrhenian Sea move like the Eurasian plate, the overall motion of the Sicily Rift Zone region matches African plate motion. Unexpected are the northnorthwest directed motions of northeastern Sicily and the Eolian islands. Most striking on the deformation field are a north-south oriented compression along the northern Sicilian

coast, compression between Apulia and northwestern Greece as well as extension in the Sicily Rift Zone and the interior of Sicily.

A.2 Introduction

The collision zone between Africa and Eurasia spans the entire Mediterranean and is characterized by trench rollback, back-arc extension and rotating blocks. Southern Italy is one of the key areas for understanding these complex tectonics [*Albarello et al.*, 1995]. We analyze new geodetic data from repeated GPS measurements carried out in southern Italy between 1994 and 2001. We present horizontal rates and trajectories of crustal motion, referenced to a common Eurasian reference system, and which are consistent with results obtained from the network of the International GPS Service (IGS, http://igscb.jpl.nasa.gov). The resulting geodetic strain rate field compares well with the pattern of seismicity.

A.3 Tectonic Setting

During the last 8 to 10 million years, roll-back of the Apennic subduction zone caused counterclockwise rotation of Italy and opening of the Tyrrhenian back-arc basin [*Malinverno and Ryan*, 1986; *Faccenna et al.*, 1996; *Bassi et al.*, 1997]. At the Calabrian arc, oceanic lithosphere has been subducting until at least very recently [e.g., *Wortel and Spakman*, 2000; *Cimini*, 1999]. Currently, Calabria, the Apennines and large parts of the Italian peninsula are dominated by horizontal extension [*Amato and Montone*, 1997]. The recent cessation of southern Apennic thrusting is probably due to collision of the subduction zone with the Apulian block (stations MATE and SPEC) [*Amato and Montone*, 1997; *Gueguen et al.*, 1998]. In Sicily, the eastern end of the Maghrebian thrust belt (GPS site TRAP) meets the western end of the Calabro-Peloritan arc (GPS sites MILA and PACE), and the Hyblean plateau of African origin (GPS site NOTO) [*Ghisetti and Vezzani*, 1981]. Active extension occurs in the Sicily Rift Zone (SRZ) [*Reuther et al.*, 1993] south of Sicily, near GPS sites PANT, GOZO, MLTA, and north of station LAMP.

A.4 Data Analysis, Time Series and Trajectories

The southern Italian GPS data obtained in 1994, 1996, 2000 and 2001 (see Table A.1) were analyzed using the Bernese GPS software 4.2 [*Beutler et al.*, 2001]. The computation combined these data with data from a large continuous network consisting of up to 54 European IGS and EUREF (European Reference Frame, see http://www.euref-iag.org) sites as well as Greek sites. As reference frame for the whole evaluation, we used ITRF97 [*Boucher et al.*, 1998]. For each campaign, the normal equations of daily sessions were generated and combined into a campaign solution. The velocities were estimated by combining all daily normal equations of the complete observation period (1994-2001). We used a subset of 15 selected IGS stations to constrain the network (see Fig. A.3a), fixed their velocities to the ITRF values and set up free network conditions for their coordinates (7 parameter Helmert constraints). Finally, the results were rotated from ITRF97 to a Eurasia fixed reference frame using a rotation rate of 0.257°/Myr around a pole located at 58.27°N and 102.21°W [*Sella et al.*, 2002].

To obtain a realistic margin of error, the formal statistical errors were scaled by the ratio of mean daily repeatability and a posteriori sigma of unit weight (see *Beutler et al.* [2001]). A factor of 8.5 was obtained. To account for degrading accuracy due to correlation between daily solutions, an additional scaling factor was applied: 5 for velocities of continuous stations, 2.5 for velocities of campaign stations as well as for the campaign coordinates of 1994 and 1996 (multi-day solutions) (see e.g., *Zhang et al.* [1997] and *Mao et al.* [1999]).

The campaign coordinate solutions are represented by time series (Fig. A.4) and trajectories (Fig. A.2). In contrast to average velocities, time series and trajectories display the discrete displacements in the time periods between the observation campaigns. The linear fit to the time series was evaluated by F testing χ^2 per degree of freedom. The linearity of motion of most of the stations is significant at a level of 99%. Exceptions are the sites LAMP (E-W component), PANA (N-S), PANT (E-W), and USTI (N-S). The vertical components are not reported, because the uncertainties are too large to allow reliable interpretation.

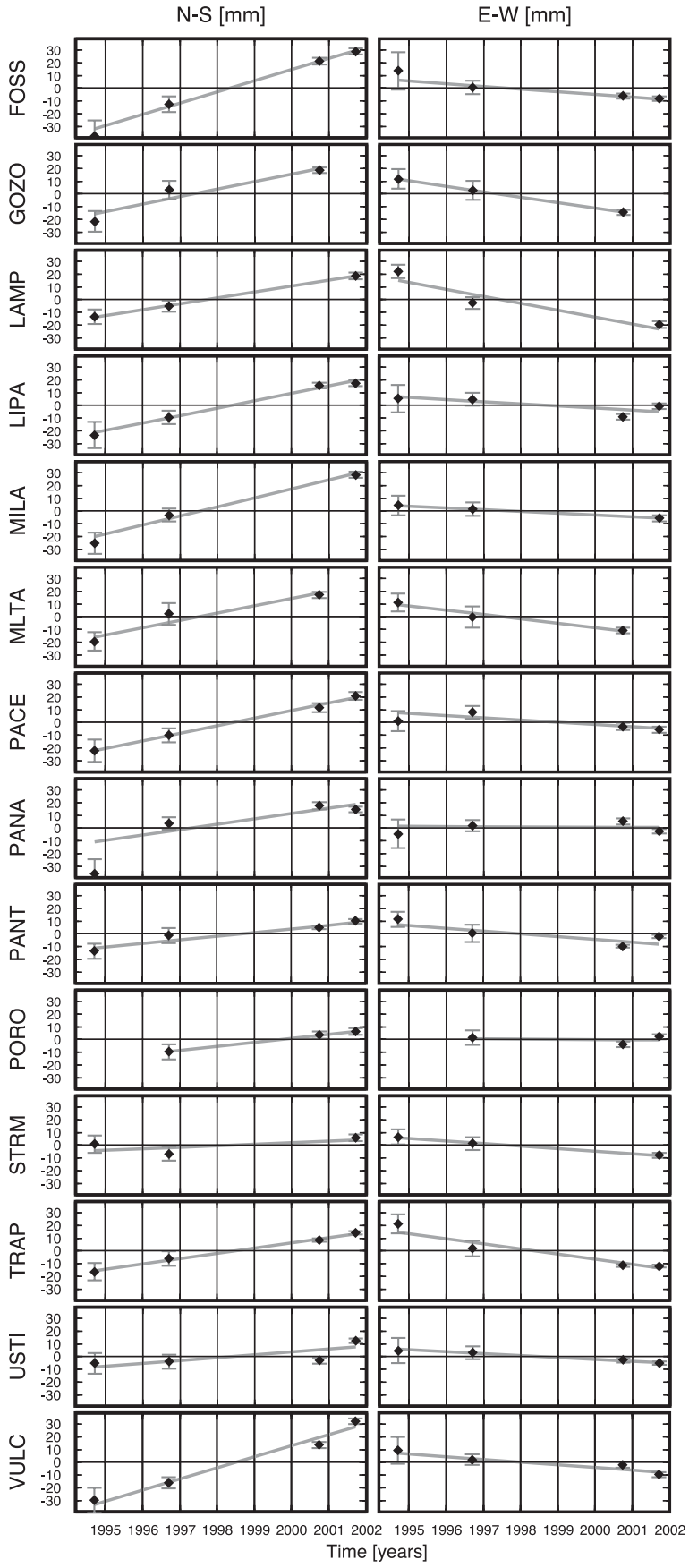

Figure A.1: Coordinate time series of campaign sites relative to Eurasia. The straight gray lines represent the weighted linear regression of the campaign solutions. The error bars show the 95% confidence interval. The stations PANT and STRM may be affected by their location near a caldera or active volcano.

Site	94	96	00	01	Perm.	Lat [°]	Lon [°]	$v_n[\frac{mm}{yr}]$	$v_e[\frac{mm}{yr}]$
AJAC					00-01	41.928	8.763	-0.9 ± 0.9	1.0 ± 0.7
APAX					95-01	39.141	20.249	2.2 ± 0.2	-0.3 ± 0.2
CAGL					96-01	39.136	8.973	-0.1 ± 0.1	-0.9 ± 0.1
FOSS	•	•	•	•		38.100	14.919	8.5 ± 0.9	-1.7 ± 0.8
GOZO	•	•	•			36.023	14.270	5.9 ± 1.0	-3.8 ± 0.9
LAMP	•	•		•	99-01	35.500	12.606	2.5 ± 0.8	-3.5 ± 0.8
LIPA	•	•	•	•		38.490	14.933	5.3 ± 0.8	-1.1 ± 0.8
MATE	•		•		94-01	40.649	16.705	3.9 ± 0.0	0.4 ± 0.0
MILA	•	•		•		38.271	15.231	6.6 ± 0.8	-1.0 ± 0.8
MLTA	•	•	•			35.946	14.453	5.6 ± 1.0	-3.0 ± 0.9
NOTO					95-01	36.876	14.990	3.6 ± 0.0	-2.4 ± 0.0
OTHF					96-00	39.865	19.429	1.1 ± 0.5	-3.2 ± 0.4
PACE	•	•	•	•		38.266	15.520	5.2 ± 0.9	-1.2 ± 0.8
PANA	•	•	•	•		38.633	15.074	4.3 ± 0.8	0.2 ± 0.7
PANT	•	•	•	•		36.832	11.945	2.4 ± 0.5	-2.0 ± 0.5
PORO		•	•	•		38.604	15.910	2.7 ± 1.2	0.2 ± 1.0
SPEC	•	•	•	•		40.063	18.458	3.1 ± 3.2	2.5 ± 2.7
STRM	•	•		•		38.801	15.242	0.0 ± 0.8	-1.6 ± 0.7
TRAP	•	•	•	•		38.004	12.582	3.5 ± 0.5	-3.9 ± 0.6
UNPG					98-01	43.119	12.356	1.0 ± 0.3	-0.8 ± 0.2
USTI	•	•	•	•		38.699	13.154	1.5 ± 0.7	-0.9 ± 0.6
VULC	•	•	•	•		38.378	14.985	8.0 ± 0.8	-1.5 ± 0.7

Table A.1: Observation History and Velocities Relative to Eurasia.
• : campaign measurements, 1994 and 1996: 5-8 h per day during 2-11 days, 2000 and 2001: at least 12 h; Perm.: time span of continous measurements; v_n: north component of the site velocity, v_e: east component. The errors given are obtained by scaling the formal statistical errors as described in Section A.4.

A.5 Velocity Field, Strain Rates and Comparison With Seismic Activity

The site velocities (Table A.1 and Fig. A.3) in central Italy (UNPG), Corsica (AJAC) and Sardinia (CAGL) are less than 1.4 mm/yr relative to Eurasia. Due to a lack of islands, the deformation of the Tyrrhenian can only be deduced from the stations USTI and STRM, which show rates of 1.7 ± 0.7 mm/yr towards northwest and west, respectively. There is no indication that the opening of the Tyrrhenian Sea is still active.

The motion of this whole area differs little from Eurasian plate motion.

In contrast, the velocities of Lampedusa (LAMP) and western Sicily (TRAP) towards the northwest fit within 1.8 mm/yr the African (Nubia) plate motion of the REVEL model [*Sella et al.*, 2002]. GOZO, MLTA and NOTO show slightly different directions of motion, but their kinematic pattern is still similar to the one of the African plate. PANT, located at the northwestern end of the SRZ, displays a smaller velocity to the northwest than expected from its geographic position. The reason can be found in the GPS solution of the 2001 campaign for which the east component shows a 6.1 ± 0.7 mm deviation from the linear trend (Fig. A.4 and A.2). This could be caused by the location of the site near the northwestern rim of the Pantelleria caldera, which has experienced deflation phenomena [*Bonaccorso and Mattia*, 2000].

An interesting feature is observed in northeastern Sicily and the Eolian Islands. Their motion is significantly more northerly directed than the other Sicilian and SRZ sites. From the relatively large rate of 8.7 ± 0.9 mm/yr at FOSS, the velocities decrease eastwards (down to 2.8 ± 1.2 mm/yr at PORO) and northwards (down to 1.6 ± 0.7 mm/yr at STRM). When referenced to the African plate, the velocity field for northeastern Sicily resembles a clockwise rotation (compare (Fig. A.3b). The rates of VULC and LIPA indicate a shortening of 2.7 ± 1.1 mm/yr between the two islands Vulcano and Lipari. This agrees with results of terrestrial measurements repeated over the last 20 years, which revealed right-lateral movement with a shortening of the same order of magnitude [*Bonaccorso*, 2002].

Extension across the Strait of Messina [*Anzidei et al.*, 1997] can only be assessed from the sites PACE and PORO which show a small lengthening of the east-west component of $1.31 \pm .3$ mm/yr which is considered to be insignificant. The Apulian sites - MATE and SPEC - move towards the north-northeast and northeast, respectively, with velocities of 4.0 mm/yr. This indicates a significantly different kinematic pattern than found in Calabria and Sicily or in northwestern Greece and supports a model of counterclockwise rotation of the Apulia/Adriatic region. The large uncertainty at SPEC is caused by a re-monumentation of the site.

From the GPS velocities, we calculated the strain rate field with the method of collocation [*Kahle et al.*, 2000] using a correlation length of 150 km and a sigma of the signal of 3.25 mm/yr (Fig. A.4). The strain rates are relatively weakly constrained, due

to the inhomogeneous site distribution dictated by the uneven coverage of islands. Error propagation yields uncertainties of 10 to 30 nstrain/yr. Caution should, therefore, be exercised when interpreting details in the deformation field. The regional features are, however, well represented.

Compression occurs between Apulia and northwestern Greece. Extension to the west and southwest of Matera fits the location and focal mechanisms of seismicity well (Fig. A.4).

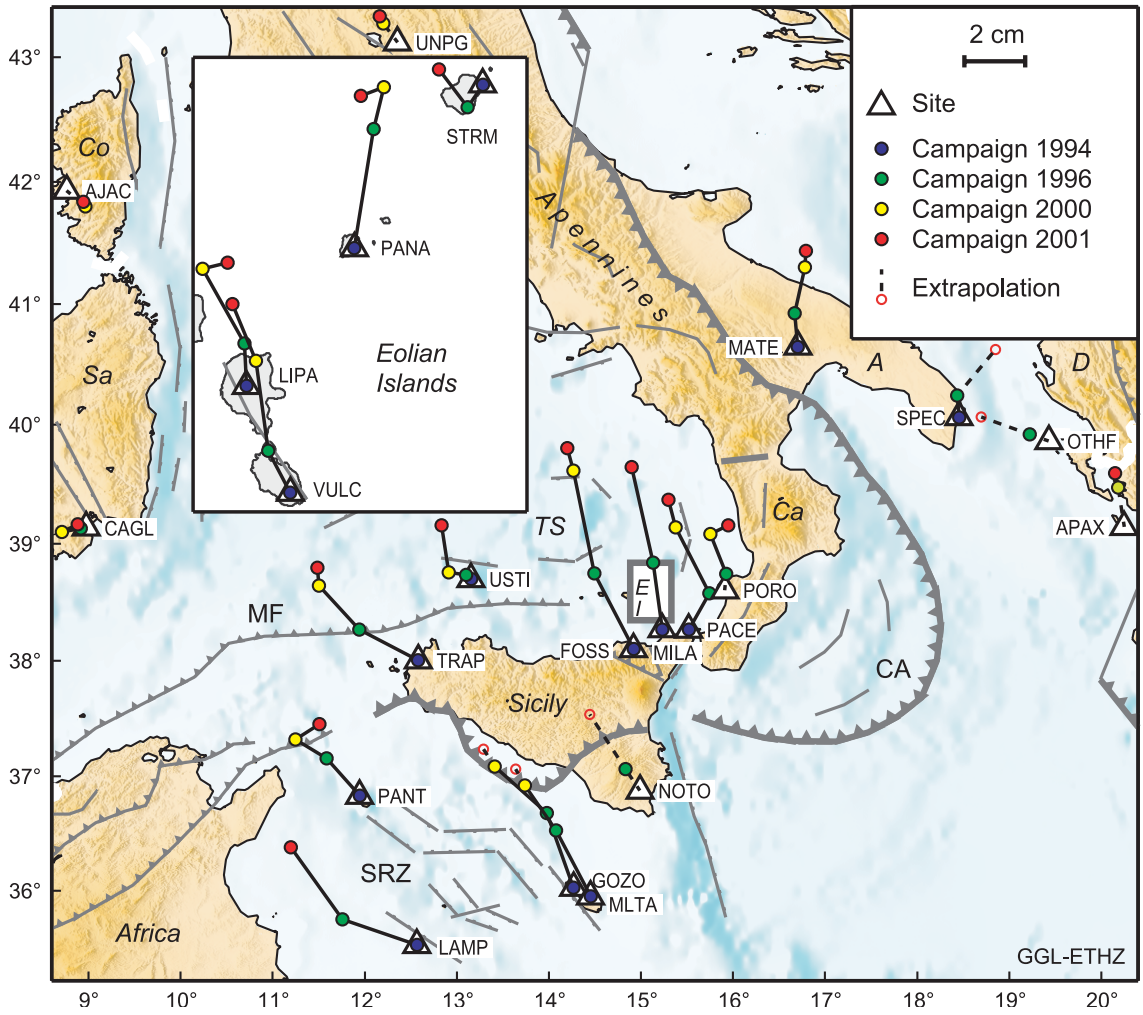

Figure A.2: Trajectories of crustal motion relative to Eurasia for the time period 1994-2001 based on the time series of the campaign solutions. For sites where start or end points are missing, the trajectories were completed by extrapolation, based on the velocity solution (see Table A.1). The uncertainties of the individual coordinate solutions are shown (component-wise) as error bars in Fig. A.4. (A: Apulia, CA: accretionary wedge of the Calabrian arc, Ca: Calabria, Co: Corsica, D: Dalmatia, EI: Eolian Islands, MF: Maghrebian front, Sa: Sardinia, SRZ: Sicily Rift Zone, TS: Tyrrhenian Sea)

Normal and shear strain rates projected perpendicular and parallel to the faults of

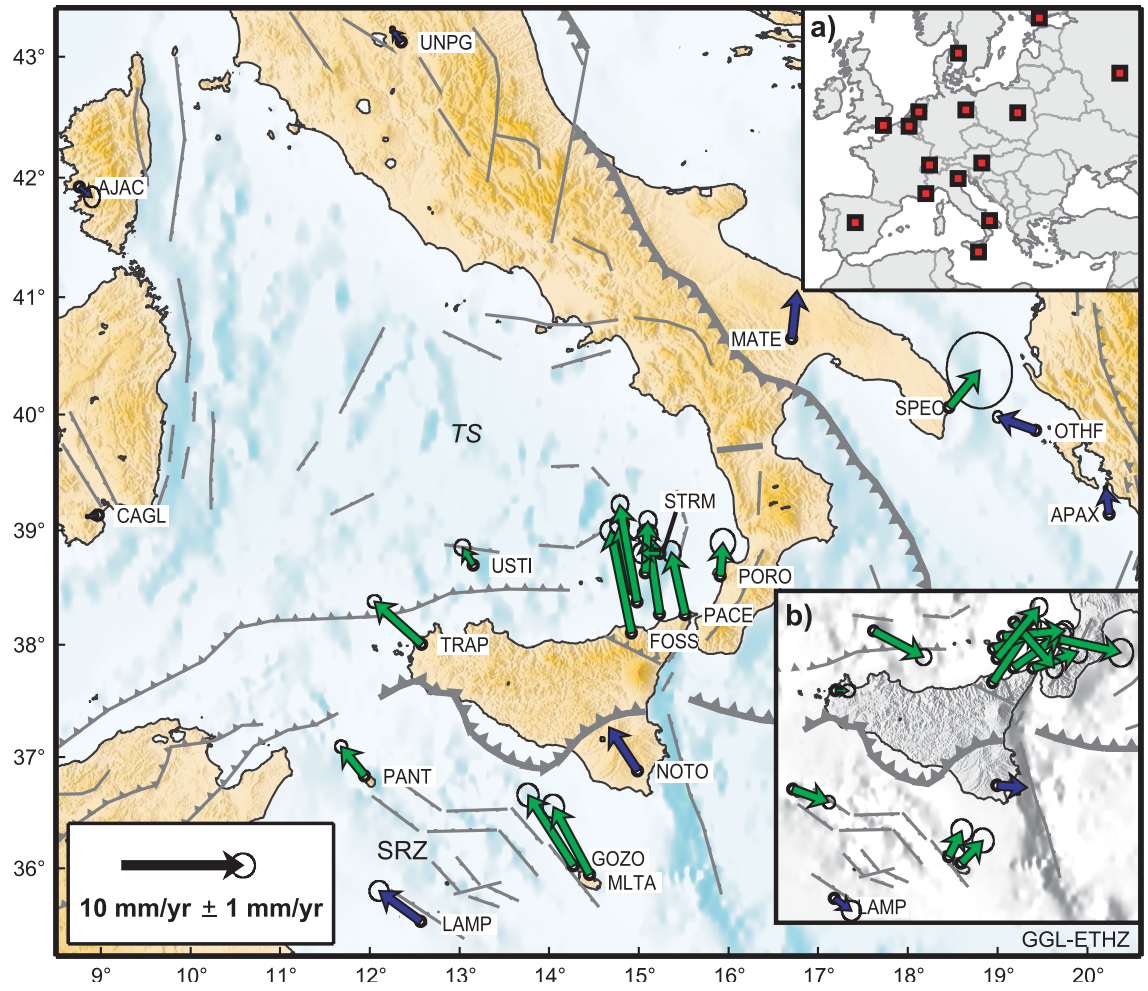

Figure A.3: GPS velocities relative to Eurasia. Green arrows: based on repeated GPS measurements between 1994 and 2001 (compare Table A.1). Blue arrows: based on continuous GPS measurements. Error ellipses: Formal statistical errors scaled by factors described in Section A.4. Insets: (a) IGS sites used as reference stations. (b) GPS velocities relative to the African plate.

the Sicily Rift Zone, show extensional and dextral motion, respectively (Fig. A.4 inset a2). This agrees with findings of [*Cello*, 1987] who invoked a combination of pull-apart and dextral strike-slip in order to explain the tectonic processes in this region.

The dominant feature of the strain rate field is the strong north-south compression of up to 60 ± 23 nstrain/yr along the Maghrebian front north of Sicily (see Fig. A.4 inset a1). The magnitude of this compression was not known before, but it is in general agreement with numerous intermediate size earthquakes with compressional fault plane solutions. Most of the compression between the African and Eurasian plates seems to be taken up along this belt. Compression in the northeast of Sicily even exceeds the

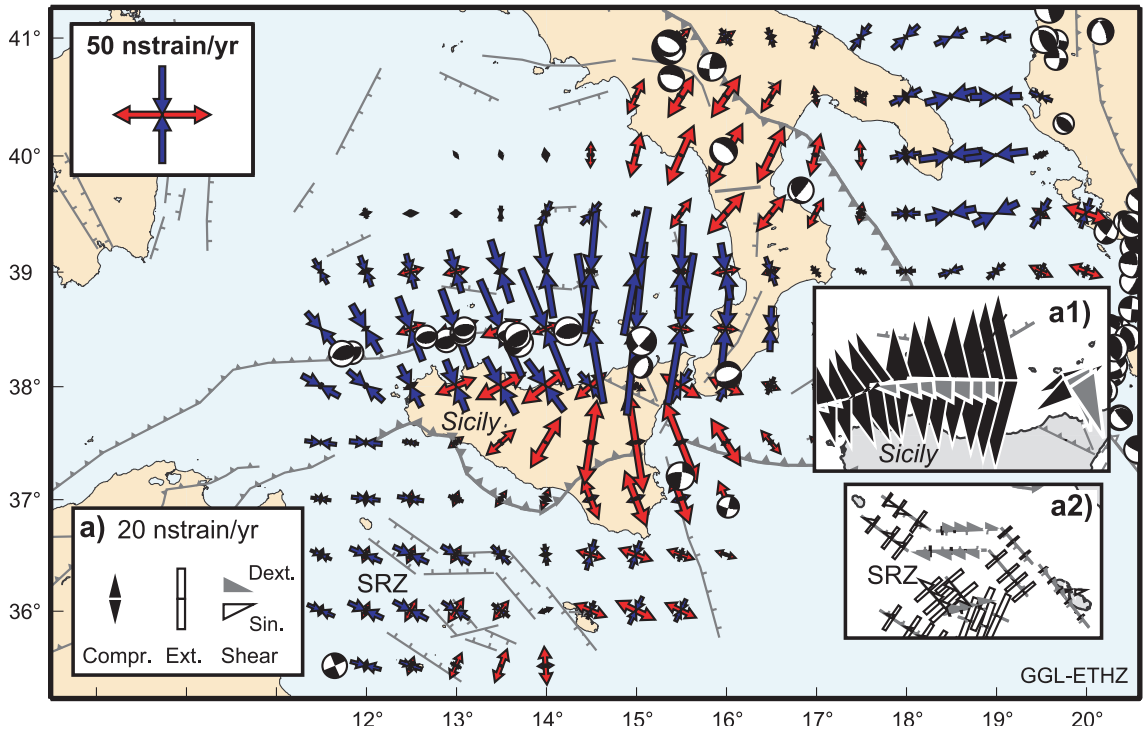

Figure A.4: Principal axes and eigenvalues of the strain rate tensor calculated from the velocity field shown in Fig. A.3. Red arrows indicate extension, blue arrows compression. 10 nstrain/yr correspond to a relative motion of 1 mm/yr over a distance of 100 km. Focal mechanisms of larger earthquakes (depth < 40 km) between 1976 and 2002 [Harvard CMT solutions, http://www.seismology.harvard.edu; *Pondrelli et al.* [2002], http://www.ingv.it/seismoglo/RCMT/]. Insets: Normal and shear strain rates projected perpendicular and parallel to selected faults, respectively. (a1) Area north of Sicily. (a2) Sicily Rift Zone (SRZ).

shortening between the plates, by more than 2.5 mm/yr. In the Eolian Islands region, a dextral shear strain reaching 40 ± 10 nstrain/yr is superimposed on the compression. The interior of Sicily shows extension. Both the compression and extension are mainly constrained by the differential velocities between the sites in northeastern, southern (NOTO) and western (TRAP) Sicily. Because of the site distribution it cannot be determined whether the extension is confined to a particular fault system or evenly distributed across the interior of the island.

A.6 Discussion and Conclusions

The southern Italian GPS data document small, but mostly stable deformation rates. The new GPS results define a pattern of crustal motion in southern Italy that is generally

consistent with geological and seismological data.

The GPS velocities and strain rates support the following results of previous work: compression between Apulia and northwestern Greece, extension across the southern Apennines [*Amato and Montone*, 1997; *Hunstad et al.*, 2003], right-lateral movement between Vulcano and Lipari [*Bonaccorso*, 2002], as well as extension and dextral strike-slip in the Sicily Rift Zone [*Cello*, 1987].

In addition, new kinematic constraints have been obtained: Corsica, Sardinia and the Tyrrhenian Sea move like the Eurasian plate. In contrast, Lampedusa, the Sicily Rift Zone and the southwestern coast of Sicily are dominated by African motion. The compression between the African and Eurasian plates seems to be concentrated along the Maghrebian front to the northwest and north of Sicily, which is consistent with compressional focal mechanisms of earthquakes along this belt. Unexpected, large north components of the velocities in northeastern Sicily enhance compression to the north of it and cause extension in the interior of Sicily.

A.7 Acknowledgments

.

We acknowledge with gratitude the support of Centro Spaziale di Matera, Italy, for providing personnel and instruments during the field campaigns 2000 and 2001. We are grateful to Dr. D. DelRosso and Dr. F. Vespe for field work assistance. The project originates from an earlier collaboration of ETH Zürich with the Dipartimento di Fisica, University of Bologna, Italy (Prof. S. Zerbini) and the Deutsches Geodätisches Forschungsinstitut, München, Germany (Prof. H. Drewes). The valuable contribution of these institutes in the 1994 and 1996 campaigns is gratefully acknowledged. We thank Prof. M. Cocard, Université Laval, Canada, for thoughtful comments and help at an earlier stage of this project. Valuable comments of the editor and two reviewers substantially helped to improve the manuscript. Research grants were provided by ETH Zürich and Munich Re.

Bibliography

Abe, K., and S. Noguchi, Revision of magnitudes of large shallow earthquakes, 1897-1912, *Phys. Earth Planet. Int.*, *33*, 1–11, 1983.

Aki, K., Maximum likelihood estimate of the parameter b in the formula log N = a - bm and its confidence limits, *Bull. Earthquake Res. Inst. Tokyo Uni.*, *43*, 237–239, 1965.

Albarello, D., E. Mantovani, D. Babbuci, and C. Tanburelli, Africa-Eurasia kinematics: main constraints and uncertainties, *Tectonophysics*, *243*, 25–36, 1995.

Albarello, D., E. Mantovani, and M. Viti, Finite element modelling of the recent-present deformation pattern in the calabrian arc and surrounding regions, *Ann. Geofis.*, *40*(4), 833–848, 1997.

Amato, A., and P. Montone, Present-day stress field and active tectonics in southern peninsular Italy, *Geophys. J. Int.*, *130*, 519–5345, 1997.

Ambraseys, N. N., Reassessment of earthquakes, 1900-1999, in the Eastern Mediterranean and the Middle East, *Geophys. J. Int.*, *145*, 471–485, 2001a.

Ambraseys, N. N., The Kresna earthquake of 1904 in Bulgaria, *Ann. Geofis.*, *44*, 95–117, 2001b.

Ambraseys, N. N., and J. A. Jackson, Seismicity of the Sea of Marmara (Turkey) since 1500, *Geophys. J. Int.*, *141*, F1–F6, 2000.

Ambrosetti, P., C. Bartolini, C. Bosi, F. Carraro, N. Ciaranfi, F. Ghisetti, G. Papani, L. Vezzani, A. Zanferrari, and N. Zitellini, Neotectonic model of Italy, Consiglio Nazionale delle Ricerche, Florence, Italy, 1987.

Amelung, F., and G. King, Large-scale tectonic deformation inferred from small earthquakes, *Nature*, *386*, 702–705, 1997.

Anderson, H., Is the Adriatic an African promontory?, *Geology*, *15*, 212–215, 1987.

Anderson, H., and J. A. Jackson, Active tectonics of the Adriatic region, *Geophys. J. R. astr. Soc.*, *91*, 937–983, 1987.

Anzidei, M., P. Baldi, C. Bonini, G. Casula, S. Gandolfi, and F. Riguzzi, Geodetic surveys across the Messina Straits (southern Italy) seismogenetic area, *J. Geodynamics*, *25*, 85–97, 1997.

Argnani, A., The Strait of Sicily rift zone: foreland deformation related to the evolution of a back-arc basin, *J. Geodynamics*, *12*(2-4), 311–331, 1990.

Argnani, A., and C. Bonazzi, Neotectonics of the Eastern Sicily offshore: recent reactivation of an old structure, in *Workshop on: Seismogenic faulting and seismic activity in the Calabrian Arc region*, pp. 12–13, Università degli Studi di Messina, Istituto Nazionale di Geofisica e Vulcanologia, Taormina, Sicily, 2003.

Argnani, A., and L. Torelli, The Pelagian Shelf and its graben system (Italy/Tunesia), in *Peri-Tethys Memoir 6: Peri-Tethyan Rift/Wrench Basins and Passive Margins*, *Mém. natn. Hist. nat.*, vol. 186, edited by S. Crasquin-Soleau, pp. 529–544, Publications Scientifique du Musée, 2001.

Argus, D. F., and M. B. Heflin, Plate motion and crustal deformation estimated with geodetic data from GPS, *Geophys. Res. Lett.*, *22*(15), 1973–1976, 1995.

Armijo, R., H. Lyon-Caen, and D. Papanastassiou, E-W Extension and Holocene normal-fault scarps in the Hellenic arc, *Geology*, *20*, 491–494, 1992.

Armijo, R., A. Hubert, and A. Barka, Westward propagation of the North Anatolian Fault into the northern Aegean: Timing and kinematics, *Geology*, *27*(3), 267–270, 1999.

Baratta, M., I Terremoti d'Italia, Arnaldo Forni, Bologna, 1901.

Barka, A., The North Anatolian Fault Zone, *Annales Tectonicae*, *Suppl. to Vol. VI*, 164–195, 1992.

Barka, A., Neotectonics of the Marmara Sea region, in *Active tectonics of the Northwestern Anatolia -The MARMARA Poly-Project*, edited by C. Schindler and M. Pfister, pp. 55–88, VdF Hochschulverlag AG, 1997.

Barka, A., and K. Kandinsky-Cade, Strike-slip fault geometry in Turkey and its influence on earthquake activity, *Tectonics*, *7*(3), 663–684, 1988.

Bassi, G., R. Sabadini, and S. Reba, Modern tectonic regime in the Tyrrhenian area: observations and models, *Geophys. J. Int.*, *129*, 330–346, 1997.

Beavan, J., and J. Haines, Contemporary horizontal velocity and strain rate fields of the Pacific-Australian plate boundary zone through New Zealand, *J. geophys. Res.*, *106*, 741–770, 2001.

Ben-Zion, Y., and L. Zhu, Potency-magnitude scaling relations for southern California earthquakes with $1.0 < M - L < 7.0$, *Geophys. J. Int.*, *148*(3), F1–F5, 2002.

Ben-Zion, Y., M. Eneva, and Y. F. Liu, Large earthquake cycles and intermittent criticality on heterogeneous faults due to evolving stress and seismicity, *J. geophys. Res.*, *108*(B6), 2307, doi:10.1029/2002JB002121, 2003.

Beutler, G., et al., Bernese GPS Software Version 4.2, Astronomical Institute, University of Berne, 2001.

Bianca, M., C. Monaco, L. Tortorici, and L. Cernobori, Quaternary normal faulting in south-eastern Sicily (Italy): a seismic source for the 1693 large earthquake, *Geophys. J. Int.*, *139*, 1999.

Bijwaard, H., W. Spakman, and E. R. Engdahl, Closing the gap between regional and global travel time tomography, *J. geophys. Res.*, *103*(B12), 30'055–30'078, 1998.

Boccaletti, M., G. Cello, and L. Tortorici, Transtensional tectonics in the sicily channel, *Journal of Structural Geology*, *9*(7), 869–876, 1987.

Boccone, P., Intorno al terremoto della Sicilia seguito l'anno 1693, Museo di Fisica, Venezia, 1697.

Bonaccorso, A., Ground deformation of the southern sector of the Aeolian islands volcanic arc from geodetic data, *Tectonophysics*, *351*(3), 181–192, 2002.

Bonaccorso, A., and M. Mattia, Deflation acting on Pantelleria island (Sicily Channel) inferred through geodetic data, *Earth Planet. Sci. Lett.*, *180*(1-2), 91–101, 2000.

Bordoni, P., and G. Valensise, Deformation of the 125 Ka marine terraces in Italy: tectonic implications, *Coastal Tectonics, Geol. Soc. Spec. Publ.*, *146*, 71–110, 1998.

Boschi, E., P. Gasperini, and F. Mulargia, Forecasting where larger crustal earthquakes are likely to occur in Italy in the near future, *Bull. seism. Soc. Am.*, *85*(5), 1475–1482, 1995a.

Boschi, E., E. Guidoboni, and D. Mariotti, Seismic effects of the strongest historical earthquakes in the Syracuse area, *Ann. Geofis.*, *38*, 223–253, 1995b.

Boucher, C., Z. Altamini, and P. Sillard, Results and analysis of the ITRF96, *Technical note 24*, Central Bureau of IERS, Observatoire de Paris, Paris, 1998.

Braunmiller, J., U. Kradolfer, M. Baer, and D. Giardini, Regional moment tensor determination in the European-Mediterranean area - initial results, *Tectonophysics*, *356*, 5–22, 2002.

Buiter, S. J. H., R. Govers, and M. J. R. Wortel, Two-dimensional simulations of surface deformation caused by slab detachment, *Tectonophysics*, *354*, 195–210, 2002.

Carletti, F., and P. Gasperini, Lateral variations of seismic intensity attenuation in italy, *Geophys. J. Int.*, *155*, 839–856, 2003.

Carminati, E., M. J. R. Wortel, P. T. Meijer, and R. Sabadini, The two-stage opening of the western-central Mediterranean basins: a forward modeling test to a new evolutionary model, *Earth Planet. Sci. Lett.*, *160*(3-4), 667–679, 1998a.

Carminati, E., M. J. R. Wortel, W. Spakman, and R. Sabadini, The role of slab detachment processes in the opening of the western-central Mediterranean basins: some geological and geophysical evidence, *Earth Planet. Sci. Lett.*, *160*(3-4), 651–665, 1998b.

Catalano, S., and G. De Guidi, Late Quaternary uplift of northeastern Sicily: relation with the active normal faulting deformation, *J. Geodynamics*, *36*, 445–467, 2003.

Catalano, S., A. Di Stefano, A. Sulli, and F. P. Vitale, Paleogeography and structure of the central Mediterranean: Sicily and its offshore area, *Tectonophysics*, *260*, 291–323, 1996.

Cello, G., Structure and deformation processes in the Strait of Sicily Rift Zone, *Tectonophysics*, *141*, 237–247, 1987.

Chen, W. P., and J. Nabelek, Seismogenic strike-slip faulting and the development of the North China Basin, *Tectonics*, *7*(5), 975–989, 1988.

Cimini, G., P-wave deep velocity structure of the Southern Tyrrhenian Subduction Zone from nonlinear teleseismic traveltime tomography, *Geophys. Res. Lett.*, *26*(24), 3'709–3'712, 1999.

Clarke, P., et al., Crustal strain in Central Greece from repeated GPS measurements in the interval 1989-1997, *Geophys. J. Int.*, *134*(4), 195–214, 1998.

Cocard, M., H.-G. Kahle, Y. Peter, A. Geiger, G. Veis, S. Felekis, H. Billiris, and D. Paradissis, New constraints on the rapid crustal motion of the Aegean region: Recent results inferred from GPS measurements (1993-1998) across the West Hellenic Arc, Greece, *Earth Planet. Sci. Lett.*, *172*, 39–47, 1999.

D'Agostino, N., and G. Selvaggi, Present-day kinematics of the Calabrian subduction zone from continuous GPS measurements, in *Workshop on: Seismogenic faulting and seismic activity in the Calabrian Arc region*, pp. 28–29, Università degli Studi di Messina, Istituto Nazionale di Geofisica e Vulcanologia, Taormina, Sicily, 2003.

Davies, R., P. England, B. Parsons, H. Billiris, D. Paradissis, and G. Veis, Geodetic strain of Greece in the interval 1892-1992, *J. geophys. Res.*, *102*, 24,571–24,588, 1997.

Davis, G. A., Y. Zheng, C. Zhang, and B. Xu, The Mesozoic Fengning-Longhua and Jiaoqier fault zones, north China: new interpretations of controversial structures, Cordilleran Section - 97th Annual Meeting, and Pacific Section, American Association of Petroleum Geologists (April 9-11), Universal City, CA, USA, 2001.

De Astis, G., A. Peccerillo, P. D. Kempton, L. La Volpe, and T. W. Wu, Transition from calc-alkaline to potassium-rich magmatism in subduction environments: geochemical

and Sr, Nd, Pb isotopic constraints from the island of Vulcano (Aeolian arc), *Contrib. Miner. Petrol.*, *139*(6), 684–703, 2000.

De Rosa, R., H. Guillou, R. Mazzuoli, and V. G., New unspiked K-Ar ages of volcanic rocks of the central and western sector of the Aeolian Islands: reconstruction of the volcanic stages, *J. Volcanol. Geoth. Res.*, *120*, 161–178, 2003.

DeMets, C., R. Gordon, D. Argus, and S. Stein, Current plate motions, *Geophys. J. Int.*, *101*, 425–478, 1994.

Devoti, R., et al., Geodetic control on recent tectonic movements in the central Mediterranean area, *Tectonophysics*, *346*(3-4), 151–167, 2002.

Dewey, J. F., M. Helman, E. Turco, D. Hutton, and S. Knott, Kinematics of the Western Mediterranean, in *Alpine Tectonics*, vol. 45, edited by M. Coward, D. Dietrich, and R. Park, pp. 265–283, Spec. Publ. Geol. Soc. London, blackwell Scientific Publications, 1989.

Ding, X., Y. Chen, Q. Huang, and G. Chen, Map 49: Major active faults and their recent movement, in *Lithospheric Dynamics Atlas of China*, edited by X. Ma, China Cartogr. Pub. House, Beijing, 1989.

Doglioni, C., F. Innocenti, and G. Mariotti, Why Mt Etna?, *Terra Nova*, *13*(1), 25–31, 2001.

Dziewonski, A., T.-A. Chou, and J. Woodhouse, Determination of earthquake source parameters from waveform data for studies of global and regional seismicity, *J. geophys. Res.*, *86*, 2825–2852, 1981.

Erdik, M., Y. A. Biro, T. Onur, K. Sesetyan, and G. Birgoren, Assessment of earthquake hazard in Turkey and neighboring regions, *Ann. Geofis.*, *42*(6), 1125 –1138, 1999.

Eyidoğan, H., Rates of crustal deformation in western Turkey as deduced from major earthquakes, *Tectonophysics*, *148*, 83–92, 1988.

Faccenna, C., P. Davy, J. P. Brun, R. Funiciello, D. Giardini, M. Mattei, and T. Nalpas, The dynamics of back-arc extension: An experimental approach to the opening of the Tyrrhenian Sea, *Geophys. J. Int.*, *126*(3), 781–795, 1996.

Faccenna, C., T. W. Becker, F. P. Lucente, L. Jolivet, and F. Rossetti, History of subduction and back-arc extension in the Central Mediterranean, *Geophys. J. Int.*, *145*, 809–820, 2001a.

Faccenna, C., F. Funiciello, D. Giardini, and P. Lucente, Episodic back-arc extension during restricted mantle convection in the Central Mediterranean, *Earth Planet. Sci. Lett.*, *187*, 105–116, 2001b.

Faccenna, C., C. Piromallo, A. Crespo-Blanc, L. Jolivet, and F. Rossetti, Lateral slab deformation and the origin of the western Mediterranean arcs, *Tectonics*, *23*(1), doi: 10.1029/2002TC001488, 2004.

Fernandes, R., B. Ambrosius, R. Noomen, L. Bastos, M. J. R. Wortel, W. Spakman, and R. Govers, The relative motion between Africa and Eurasia as derived from ITRF2000 and GPS data, *Geophys. Res. Lett.*, *30*(16), doi:10.1029/2003GL017089, 2003.

Field, E. H., D. D. Johnson, and J. F. Dolan, A mutually consistent seismic-hazard source model for Southern California, *Bull. seism. Soc. Am.*, *89*(3), 559–578, 1999.

Flesch, L. M., A. J. Haines, and W. E. Holt, Dynamics of the India-Eurasia collision zone, *J. geophys. Res.*, *106*(B8), 16,435–16,460, 2001.

Frepoli, A., and A. Amato, Fault plane solutions of crustal earthquakes in Southern Italy (1988-1995): seismotectonic implications, *Ann. Geofis.*, *43*(3), 437–467, 2000.

Galli, P., and V. Bosi, Catastrophic 1638 earthquakes in Calabria (southern Italy): New insights from paleoseismological investigation, *J. geophys. Res.*, *108*(B1), 2004, doi:10.1029/2001JB001713, 2003.

Gao, W., Z. Chen, and X. Xie, Fundamental characteristics of active faults in China, *Quat. Int.*, *25*, 13–17, 1995.

Gasperini, P., The attenuation of seismic intensity in Italy: a bilinear shape indicates the dominance of deep phases at distances longer than 45 km, *Bull. seism. Soc. Am.*, *91*(2), 826–841, 2001.

Gasperini, P., and G. Ferrari, Deriving numerical estimates from descriptive information: the estimation of earthquake synthetic parameters, *Ann. Geofis.*, *43*, 729–746, 2000.

Gautier, P., J. P. Brun, R. Moriceau, D. Sokoutis, J. Martinod, and L. Jolivet, Timing, kinematics and cause of Aegean extension: a scenario based on a comparison with simple analogue experiments, *Tectonophysics*, *315*, 31–72, 1999.

Ghisetti, F., and L. Vezzani, Contribution of stuctural analysis to understanding the geodynamic evolution of the Calabrian arc (Southern Italy), *Journal of Structural Geology*, *3*(4), 371–381, 1981.

Ghisetti, F., and L. Vezzani, Normal faulting, transcrustal permeability and seismogenesis in the Apennines (Italy), *Tectonophysics*, *348*(1-3), 155–168, 2002.

Giardini, D., The Global Seismic Hazard Assessment Program (GSHAP) 1992-1999, *Ann. Geofis.*, *42*(6), 957–974, 1999.

Giardini, D., and P. Basham, The Global Seismic Hazard Assessment Program (GSHAP), *Ann. Geofis.*, *36*(3-4), 3–13, 1993.

Gioncada, A., R. Mazzuoli, M. Bisson, and M. T. Pareschi, Petrology of volcanic products younger than 42 ka on the Lipari-Vulcano complex (Aeolian Islands, Italy): an example of volcanism controlled by tectonics, *J. Volcanol. Geoth. Res.*, *122*, 191–220, 2003.

Giunchi, C., A. Kiratzi, R. Sabadini, and E. Louvari, A numerical model of the Hellenic subduction zone: Active stress field and sea-level changes, *Geophys. Res. Lett.*, *23*(18), 2485–2488, 1996a.

Giunchi, C., R. Sabadini, E. Boschi, and P. Gasperini, Dynamic models of subduction; geophysical and geological evidence in the Tyrrhenian Sea, *Geophys. J. Int.*, *126*(2), 555–578, 1996b.

Godano, C., and F. Pingue, Is the seismic moment-frequency relation universal?, *Geophys. J. Int.*, *142*, 193–198, 2000.

Goes, S., D. Giardini, S. Jenny, C. Hollenstein, H.-G. Kahle, and A. Geiger, A recent tectonic reorganization in the South-Central Mediterranean, *Earth Planet. Sci. Lett.*, 2004.

Gomberg, J., P. Bodin, K. Larson, and H. Dragert, Earthquake nucleation by transient deformations caused by the M=7.9 Denali, Alaska, earthquake, *Nature*, *427*(6975), 621–624, 2004.

Gueguen, E., C. Doglioni, and M. Fernandez, On the post-25 Ma geodynamic evolution of the western Mediterranean, *Tectonophysics*, *298*(1-3), 259–269, 1998.

Guidi, D. G., S. Catalano, C. Monaco, and L. Tortorici, Morphological evidence of Holocene coseismic deformation in the Taormina region (NE Sicily), *J. Geodynamics*, *36*, 193–211, 2003.

Gvirtzman, Z., and A. Nur, The formation of Mount Etna as the consequence of slab rollback, *Nature*, *401*, 782–785, 1999.

Haines, A. J., and W. E. Holt, A procedure for obtaining the complete horizontal motions within zones of distributed deformation from the inversion of strain rate data, *J. geophys. Res.*, *98*, 12,057–12,082, 1993.

Haines, A. J., J. A. Jackson, W. E. Holt, and D. C. Agnew, Representing distributed deformation by continuous velocity fields, in *Sci. Rept. 98/5, inst. of Geol. and Nucl. Sci.*, Wellington, New Zealand, 1998.

Hanks, T., and H. Kanamori, A moment magnitude scale, *J. geophys. Res.*, *84*, 2348–2350, 1979.

Harris, R. A., and R. W. Simpson, The 1999 M-w 7.1 Hector Mine, California, earthquake: A test of the stress shadow hypothesis?, *Bull. seism. Soc. Am.*, *92*(4), 1497–1512, 2002.

Hattori, S., Regional distribution of b value in the world, *Bull. Inst. seism. Earthq. Eng.*, *12*, 39–57, 1974.

Hatzfeld, D., M. Ziazia, D. Kementzetzidou, P. Hatzidimitriou, D. Panagiotopoulos, K. Makropoulos, P. Papadimitriou, and A. Deschamps, Microseismicity and focal mechanisms at the western termination of the North Anatolian Fault and their implications for continental tectonics, *Geophys. J. Int.*, *137*(3), 891–908, 1999.

Hippolyte, J. C., J. Angelier, and E. Barrier, Compressional and extensional tectonics in an arc system - example of the Southern Apennines, *Journal of Structural Geology*, *17*(12), 1725–1740, 1995.

Hirn, A., R. Nicolich, J. Gallart, M. Laigle, L. Cernobori, and ETNASEIS Scientific Group, Roots of Etna volcano in faults of great earthquakes, *Earth Planet. Sci. Lett.*, *148*, 171–191, 1997.

Hoernle, K., Y. Zhang, and D. Graham, Seismic and geochemical evidence for large-scale mantle upwelling beneath the eastern Atlantic and western and central Europe, *Nature*, *374*, 34–39, 1995.

Hollenstein, C., H.-G. Kahle, A. Geiger, S. Jenny, S. Goes, and D. Giardini, New GPS constraints on the Africa-Eurasia Plate Boundary Zone in Southern Italy, *Geophys. Res. Lett.*, *30*(18), 1935, doi:10.1029/2003GL017554, 2003.

Holt, W. E., and A. J. Haines, The kinematics of northern South Island, New Zealand, determined from geologic strain rates, *J. geophys. Res.*, *100*, 17,991–18,010, 1995.

Holt, W. E., N. Chamot-Rooke, X. Le Pichon, A. J. Haines, B. Shen-Tu, and J. Ren, Velocity field in Asia inferred from Quaternary fault slip rates and Global Positioning System observations, *J. geophys. Res.*, *105*(B8), 19,185–19,209, 2000.

Hunstad, I., G. Selvaggi, N. D'Agostino, P. England, P. Clarke, and M. Pierozzi, Geodetic strain in peninsular Italy between 1875 and 2001, *Geophys. Res. Lett.*, *30*(4), 1181, 2003.

Instrumental Catalog Working Group CSTI, Catalogo Strumentale dei terremoti italiani dal 1981 al 1996, Versione 1.0, Clueb, Bologna, CD-ROM, 2001.

Jackson, J. A., and D. P. McKenzie, Active tectonics of the Alpine-Himalayan belt between western Turkey and Pakistan, *Geophys. J. R. astr. Soc.*, *77*, 185–264, 1984.

Jackson, J. A., and D. P. McKenzie, The relationship between plate motions and seismic moment tensors, and the rates of active deformation in the Mediterranean and Middle East, *Geophys. J. R. astr. Soc.*, *93*, 45–73, 1988.

Jackson, J. A., J. Haines, and W. Holt, The horizontal velocity field in the deforming Aegean Sea region determined from the moment tensors of earthquakes, *J. geophys. Res.*, *97*(B12), 17,657–17,683, 1992.

Jackson, J. A., J. Haines, and W. Holt, A comparison of satellite laser ranging and seismicity data in the Agean region, *Geophys. Res. Lett.*, *21*(25), 2849–2852, 1994.

Jacques, E., C. Monaco, P. Tapponnier, L. Tortorici, and T. Winter, Faulting and earthquake triggering during the 1783 Calabria seismic sequence, *Geophys. J. Int.*, *147*(3), 499–516, 2001.

Jenny, S., S. Goes, D. Giardini, and H.-G. Kahle, Earthquake recurrence parameters from seismic and geodetic strain rates in the eastern Mediterranean, *Geophys. J. Int.*, *157*, 1331–1347, doi:10.1111/j.1365-246X.2004.02261.x, 2004.

Jolivet, L., A comparison of geodetic and finite strain pattern in the Aegean, geodynamic implications, *Earth Planet. Sci. Lett.*, *187*, 95–104, 2001.

Jolivet, L., J. Brun, P. Gautier, S. Lallemant, and M. Patriat, 3D kinematics of extension in the Aegean region from the early Miocene to the present, insights from the ductile crust, *Bull. Soc. géol. France*, *165*(3), 195–209, 1994.

Kagan, Y. Y., Seismic moment distribution, *Geophys. J. Int.*, *106*, 123–134, 1991.

Kagan, Y. Y., Seismic moment-frequency relation for shallow earthquakes: Regional comparison, *J. geophys. Res.*, *102*(B2), 2835–2852, 1997.

Kagan, Y. Y., Seismic moment distribution revisited: I. Statistical results, *Geophys. J. Int.*, *148*, 520–541, 2002a.

Kagan, Y. Y., Seismic moment distribution revisited: II. Moment conservation principle, *Geophys. J. Int.*, *149*, 731–754, 2002b.

Kahle, H.-G., M. V. Müller, and G. Veis, Trajectories of crustal deformation of western Greece from GPS observations 1989-1994, *Geophys. Res. Lett.*, *23*(6), 677–680, 1996.

Kahle, H.-G., M. Cocard, Y. Peter, A. Geiger, R. Reilinger, S. McClusky, R. W. King, A. Barka, and G. Veis, The GPS strain rate field in the Agean Sea and western Anatolia, *Geophys. Res. Lett.*, *26*(16), 2513–2516, 1999.

Kahle, H.-G., M. Cocard, Y. Peter, A. Geiger, R. Reilinger, A. Barka, and G. Veis, GPS-derived strain rate field within the boundary zones of the Eurasian, African, and Arabian Plates, *J. geophys. Res.*, *105*, 23,353–23,370, 2000.

Kanamori, H., The energy release in great earthquakes, *J. geophys. Res.*, *82*, 2981–2987, 1977.

Kanamori, H., and D. L. Anderson, Theoretical basis of some empirical relations in seismology, *Bull. seism. Soc. Am.*, *65*, 1073–1096, 1975.

King, G., D. Sturdy, and J. Whitney, The landscape geometry and active tectonics of northwestern Greece, *Geol. Soc. Am. Bull.*, *105*, 137–161, 1993.

Kiratzi, A. A., Study on the active crustal deformation of the North and East Anatolian Fault zones, *Tectonophysics*, *225*, 191–203, 1993.

Koravos, G. C., I. G. Main, T. M. Tsapanos, and R. M. W. Musson, Maximum earthquake magnitudes in the Aegean area constrained by tectonic moment release rates, *Geophys. J. Int.*, *152*, 94–112, 2003.

Kostrov, V. V., Seismic moment and energy of earthquakes, and seismic flow of rocks, *Izv. Acad. Sci. USSR Phys. Solid Earth*, *1*, 23–44, engl. Trans, 1974.

Kotzev, V., R. Nakov, B. Burchfiel, R. King, and R. Reilinger, GPS study of active tectonics in Bulgaria: results from 1996 to 1998, *J. Geodynamics*, *31*, 189–200, 2001.

Kreemer, C., and N. Chamot-Rooke, Contemporary kinematics of the Southern Aegean and the Mediterranean Ridge, *Geophys. J. Int., In Press*, 2004.

Kreemer, C., W. E. Holt, S. Goes, and R. Govers, Active deformation in the eastern Indonesia and Philippines from GPS and seismicity data, *J. geophys. Res.*, *105*, 663–680, 2000.

Kreemer, C., W. E. Holt, and J. A. Haines, An integrated global model of present-day plate motions and plate boundary deformation, *Geophys. J. Int.*, *154*, 8–34, 2003.

Lay, T., and T. Wallace, *Modern Global Seismology*, chap. Seismotectonics, pp. 434–495, Academic Press, San Diego, California, 1995.

Le Pichon, X., and J. Angelier, The Hellenic Arc and Trench system: A key to the neotectonic evolution of the Eastern Mediterranean area, *Tectonophysics*, *60*, 1–42, 1979.

Le Pichon, X., N. Chamot-Rook, S. Lallemant, R. Noomen, and G. Veis, Geodetic determination of the kinematics of Central Greece with respect to Europe: Implication for Eastern Mediterranean tectonics, *J. geophys. Res.*, *100*(B7), 12,675–12,690, 1995.

Leonard, T., O. Papasouliotis, and I. G. Main, A Poisson model for identifying characteristic size effects in frequency data: Application to frequency-size distributions for global earthquakes, "starquakes", and fault lengths, *J. geophys. Res.*, *106*(B7), 13,473–13,484, 2001.

Lickorish, W. H., M. Grasso, R. W. H. Butler, A. Argnani, and R. Maniscalco, Structural styles and regional tectonic setting of the "Gela Nappe"and frontal part of the Maghrebian thrust belt in Sicily, *Tectonics*, *18*(4), 655–668, 1999.

Lin, J., and R. S. Stein, Stress triggering in thrust and subduction earthquakes and stress interaction between the southern San Andreas and nearby thrust and strike-slip faults, *J. geophys. Res.*, *109*(B2), B02,303, doi:10.1029/2003JB002607, 2004.

Liu, G. D., The Cenozoic rift system of the North China plain and the deep internal process, in *Deep Internal Processes and Continental Rifting*, vol. 308, edited by C. Froidevaux and T. Tan, pp. 99–118, Tectonophysics, 1987.

Louvari, E., A. A. Kiratzi, and B. C. Papazachos, The Cephalonia transform fault and its extension to western Lefkada island (Greece), *Tectonophysics*, *308*, 223–226, 1999.

Lundgren, P., F. Saucier, R. Palmer, and M. Langon, Alaska crustal deformation: Finite element modeling constrained by geologic and very long baseline interferometry data, *J. geophys. Res.*, *100*(B11), 22,033–22,045, 1995.

Lundgren, P., D. Giardini, and R. Russo, A geodynamic framework for eastern Mediterranean kinematics, *Geophys. Res. Lett.*, *25*, 4007–4010, 1998.

Lyberis, N., T. Yurur, J. Chorowicz, E. Kasapoglu, and N. Gundogdu, The East Anatolian fault: An oblique collisional belt, *Tectonophysics*, *204*, 1–15, 1992.

Lyon-Caen, H., et al., The 1986 Kalamata (South Peloponessus) earthquake: Detailed study of a normal fault, evidences for east-west extension in the Hellenic arc, *J. geophys. Res.*, *93*, 14,967–15,000, 1988.

Main, I., Apparent breaks in scaling in the earthquake cumulative frequncy-magnitude distribution: fact or artifact?, *Bull. seism. Soc. Am.*, *90*, 86–97, 2000.

Main, I. G., and P. W. Burton, Seismotectonics and the earthquake frequency magnitude distribution in the Aegean area, *Geophys. J. Int.*, *98*(3), 575–586, 1989.

Makris, J., Some geophysical consideration on the geodynamic situation in Greece, *Tectonophysics*, *46*, 251–268, 1978.

Malinverno, A., and W. Ryan, Extension in the Tyrrhenian Sea and shortening in the Apennines as result of arc migration driven by sinking of the lithosphere, *Tectonics*, *5*, 227–245, 1986.

Mantovani, E., M. Viti, D. Albarello, C. Tamburelli, D. Babbucci, and N. Cenni, Role of kinematically induced horizontal forces in Mediterranean tectonics: insights from numerical modeling, *J. Geodynamics*, *30*(3), 287–320, 2000.

Mantovani, E., N. Cenni, D. Albarello, M. Viti, D. Babbucci, C. Tamburelli, and F. D'onza, Numerical simulation of the observed strain field in the central-eastern Mediterranean region, *J. Geodynamics*, *31*, 519–556, 2001.

Mao, A., C. G. A. Harrison, and T. H. Dixon, Noise in GPS coordinate time series, *J. geophys. Res.*, *104*(B2), 2797–2816, 1999.

Mascle, J., K. Kastens, C. Auroux, and L. S. D. Party, A land-locked back-arc basin: preliminary results from ODP Leg 107 in the Tyrrhenian Sea, *Tectonophysics*, *146*, 149–162, 1988.

Mazzuoli, R., L. Tortorici, and G. Ventura, Oblique rifting in Salina, Lipari and Vulcano Islands, *Terra Nova*, *7*, 444–452, 1995.

McClusky, S., et al., Global Positioning System constraints on plate kinematics and dynamics in the eastern Mediterranean and Caucasus, *J. geophys. Res.*, *105*, 5696–5719, 2000.

McGuire, J. J., and P. Segall, Imaging of aseismic fault slip transients recorded by dense geodetic networks, *Geophys. J. Int.*, *155*(3), 778–788, 2003.

McKenzie, D. P., Active tectonics of the Alpine-Himalayan belt: the Aegean sea and surrouding regions, *Geophys. J. R. astr. Soc.*, *55*, 217–254, 1978.

Meijer, P., and M. Wortel, Present-day dynamics of the Aegean region: A model analysis of the horizontal pattern of stress and deformation, *Tectonics*, *16*(6), 879–895, 1997.

Meletti, C., E. Pattaca, and P. Scandone, Construction of a seismotectonic model: The case of italy, *Pageoph*, *157*, 11–35, 2000.

Monachesi, G., and M. Stucchi, DOM4.1: an intensity database of damaging earthquakes in the Italian area, 1997.

Monaco, C., and L. Tortorici, Tettonica estensionale quaternaria nell'Arco Calabro e in Sicilia orientale, *Studi Geologici Camerti*, *2*, 351–362, 1995.

Monaco, C., and L. Tortorici, Active faulting in the Calabrian arc and eastern Sicily, *Journal of Geodynamics*, *29*, 407–424, 2000.

Monaco, C., S. Mazzoli, and L. Tortorici, Active thrust tectonics in western Sicily (southern Italy): the 1968 Belice earthquake sequence, *Terra Nova*, *8*(4), 372–381, 1996.

Monaco, C., P. Tapponnier, L. Tortorici, and P. Y. Gillot, Late Quaternary slip rates on the Acireale-Piedimonte normal faults and tectonic origin of Mt. Etna (Sicily), *Earth Planet. Sci. Lett.*, *147*(1-4), 125–139, 1997.

Moretti, A., and I. Guerra, Tettonica dal Messiniano ad oggi in Calabria: Implicazioni sulla geodinamica del sistema Tirreno-Arco Calabro, *Bol. Soc. Geol. Ital.*, *116*, 125–142, 1997.

Mulargia, F., F. Broccio, V. Achilli, and P. Baldi, Evaluation of a seismic quiescence pattern in southeastern Sicily, *Tectonophysics*, *116*, 335–364, 1985.

Mulargia, F., P. Gasperini, and S. Tinti, Contour mapping of italian seismicity, *Tectonophysics*, *142*, 203–216, 1987.

Nocquet, J.-M., and E. Calais, Crustal velocity field of western Europe from permanent GPS array solutions, *Geophys. J. Int.*, *154*, 72–88, 2003.

Nyst, M. C. J., A new approach to model the kinematics of crustal deformation with applications to the aegean and southeast asia, Ph.D. thesis, Delft University of Technologie, The Netherland, 2001.

Okal, E. A., and B. A. Romanowicz, On the variation of b-values with earthquake size, *Phys. Earth Planet. Int.*, *87*(1-2), 55–76, 1994.

Pantosti, D., and G. Schwartz, D.P.and Valensise, Paleoseismology along the 1980 Irpinia earthquake fault and implication for earthquake recurrence in the southern Apennines, *J. geophys. Res.*, *98*, 6561–6577, 1993.

Papadimitriou, E. E., and L. R. Sykes, Evolution of the stress field in the northern Aegean Sea (Greece), *Geophys. J. Int.*, *146*(3), 747–759, 2001.

Papaioannou, C., and B. Papazachos, Time-Independent and Time-Dependent Seismic Hazard in Greece Based on Seismogenic Sources, *Bull. seism. Soc. Am.*, *90*, 22–33, 2000.

Papazachos, B. C., A. A. Kiratzi, and B. G. Karacostas, Toward a homogeneous moment-magnitude determination for earthquakes in Greece and the surrouding area, *Bull. seism. Soc. Am.*, *87*(2), 474–483, 1997.

Papazachos, B. C., P. E. Comninakis, G. F. Karakaisis, B. G. Karakostas, C. A. Papaioannou, C. B. Papazachos, and E. M. Scordilis, A catalogue of earthquakes in Greece and surrounding area for the period 550BC-1999, in *International handbook of Earthquake and Engineering Seismology IASPEI*, 2000.

Papazachos, B. C., V. G. Karakostas, A. A. Kiratzi, B. N. Margaris, C. B. Papazachos, and E. M. Scordilis, Uncertainties in the estimation of earthquake magnitudes in greece, *J. of Seismology*, *6*, 557–570, 2002.

Papazachos, C. B., An alternative method for a reliable estimation of seismicity with an application in Greece and the surrouding area, *Bull. seism. Soc. Am.*, *89*, 1999.

Papazachos, C. B., and A. Kiratzi, A formulation for reliable estimation of active crustal deformation and its application to Central Greece, *Geophys. J. Int.*, *111*, 424–432, 1992.

Patane, D., P. De Gori, C. Chiarabba, and A. Bonaccorso, Magma ascent and the pressurization of Mount Etna's volcanic system, *Science*, *299*, 2061–2063, 2003.

Pavlides, S., N. Zouros, Z. Fang, S. Cheng, M. Tranos, and A. Chatzipetros, Geometry, kinematics and morphotectonics of the Yanqing-Huailai active faults (northern China), *Tectonophysics*, *308*(1-2), 99–118, 1999.

Piatanesi, A., and S. Tinti, A revision of the eastern Sicily earthquake and tsunami, *J. geophys. Res.*, *103*, 2749–2758, 1998.

Piromallo, C., and A. Morelli, Imaging the Mediterranean upper mantle by P-wave travel time tomography, *Ann. Geofis.*, *40*(4), 963–979, 1997.

Pondrelli, S., Pattern of seismic deformation in the Western Mediterranean, *Ann. Geofis.*, *42*(1), 57–70, 1999.

Pondrelli, S., A. Morelli, G. Ekström, S. Mazza, E. Boschi, and A. M. Dziewonski, European-Mediterranean regional centroid-moment tensors: 1997-2000, *Phys. Earth Planet. Int.*, *130*, 71–101, 2002.

Postpischl, D., Atlas of Isoseismal Maps of Italian Earthquakes, CNR, Progetto Finalizzato Geodinamica, Graficoop, Bologna, 1985.

Reilinger, R. E., S. C. McClusky, M. B. Oral, R. W. King, M. N. Toksöz, A. A. Barka, I. Kinik, O. Lenk, and I. Sanli, Global Positioning System measurements of present-day crustal movements in the Arabia-Africa-Eurasia plate collision zone, *J. geophys. Res.*, *102*(B5), 9983–9999, 1997.

Research Group for Estimating Losses from Future Earthquakes, State Seismological Bureau, *Estimating losses from earthquakes in China in the forthcoming 50 years*, 60 and 1 map pp., State Seismological Press, Beijing, 1992.

Reuther, C.-D., Z. Ben-Avraham, and M. Grasson, Origin and role of major strike-slip transfers during plate collision in the Central Mediterranean, *Terra Nova*, *5*, 249–257, 1993.

Robertson, A., and M. Shallo, Mesozoic-Tertiary tectonic evolution of Albania in its regional Eastern Mediterranean context, *Tectonophysics*, *316*, 197–254, 2000.

Robinson, R., and R. Benites, Upgrading a synthetic seismicity model for more realistic fault ruptures, *Geophys. Res. Lett.*, *28*(9), 1843–1846, 2001.

Sauter, F., Damage Prediction for Earthquake Insurance, pp. 99–108, 2nd US Nat. Conf. Earthqu. Eng., Aug. 22-24, Stanford University, California, USA, 1979.

Savage, J. C., and R. W. Simpson, Surface strain accumulation and the seismic moment tensor, *Bull. seism. Soc. Am.*, *87*, 1345–1353, 1997.

Schiano, P., R. Clocchiatti, L. Ottolini, and L. Busà, Transition of Mount Etna lavas from from a mantle-plume to an island-arc magmatic source, *Nature*, *412*, 900–904, 2001.

Scholz, C. H., and J. Campos, On the mechanism of seismic decoupling and back arc spreading at subduction zones, *J. geophys. Res.*, *100*(B11), 22,103–22,115, 1995.

Schorlemmer, D., S. Wiemer, and D. Wyss, M.and Jackson, Testing seismicity forecasts at parkfield: Hypotheses of spatially varying versus constant *b*-values. part ii: Superior performance of the model including variations, *submitted to J. geophys. Res.*, 2004a.

Schorlemmer, D., S. Wiemer, and M. Wyss, Testing Seismicity Forecasts at Parkfield: Hypotheses of Spatially Varying Versus Constant *b*-values. Part I: Stationarity of Spatial *b*-value Patterns, *submitted to J. geophys. Res.*, 2004b.

Sella, G. F., T. H. Dixon, and A. L. Mao, REVEL: A model for Recent plate velocities from space geodesy, *J. geophys. Res.*, *107*(B4), 2081, doi:10.1029/2000JB000033, 2002.

Selvaggi, G., and C. Chiarabba, Seismicity and P-wave velocity image of the Southern Tyrrhenian subduction zone, *Geophys. J. Int.*, *121*(3), 818–826, 1995.

Serpelloni, E., S. Pondrelli, M. Anzidei, P. Baldi, G. Casula, N. Cenni, and A. Pesci, Crustal deformation in Italy and surrounding regions inferred from GPS data and earthquake focal mechanisms, *Geophys. Res. Abs*, *5*, EAE03–A–02,573, 2003.

Serri, G., Neogene-Quaternary magmatism of the Tyrrhenian region: characterization of the magma sources and geodynamic implications, *Mem. Soc. Geol. It.*, *41*, 219–242, 1990.

Seyitoglu, G., and B. C. Scott, The cause of N-S extensional tectonics in western Turkey: tectonic escape vs back-arc spreading vs orogenic collapse, *J. Geodynamics*, *22*, 145–153, 1996.

Shen-Tu, B., W. E. Holt, and A. J. Haines, Deformation kinematics in the western United States determined from Quartenary fault slip rates and recent geodetic data, *J. geophys. Res.*, *104*, 28,927–28,955, 1999.

Slejko, D., L. Peruzza, and A. Rebez, Seismic hazard maps of Italy, *Ann. Geofis.*, *41*, 183–214, 1998.

Slejko, D., et al., GSHAP Seismic hazard assessment for Adria, *Annali di Geofisica, GSHAP Special Volume*, *42*(6), 1085–1107, 1999.

Sorel, D., A Pleistocene and still-active detachment fault and the origin of the Corinth-Patras rift, Greece, *Geology*, *28*(1), 83–86, 2000.

Speranza, F., R. Maniscalco, M. Mattei, A. Di Stefano, R. W. H. Butler, and R. Funiciello, Timing and magnitude of rotations in the frontal thrust systems of southwestern Sicily, *Tectonics*, *18*(6), 1178–1197, 1999.

Speranza, F., I. M. Villa, L. Sagnotti, F. Florindo, D. Cosentino, P. Cipollari, and M. Mattei, Age of the Corsica-Sardinia rotation and Liguro-Provencal Basin spreading: new paleornagnetic and Ar/Ar evidence, *Tectonophysics*, *347*(4), 231–251, 2002.

Speranza, F., R. Maniscalco, and M. Grasso, Pattern of orogenic rotations in central-eastern Sicily: implications for the timing of spreading in the Tyrrhenian Sea, *J. Geol. Soc. London*, *160*, 183–195, 2003.

State Seismological Bureau of China, *Explanation of seismic intensity zoning map of China*, Seismological Press, 1991.

Stein, R., A. Barka, and J. Dieterich, Progressive failure on the North Anatolian fault since 1939 by earthquake stress triggering, *Geophys. J. Int.*, *128*, 594–604, 1997.

Stein, R. S., G. C. P. King, and J. Lin, Stress triggering of the 1994 M=6.7 Northridge, California, earthquake by its predecessors, *Science*, *265*(5177), 1432–1435, 1994.

Stein, S., Space geodesy and plate motions, in *Contributions of Space Geodesy to Geodynamics: Crustal Dynamics*, edited by D. E. Smith and D. L. Turcotte, pp. 5–20, American Geophysical Union, 1993.

Stein, S., and M. Wysession, *An Introduction to Seismology, Earthquakes, and Earth Structure*, chap. Seismology and Plate Tectonics, pp. 286–368, Blackwell Publishing, Malden, U.S.A., 2003.

Stewart, I. S., A. Cundy, S. Kershaw, and C. Firth, Holocene coastal uplift in the Taormina area, northeastern Sicily: Implications for the southern prolongation of the Calabrian seismogenic belt, *J. Geodynamics*, *24*(1-4), 37–50, 1997.

Straub, C., H.-G. Kahle, and C. Schindler, GPS and geologic estimates of the tectonic activity in the Marmara Sea region, NW Anatolia, *J. geophys. Res.*, *102*(B12), 27,587–27,601, 1997.

Tanguy, J. C., M. Condomines, and G. Kieffer, Evolution of the Mount Etna magma: Constraints on the present feeding system and eruptive mechanism, *J. Volcanol. Geoth. Res.*, *75*, 221–250, 1997.

Tapponnier, P., and P. Molnar, Active faulting and tectonics in china, *J. geophys. Res.*, *82*(20), 2905–2930, 1977.

Taymaz, T., H. Eyidogan, and J. Jackson, Source parameters of large earthquakes in the East Anatolian fault zone, *Geophys. J. Int.*, *106*, 537–550, 1991a.

Taymaz, T., J. Jackson, and D. McKenzie, Active tectonics of the north and central Aegean Sea, *Geophys. J. Int.*, *106*, 433–490, 1991b.

Thatcher, W., Present-day crustal movements and the mechanics of cyclic deformation, in *The San Andreas Fault System, California*, edited by R. E. Wallace, pp. 189–206, U.S. Geological Survey Professional Paper 1515, 1990.

Tortorici, L., C. Monaco, T. Carlo, and C. Ornella, Recent and active tectonics in the Calabrian arc (Southern Italiy), *Tectonophysics*, *243*, 37–55, 1995.

Tortorici, L., C. Monaco, S. Mazzoli, and M. Bianca, Timing and modes of deformation in the western Sicilian thrust system, southern Italy, *Journal of Petroleum Geology*, *24*(2), 191–211, 2001.

Trasatti, E., C. Giunchi, and M. Bonafede, Effects of topography and rheological layering on ground deformation in volcanic regions, *J. Volcanol. Geoth. Res.*, *122*, 89–110, 2003.

U.S. Geological Survey, Preliminary Determination of Earthquakes (PDE), Monthly Listings, U.S. Dept. of Inter., Natl. Earthquake Inf. Cent., Denver, 1998.

Utsu, T., Aftershocks and earthquakes statistics (III), Analysis of the sistribution of earthquakes in magnitude, time and space with special considerations to clustering characteristics of earthquakes occurrence, *J. Fac. Sci. Hokkaido Univ. Japan*, *VII*(3), 379–441, 1971.

Utsu, T., Representation and analysis of the earthquake size distribution: a historical review and some new approaches, *Pure and Applied Geophysics*, *155*, 509–535, 1999.

Ventura, G., G. Vilardo, G. Milano, and N. A. Pino, Relationships among crustal structure, volcanism and strike-slip tectonics in the Lipari-Vulcano Volcanic Complex (Aeolian Islands, Southern Tyrrhenian Sea, Italy), *Phys. Earth Planet. Int.*, *116*(1-4), 31–52, 1999.

Viti, M., D. Albarello, and E. Mantovani, Classification of seismic strain estimates in the Mediterranean region from a 'bootstrap' approach, *Geophys. J. Int.*, *146*(2), 399–415, 2001.

Ward, S., and S. Goes, How regularly do earthquakes recur - a synthetic seismicity model for the San-Andreas fault, *Geophys. Res. Lett.*, *20*(19), 2131–2134, 1993.

Ward, S. N., Pacific-North America plate motions: New results from very long baseline interferometry, *J. geophys. Res.*, *95*, 21,965–21,981, 1990.

Ward, S. N., On the consistency of earthquake moment release and space geodetic strain rates: Europe, *Geophys. J. Int.*, *135*, 1011–1018, 1998a.

Ward, S. N., On the consistency of earthquake moment rates, geological fault data, and space geodetic strain: the United States, *Geophys. J. Int.*, *134*, 172–186, 1998b.

Wesnousky, S. G., Crustal deformation processes and the stability of the gutenberg-richter relationship, *Bull. seism. Soc. Am.*, *89*(4), 1131–1137, 1999.

Westaway, R., The Tripoli Libya, earthquake of September 4, 1974: Implications for the active tectonics of the Central Mediterranean, *Tectonics*, *9*(2), 231–248, 1990.

Westaway, R., Seismic moment summation for historical earthquakes in Italy: tectonic implications, *J. geophys. Res.*, *97*, 15,437–15,464, 1992.

Westaway, R., Quartenary uplift of Southern Italy, *J. geophys. Res.*, *98*, 21'741–21'772, 1993.

Westaway, R., Present-day kinematics of the Middle East and eastern Mediterranean, *J. geophys. Res.*, *99*(6), 12,071–12,090, 1994.

Wiemer, S., and M. Wyss, Mapping spatial variability of the frequency-magnitude distribution of earthquakes, *Adv. Geophys.*, *45*, 259–302, 2002.

Wilson, M., and R. Patterson, Intraplate magmatism related to short-wavelength convective instabilities in the upper mantle; evidence from the Tertiary-Quaternary volcanic province of Western and Central Europe, in *Mantle plumes: their identification through time*, *Special Paper - Geol. Soc. Am.*, vol. 352, edited by K. L. Buchan, pp. 37–58, Geological Society of America, 2001.

Working Group CPTI, Catalogo parametrico dei terremoti italiani, GNDT, SGA, SSN, Bologna, 92pp, 1999.

Wortel, M., and W. Spakman, Subduction and slab detachment in the Mediterranean-Carpathian region, *Science*, *290*, 1910–1917, 2000.

Xu, X., and X. Ma, Geodynamics of the Shanxi rift system, China, in *Geodynamics of Rifting, 1. Case History Studies on Rifts: Europe and Asia*, edited by P. Ziegler, pp. 325–340, Tectonophysics, 1992.

Xu, X., X. Ma, and Q. Deng, Neotectonic activity along the Shanxi Rift System, China, *Tectonophysics*, *219*(4), 305–325, 1993.

Zhang, J., Y. Bock, H. Johnson, P. Fang, S. Williams, G. Joachim, S. Wdowinski, and J. Behr, Southern California Permanent GPS Geodetic Array: Error analysis of daily position estimates and site velocities, *J. geophys. Res.*, *102*(B8), 18,035–18,055, 1997.

Zhang, Y. Q., and J. L. Vergely, P. amd Mercier, Active faulting in and along the Qinling Range (China) inferred from SPOT imagery analysis and extrusion tectonics of south China, *Tectonophysics*, *243*(1-2), 69–95, 1995.

Zhang, Y. Q., P. Vergely, and J. L. Mercier, Fault segmentation, active faulting and oblique extension along the Shanxi graben system (north China): observations from SPOT images, *Annales Tectonicae*, *8*, 3–22, 1994.

Zhang, Y. Q., J. L. Mercier, and P. Vergely, Extension in the graben systems around the Ordos (China), and its contribution to the extrusion tectonics of south China with respect to Gobi-Mongolia, *Tectonophysics*, *285*(1-2), 41–75, 1998.

Zhang, Z., and D. Chen, Seismic hazard analysis for site intensity evaluation, in *3rd Int. Earthquake Microzonation Conference Proceedings*, Seattle, USA, 1982.

Acknowledgments

I would foremost like to thank my direct supervisor Prof. Saskia Goes with whom I interacted the most. Saskia has invested a lot of time, energy and enthousiasm in supervising this work. She was always willing to answer my questions or discuss critical issues. I am grateful for her patience helping me to shape ideas and present results in a concise way and write them down in a precise English.

I want to thank Prof. Domenico Giardini for suggesting the theme of this thesis, which motivated me to begin a Ph.D. Many ideas in this study originate from several discussions I and Saskia had with him. This thesis has very much benefited, as have I, from his expertise in seismic hazard and knowledge about the Mediterranean tectonics. I am also grateful for the financial assistance he secured for my project.

I spent the first part of this study within the group of Prof. Hans-Gert Kahle. I want to thank him and his group for their help in getting me started with geodetic data and crustal motion. My programming at the early stage of this project has beneficiated from the experience of Dr. Marc Cocard and Dr. Etienne Favey. I am grateful to Prof. Kahle for having taken contact with Dr.D. Del Rosso and Dr. F. Vespe for field work assistance. Special thanks are going to Christine Hollenstein who has processed the italian geodetic data. Her expert knowledge has allowed us to get high quality geodetic data. Without her outstanding job, half of this project wouldn't have been possible. I am also grateful to Prof. Hans-Gert Kahle for having partly financed this project.

I am very grateful to Dr. Anselm Smolka and Dr. Gerhard Berz from the Munich Reinsurance Company in Munich (Germany) for having spontaneously accepted to partly finance this project. I wouldn't have been able to begin this study otherwise. I

would like to thank Dr. Anselm Smolka for his interest in this project and for hosting me at the MunichRe during the summer 2003. The expert knowledge and friendly attitude of himself and his group (Alex Allmann and Dr. Dirk Hollnack) made this internship very interesting and enjoyable.

I thank Prof. Bill Holt and Dr. John Haines for making the strain rate mapping program available. Dr. Corné Kreemer deserves special mention for having been very patient in helping me running this code. The finite element strain rate code has been provided by Dr. Paul Lundgren, who took time helping us run it.

Dr. Paolo Gasperini has been very helpful in providing seismic data for Italy and in answering all kind of questions about them.

Thanks to Dr. Jochen Braunmiller and Fabrizio Bernardi for providing moment tensor solutions.

I would like to express my gratitude to those who took the time and the effort to give me useful advice and/or discuss my results with me. These are Dr. Nicolas Deichmann, Dr. Alain Geiger, Prof. Dave Jackson, Dr. Corné Kreemer, Dr. Enrico Serpelloni, Dr. Steve Ward, Dr. Stefan Wiemer and Jochen Woessner.

I would like to thank my officemates that contributed to a very nice working atmosphere. They are Lapo Boschi, Nicolas Deichmann, Paul Flück, Jeroen van Hunen, Steve Miller, Jérome Salichon (who provided me with nice cookies), Marc Troller and the women power group (Dominique Ballarin, Iris Marschall (thanks for translating the abstract in to German), Souad Sellami and Alba Zappone). Thanks to the Italian group (Fabio Antonio, Fabrizio Bernardi, Fabio Cammarano, Francesca Funiciello, Gabriele Mora and Rafaele di Stefano) for bringing a Mediterranean climate to the offices. It has always been very nice to have a small chat with Remco Muijs in the coffee room.

I would like to thanks my friends Francesca Bay, Philippe Roth and Sibylle Steimen for their understanding of the ups and downs related to such a work, their always lis-

tening ear, their support and humor.

Special thanks are going to my mother, Geneviève, who made my studies in geophysics possible and always encouraged and supported me during this work.

Last but not least, I would like to thank Marc for his moral and technical support. I am very grateful to him for having been my highly appreciated personal system administrator and for having solved countless problems related to informatics. This work has benefited from the time he took to teach me how to use GIS ArcView. Thank you Marc for having let me feel like eating in a five-star restaurant nearly every evening during the last month. Although the stress level was pretty high, it has been a culinary highlight period.

There were a lot more helpful and supportive people that I could not list here. Whoever reads these words most probably is part of that crowd.

Curriculum Vitae

Personal

Name:	Sarah Jenny
Date of Birth:	29 January 1974
Place of Birth:	Fribourg, Switzerland
Citizen of:	Switzerland and France

Education

2000 - 2004	Ph.D. in Geophysics, Swiss Federal Institute of Technology (ETH), Zürich, Switzerland.
1994 - 1999	Diploma in Applied Geophysics, Swiss Federal Institute of Technology (ETH) Zürich, Switzerland and Geological Survey of Canada, Ottawa, Canada.
1989 - 1993	Matura type C (High school degree), Collège St. Michel, Fribourg, Switzerland.

Award

2003	Award of the American Geophysical Union for outstanding student paper at the fall meeting, San Francisco, December 2002.